

**Mesostructuring of SiCN Materials and Catalysts *via*
Microphase Separation Technique *utilizing*
High-Density Polyethylene Blocks**

DISSERTATION

zur Erlangung des akademischen Grades eines Doktors der
Naturwissenschaften (Dr. rer. nat.)
Im Fach Chemie der Fakultät für Biologie, Chemie und
Geowissenschaften der Universität Bayreuth

vorgelegt von

M.Sc. Saravana Kumar Thaman Pillai (M.S.)

geboren in Trichy, Tamilnadu, India.

Bayreuth, Germany, 2013

This doctoral thesis was prepared at the Chair of Inorganic Chemistry II, University of Bayreuth, from November 2010 until November 2013 supervised by Prof. Dr. Rhett Kempe.

This is a full reprint of the dissertation submitted to obtain the academic degree of Doctor of Natural Sciences (Dr. rer. nat.) and approved by the Faculty of Biology, Chemistry and Geological Sciences of the University of Bayreuth.

Acting Dean: Prof. Dr. Rhett Kempe

Date of submission: 13-09-2013

Date of defence (disputation): 21-11-2013

Doctoral Committee:

Prof. Dr. Rhett Kempe (1st reviewer)

Prof. Dr. Josef Breu (2nd reviewer)

Prof. Dr. Stephan Förster (Chairman)

Prof. Dr. Mukundan Thelakkat

To my Parents and Roopa

கற்றது கை மண் அளவு, கல்லாதது உலகளவு.

-ஒளவையார், பொ. ஊ. 100-200.

Known is a Drop, Unknown is an Ocean.

Avvaiyar, 100-200 CE.

Abbreviations

AFM	atomic force microscopy
Au@SiCN	gold nanoparticles containing silicon carbonitride
Ag@SiCN	silver nanoparticles containing silicon carbonitride
Ap ^{TMS} H	4-Methyl-2-2((trimethylsilyl)-amino)-pyridine
ATRP	atom transfer radical polymerization
BET	brunauer-emmett-teller
BJH	barrett-joyner-helenda
CTA	chain transfer agents
CTS	chain transfer state
CGS	chain growing state
CCTP	coordinative chain transfer polymerization
DCP	dicumyl peroxide
DFT	density functional theory
DSC	differential scanning calorimetric
d-spacing	domain spacing
FTIR	fourier transform infrared spectroscopy
FIB	fiber
f _{PL}	volume fraction of poly Lactide block
GPC	gel permeation chromatography
Gyroid	a self assembled morphology defined by infinitely connected triply periodic surface
HT GPC	high temperature gel permeation chromatography
HTT-1800	commercially available ceramic precursor
HD	high-density
hPB	hydrogenated PolyButadiene

IR	infrared
LPE	linear polyethylene
LAM	lamellae
M@SiCN	metal nanoparticles containing silicon carbonitride
MAS	magic angle spinning
Mn	molecular number
Mw	molecular weight
NL-DFT	non linear density functional theory
NMR	nuclear magnetic resonance
ODT	order to disorder transition
RAFT	reversible addition-fragmentation chain transfer
RE	rare earth metal
PE-OH	hydroxyl terminated polyethylene
PCCP	precursor ceramic carbosilazane polymer
PEOPL	polyethylene- <i>b</i> -polylactide
PEOHTT	polyethylene- <i>b</i> -polycarbosilane
PDMS	polydimethylsilokane
ppm	parts per million
PDI	polydispersity index
Porogen	pore generating polymer
PL	polylactide
Rg	surface roughness
rpm	rate per minute
SI	supporting information
SiCN	silicon carbonitride
SEM	scanning electron microscopy
SAXS	small angle x-ray scattering

SEC	size- exclusive chromatography
T _m	melting point
T _c	crystallization point
TEM	transmission electron microscopy
TMA	tri-methyl aluminum
TiBA	tri-isobutyl aluminim
TEA	triethyl aluminum
TGA	thermo gravimetric analysis
thf	Tetrahydrofuran
XRD	X-ray Diffraction
ΔH _m	enthalpy of formation
X _E	crystallinity
χ	Flory-Huggins interaction parameter

Table of Contents

1. Zusammenfassung/Summary	1
2. Introduction	4
2.1. Brief introduction on SiCN ceramics.....	4
2.2. From non-porous to mesoporous SiCN.....	5
2.3. (Mesoporous) SiCN supported metal catalysts	7
2.4. References	8
3. Overview of the Thesis	12
3.1. Individual Contribution to Joint Publications.....	16
4. Tailored Nano-Structuring of End-Group Functionalized HD-Polyethylene Synthesized via an Efficient Catalytic Version of Ziegler's "Aufbaureaktion"	20
4.1. Abstract.....	20
4.2. Introduction, Results and Discussion.....	20
4.3. Conclusion.....	31
4.4. Acknowledgements	31
4.5. References	31
4.6. Experimental Section (Supporting Information)	34
4.6.1. Synthesis and Characterization of the Polymerization Catalysts	37
4.6.2. Ethylene Polymerization Studies.....	39
4.6.3. General procedure for block copolymer synthesis	45
4.6.4. Characterization of the diblock copolymers.....	46
4.6.5. Microphase separation of PEOPL	48
4.7. References (Supporting Information)	51
5. SiCN nanofibers with a diameter below 100 nm synthesized via concerted block copolymer formation, microphase separation, and crosslinking	52
5.1. Abstract.....	52
5.2. Introduction, Results and Discussion.....	53
5.3. Conclusion	61
5.4. Acknowledgement.....	61
5.5. References	62
5.6. Experimental Section (Supporting Information).....	65

5.6.1. Characterization of hydroxyl terminated PE block.....	67
5.6.2. Characterization of HTT-1800	67
5.6.3. Synthesis of SiCN fibers.....	68
5.6.4. Characterization of cross-linked “green body”	69
5.6.5. Pyrolysis of the green body and characterization of the nano- structured SiCN material	73
5.7. References (Supporting Information)	78
6. Robustly Supported Porous Au and Ag Catalysts for the Selective Oxidation of Alkenes using Air/O₂ as an Oxidant...	79
6.1. Abstract.....	79
6.2. Introduction	80
6.3. Results and Discussion.....	82
6.4. Conclusion	88
6.5. Acknowledgments.....	88
6.6. References.....	88
6.7. Experimental Section	91
6.8. References (Experimental Section)	107
7. List of Publications	108
8. Danksagung/Acknowledgement.....	109
9. Declaration/Erklärung	112

1. Zusammenfassung/Summary

Summary

The objective of this thesis is to utilize the hydroxyl terminated polyethylene (PE-OH) produced via Ziegler's "Aufbaureaktion" for the synthesis of 1) porous polyethylene templates for the synthesis of structurally inverted porous SiCN (siliconcarbonitride) 2) SiCN mesomaterials using PE-OH as porogen 3) porous SiCN supported gold catalysts.

Porous polyethylene template was synthesized from polyethylene-*block*-polylactide (PEOPL) copolymer by microphase separation technique and selective etching of polylactide block. ^1H NMR was used to confirm the formation of copolymer. Atomic Force Microscopy (AFM) was used to analyse the microphase separated PEOPL copolymer. The progress of etching polylactide block was monitored by Fourier Transform Infrared Spectroscopy (FTIR). Scanning Electron Microscopy (SEM) was used to analyse the porous polyethylene template.

The SiCN mesomaterials were synthesized from PE-OH by linking with commercially available polysilazane (HTT1800). Linked copolymer was microphase separate, cross-linked, and pyrolysed for the synthesis of SiCN mesostructures. Upon tuning the weight (volume) ratio of HTT1800 and PE-OH, various morphologies such as lamellae, fibers, and disordered bicontinuous SiCN can be synthesized (Figure 1.1). These morphologies were confirmed by AFM, TEM, SEM and Small Angle X-ray Scattering (SAXS).

Die SiCN-Mesomaterialien wurden durch Bindung des PE-OHs an kommerziell erhältlichem Polysilazan (HTT1800) erhalten. Das entstandene Copolymer wurde mikrophasensepariert, vernetzt und pyrolysiert. Durch Variation des Gewichts- (Volumen-) Verhältnisses von HTT1800 und PE-OH konnten verschiedene Morphologien wie Lamellen, Fasern und bicontinuierlem SiCN erhalten werden. Diese Morphologien wurden mittels AFM, TEM, REM und Kleinwinkelröntgenstreuung (SAXS) untersucht.

Porous SiCN supported gold ceramic (Au@SiCN) catalyst was synthesized by copolymer formation, microphase separation, crosslinking, and pyrolysis. The bicontinuous SiCN morphology has been chosen as a support for the synthesis of porous catalyst due to high surface area and the pores in the range of mesoscale (2-50 nm). Gold nanoparticles were introduced by adding tetrameric aminopyridinato gold complex. The synthesized Au@SiCN catalysts were characterized by TEM, powder XRD, and N₂ physisorption. The stability of nanoparticles may be due to the nitrogen functionality of Si-C-N network (Figure 1.2). The catalytic performance of the synthesized catalyst was demonstrated in the oxidation of cyclic and linear alkenes with air. The catalyst was highly selective for the epoxide products.

Zusammenfassung

Ziel dieser Doktorarbeit ist es, Hydroxy-terminiertes Polyethylen (PE-OH), welches über Zieglers "Aufbaureaktion" zugänglich ist, für die Synthese von 1) einem porösen Polyethylentemplat für die Herstellung von porösen SiCN 2) SiCN-Mesomaterialien mittels PE-OH als *porogen* 3) poröse SiCN getragene Gold-Katalysatoren.

Das poröse Polyethylentemplat wurde durch Mikrophasenseparation mittels einem Polyethylen-block-polylactid (PEOPL) Copolymer und selektivem Herauslösen des Polylactidblocks synthetisiert. Die Bildung des Copolymers wurde mittels ¹H-NMR bestätigt. Das mikrophasenseparierte PEOPL-Copolymer wurde mittels Rasterkraftmikroskopie (AFM) analysiert. Das Herauslösen des Polylactid-Blocks wurde mittels Fouriertransformierter Infrarotspektroskopie (FTIR) verfolgt. Das poröse Polyethylentemplat wurde mittels Rasterelektronenmikroskopie (REM) analysiert.

Die SiCN-Mesomaterialien wurden durch Bindung des PE-OHs an kommerziell erhältlichem Polysilazan (HTT1800) erhalten. Das entstandene Copolymer wurde mikrophasensepariert, vernetzt und pyrolysiert. Durch Variation des Gewichts- (Volumen-) Verhältnisses von HTT1800 und PE-OH konnten verschiedene Morphologien wie Lamellen, Fasern und

bicontinuierlichem SiCN erhalten werden. Diese Morphologien wurden mittels AFM, TEM, REM und Kleinwinkelröntgenstreuung (SAXS) untersucht.

Die porösen SiCN geträgerten Gold-Katalysatoren (Au@SiCN) wurden durch Copolymerbildung, Mikrophasenseparation, Vernetzung und Pyrolyse synthetisiert. Aufgrund der hohen Oberfläche und Poren im Mesobereich (2-50 nm) wurde die bikontinuierliche SiCN Morphologie als Träger für die Synthese von porösen Katalysatoren verwendet. Durch die Zugabe eines tetramerischen Aminopyridinato-Gold-Komplexes konnten Goldnanopartikel in die poröse SiCN-Matrix eingeführt werden. Der synthetisierte Au@SiCN Katalysator wurde mittels TEM, Pulverdiffraktometrie (XRD) und N₂-Physisorption (BET) charakterisiert. Die Nanopartikel können dabei durch die Stickstoff-Funktionen des Si-C-N-Netzwerkes stabilisiert werden. Der hergestellte Katalysator wurde in der katalytischen Oxidation von zyklischen und linearen Alkanen mit Luftsauerstoff getestet. Hierbei war der Katalysator sehr selektiv hinsichtlich der Epoxidierung.

2. Introduction

“Science cannot solve the ultimate mystery of nature. And that is because, in the last analysis, we ourselves are part of nature and therefore part of the mystery that we are trying to solve.”

---Hon. Prof. Max Ernst Ludwig Planck

2.1. Brief introduction on SiCN ceramics

The term “Keramik” (ceramics) is originated from the greek word “κεραμικ” denotes for inorganic and non-metallic materials.¹ Ceramics are divided into three classes namely, oxide ceramics (metal oxides, little or no glass phase), non-oxide ceramics and silicate ceramics (large proportion of glass phase with SiO₂).² Among these three classes, the non-oxide ceramics are an interesting class of materials that includes borides, silicides, carbides, nitrides, carbonitrides, etc.³ In particular, (polymer derived) non-oxide silicon carbonitrides (SiCN) show unique physical and chemical properties⁴ that make them suitable materials for various applications such as supports for heterogeneous catalysts.⁵

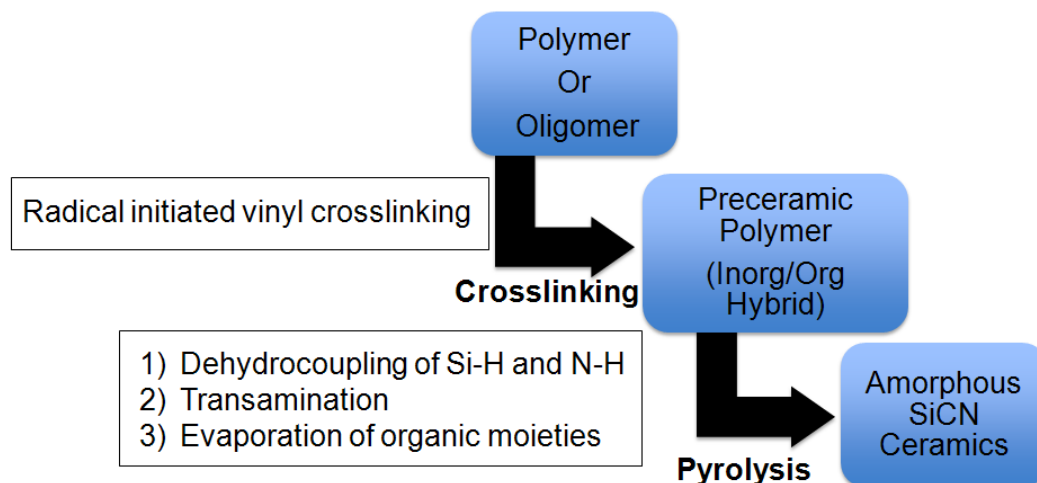


Figure 2.1. General synthetic route to polymer derived SiCN ceramics.

The synthesis of polymer derived SiCN ceramics is carried out from oligo- or polysilazane precursors via multi step process as mentioned in Figure 2.1.⁶ The precursors can be cross-linked in the presence of a

catalytic amount of radical initiator. The cross-linked precursor is called pre-ceramic polymer or green-body that can be transferred into SiCN material upon pyrolyzing at high temperature under inert atmosphere. During pyrolysis, the formation of various environments such as C_4Si , C_3SiN , C_2SiN_2 , $CSiN_3$, and SiN_4 is possible.⁷ The pre-ceramic polymer, pyrolysed at $1100^\circ C$ leads to the formation of an amorphous SiCN materials with primarily C_3SiN , C_2SiN_2 , and $CSiN_3$ environments.⁸

2.2. From non-porous to mesoporous SiCN

Since the discovery of mesoporous silica materials,⁹ the demand for the synthesis of mesoporous materials with controlled pore size and porosity has been exceptionally increased. Based on the pore diameter, porous materials are classified into microporous ($< 2nm$), mesoporous (2-50 nm) and macroporous ($> 50 nm$).¹⁰ The porous materials offer many additional features from non-porous materials such as high surface area and high adsorption capacity.¹¹ These porous materials can be synthesized by various template and non-template assisted techniques.¹² Introducing porosity to SiCN ceramics is a challenging task because of the sensitivity of the precursors.

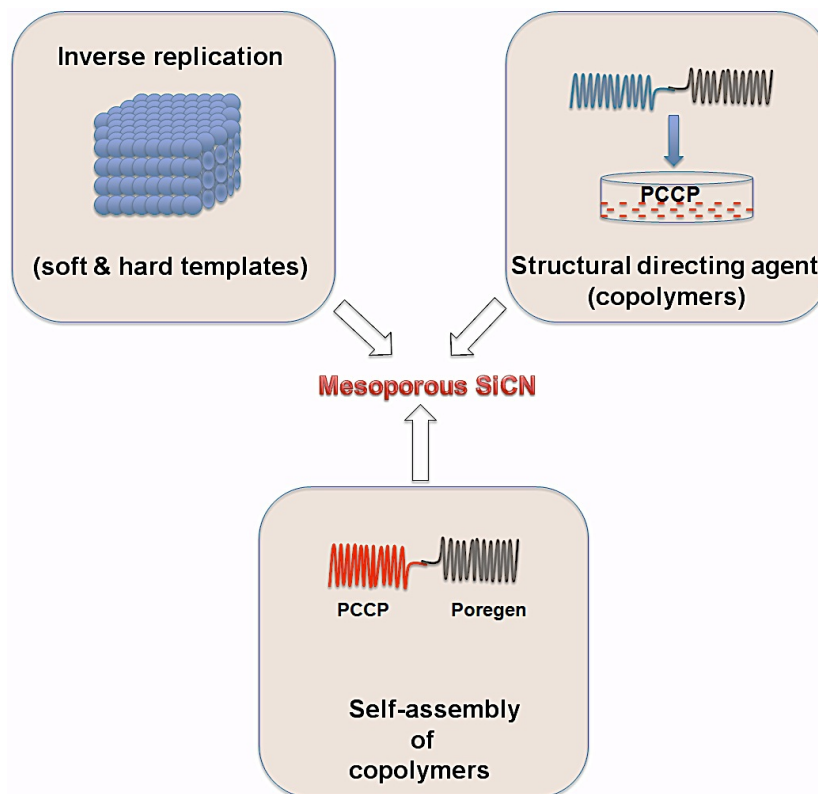


Figure 2.2. Various procedures for the synthesis of porous SiCN (PCCP-preceramic carboosilazane polymer, *porogen*-pore generating

polymer).

In general, porous SiCN ceramics¹³ can be synthesized by (i) inverse replication of hard or soft templates, (ii) employing an organic copolymers as structural directing agent, and (iii) copolymerization of ceramic precursor with an organic *porogen* block (Figure 2.2). Hard templates such as SiO₂, Al₂O₃, etc., are widely used for the synthesis of structurally inverted porous SiCN in mainly macro porous range.¹⁴ However, strong etching reagents (HF, etc.) are required for the removal of the templates. These harmful etching reagents not only etches out the templates but also causes sever damage to the SiCN. Alternative to the hard template inversion procedure, soft templates such as porous polyolefins templates have shown to avoid exposing to etching reagents.¹⁵ However, the precursor may not be effectively infiltrated. Thus, this procedure has been mainly used for the synthesis of macroporous SiCN ceramics. Alternative to the (spherical) template assisted synthesis of porous SiCN, structural directing agents such as organic block copolymers can be employed for the self-assembly of ceramic precursor.¹⁶ Pyrolyzing the morphology leading to mesostructured SiCN with only moderate surface area. In addition, this approach can introduce oxygen environment to SiCN due to the copolymers with having oxy functional groups.

Followed by the above copolymer/polymer mixture leading to a self-assembled morphology approach, the direct inorganic-organic diblockcopolymer of pre-ceramic precursor with organic *porogen* block have shown to be a promising technique for the synthesis of mesoporous SiCN.¹⁷

A chemically dissimilar block copolymer with thermodynamically incompatible and spatially segregating blocks tend to undergo microphase separation leading to various morphologies in nanoscale.¹⁸ The final morphology is based on several factors such as the volume fraction of blocks, degree of polymerization, and Flory-Huggins interaction parameters. The volume fraction can control the morphology and the degree of polymerization can control the domain size. Incompatibility between the blocks is an important factor for the microphase separation. Morphologies such as hexagonally packed cylinders, spheres arranged on body centered cubic,

lamellae, gyroidal (Figure 2.3) can be obtained.¹⁹ This direct copolymerization approach seems to be most promising approach to structure materials such as SiCN ceramics/catalysts.

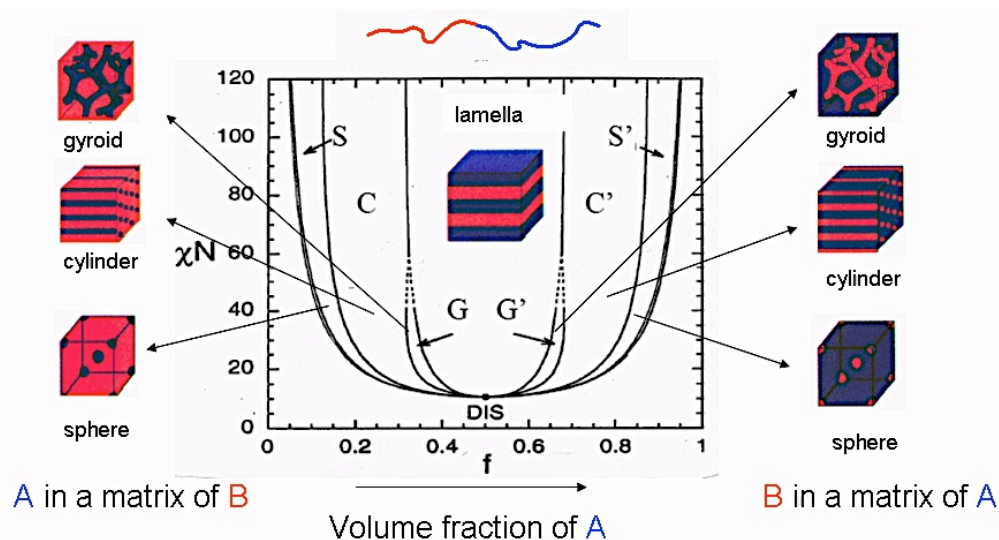


Figure 2.3. Various self-assembled morphologies (S-spherical, C-cylindrical, and G-gyroidal) derived from diblock copolymers (figure adopted from ref. 19b).

2.3. (Mesoporous) SiCN supported metal catalysts

Recently, metal containing SiCN ceramics have been introduced as interesting class of heterogeneous catalyst.^{5a} For example, copper containing SiCN catalysts were synthesized via modifying the preceramic precursor by a copper aminopyridinato complex.²⁰ The modification was accomplished by transmetallation reaction from metal complex to ceramic precursor via molecular pathway. This non-porous Cu@SiCN catalyst has shown increase in selectivity for aerobic oxidation of alkanes with increasing copper loading. In another example of non porous SiCN support, palladium silicides at SiCN catalyst was synthesized for the hydrogenation of ketones via modifying precursor ceramic by a palladium aminopyridinato complex.²¹ Recently, porous materials have been used as a support because porosity can impact on the performance of catalysts.²² Metal nanoparticles have been introduced on porous support as an additional step.^{22a} For example, the metal containing macroporous SiCN catalyst for ammonia reformation was first reported by Kim and coworkers using two-step synthetic procedure.^{14d} A macroporous SiCN was fabricated by capillary filling of preceramic polymer followed by

the deposition of ruthenium metal. To simplify this two step procedure, Wiesner and co-workers have introduced one pot synthesis of metal nanoparticles supported mesostructured catalysts using block-copolymer as structural directing agent have been established. Porous SiCN supported platinum nanoparticles have been synthesized via above mentioned approach by copolymer, ceramic precursor, and platinum complex as a part of five component system.²³ The platinum SiCN catalyst synthesized by this approach has shown 40 m²/g of surface area. Recently, microporous SiCN supported nickel catalyst with 400 m²/g for semi hydrogenation of alkynes was synthesized by Kempe and co-workers.²⁴ Controlled pyrolysis at 600°C is the reason reported for the generation of microporosity in the catalysts.

This thesis comprises of 1) the synthesis of porous polyethylene templates for the synthesis of structurally inverted porous SiCN 2) synthesis of nanostructured SiCN ceramics 3) synthesizing porous SiCN supported catalysts for alkene epoxidation. For the synthesis of porous catalysts, bicontinuously porous SiCN was used as support and gold and silver aminopyridinato metal complexes were employed to introduce nanoparticles.

2.4. References

- [1] W. Kollenberg in *Technische Keramik* (Ed.: W. Kollenberg), Vulkan, Essen **2004**, p. 3.
- [2] W. Kollenberg in *Technische Keramik* (Ed.: W. Kollenberg), Vulkan, Essen **2004**, p. 163.
- [3] E. Kroke, Y.-L. Li, C. Konetschny, E. Lecomte, C. Fasel, R. Riedel, *Mater. Sci. Eng.* **2000**, *26*, 97-199.
- [4] a) P. Colombo, G. Mera, R. Riedel, G. D. Soraru, *J. Am. Ceram. Soc.* **2010**, *93*, 1805–1837; b) E. Ionescu, H.-J. Kleebe, R. Riedel, *Chem. Soc. Rev.* **2012**, *41*, 5032–5042.
- [5] a) M. Zaheer, T. Schmalz, G. Motz, R. Kempe, *Chem. Soc. Rev.* **2012**, *41*, 5102–5116; b) D. Su, Y.-L. Li, Y. Feng, J. Jin, *J. Am. Ceram. Soc.* **2009**, *92*, 2962–2968; c) R. Riedel, H.-J. Kleebe, H. Schönfelder, F. Aldinger, *Nature* **1994**, *374*, 526–528; d) L. M. Reinold, M. Graczyk-Zajac, Y. Gao, G. Mera, R. Riedel, *J. Power Sources* **2013**, *236*, 224–229.

- [6] E. Kroke, Y.-L. Li, C. Kornetschny, *Technische Keramik* (Ed.: W. Kollenberg), Vulkan, Essen **2004**, p. 230.
- [7] Polymer Derived Ceramics (Eds: P. Colombo, G. D. Sorarú, R. Riedel, A. Kleebe, D. E. Stech), Publications Inc., Lancaster USA **2010**.
- [8] a) C. Haluschka, H.-J. Kleebe, R. Franke, R. Riedel, *J. Eur. Ceram. Soc.* **2000**, *20*, 1355–1364; b) H.-J. Kleebe, H. Störmer, S. Trassl, G. Ziegler, *Appl. Organometal. Chem.* **2001**, *15*, 858–866.
- [9] a) C. T. Kresge, M. E. Leonowicz, W. J. Roth, J. C. Vartuli, J. S. Beck, *Nature* **1992**, *359*, 710–712; b) J. S. Beck, J. C. Vartuli, W. J. Roth, M. E. Leonowicz, C. T. Kresge, K. D. Schmitt, C. T. W. Chu, D. H. Olson, E. W. Sheppard, S. B. McCullen, J. B. Higgins, J. L. Schlenker, *J. Am. Chem. Soc.* **1992**, *114*, 10834–10843.
- [10] K. S. W. Sing, D. H. Everett, R. A. W. Haul, L. Moscou, R. A. Pierotti, J. Rouquerol, T. Siemieniowska, *Pure & Appl. Chem.* **1985**, *57*, 603–619.
- [11] M. E. Devis, *Nature* **2002**, *417*, 813–821.
- [12] G. J. de A. A. Soler-Illia, C. Sanchez, B. Lebeau, J. Patarin, *Chem. Rev.* **2002**, *102*, 4093–4138.
- [13] a) P. Colombo, *Science* **2008**, *322*, 381–383; b) P. Colombo, C. Vakifahmetoglu, S. Costacurta, *J. Mater. Sci.* **2010**, *45*, 5425–5455; b) P. Colombo, M. Scheffler, Highly porous components, in *Polymer Derived Ceramics. From Nano-Structure to Applications*, (Eds: P. Colombo, R. Riedel, G. D. Sorarú, and H.-J. Kleebe), p 379, DEStech Publications Inc., Lancaster, PA, **2010**.
- [14] a) H. Wang, S.-Y. Zheng, X.-D. Lia, D.-P. Kim, *Microporous Mesoporous Mater.* **2005**, *80*, 357–362; b) J. Yan, A. Wang, D.-P. Kim, *Microporous Mesoporous Mater.* **2007**, *100*, 128–133; c) I.-K. Sung, Christian, M. Mitchell, D.-P. Kim, P. J. A. Kenis, *Adv. Funct. Mater.* **2005**, *15*, 1336–1342; d) Y. Shi, Y. Wan, Y. Zhai, R. Liu, Y. Meng, B. Tu, D. Zhao, *Chem. Mater.* **2007**, *19*, 1761–1771; e) Y. Shi, Y. Wan, D. Zhao, *Chem. Soc. Rev.* **2011**, *40*, 3854–3878.
- [15] a) B. H. Jones, T. P. Lodge, *J. Am. Chem. Soc.* **2009**, *131*, 1676–1677; b) T. Schmalz, J. M. Hausherr, W. Müller, T. Kraus, W. Krenkel, R. Kempe, G. Motz, *J. Ceram. Soc. Jpn.* **2011**, *119*, 477–482; c) P. Colombo, C. Vakifahmetoglu, S. Costacurta, *J. Mater. Sci.* **2010**, *45*, 5425–5455.

- [16] a) C. B. W. Garcia, C. Lovell, C. Curry, M. Faught, Y. Zhang, U. Wiesner, *J. Polym. Sci. Part B: Polym. Phys.* **2003**, *41*, 3346–3350; b) M. Kamperman, C. B. W. Garcia, P. Du, H. Ow, U. Weisner, *J. Am. Chem. Soc.* **2004**, *126*, 14708–14709; c) J. Wan, A. Alizadeh, S. T. Taylor, P. R. L. Malenfant, M. Manoharan, S. M. Loureiro, *Chem. Mater.* **2005**, *17*, 5613–5617; d) J. Wan, P. R. L. Malenfant, S. T. Taylor, S. M. Loureiro, M. Manoharan, *Mater. Sci. Eng. A* **2007**, *463*, 78–88; e) P. F. W. Simon, R. Ulrich, H. W. Spiess, U. Wiesner, *Chem. Mater.* **2001**, *13*, 3464–3486. f) M. Kamperman, P. Du, R. O. Scarlat, E. Herz, U. Werner-Zwanziger, R. Graf, J. W. Zwanziger, H. W. Spiess, U. Wiesner, *Macromol. Chem. Phys.* **2007**, *208*, 2096–2108; g) M. Kamperman, M. A. Fierke, C. B. W. Garcia, U. Wiesner, *Macromolecules* **2008**, *41*, 8745–8752.
- [17] a) Q. D. Nghiem, D. Kim, and D.–P. Kim, *Adv. Mater.* **2007**, *19*, 2351–2354; b) N. Q. Dat, N. C. Thanh, D.–P. Kim, *J. Polym. Sci. Part A* **2008**, *46*, 4594–4601; c) H.–C. Kim, S.–M. Park, W. D. Hinsberg, *Chem. Rev.* **2010**, *110*, 146–177; d) H. C. Kim, S.–M. Park, W. D. Hinsberg, *Chem. Rev.* **2010**, *110*, 146–177; e) S. K. T. Pillai, W. P. Kretschmer, C. Denner, G. Motz, M. Hund, A. Fery, M. Trebbin, S. Förster, R. Kempe, *Small* **2013**, *9*, 984–989.
- [18] a) The physics of block copolymers (Eds: I. W. Hamley), Oxford University Press, Inc. New York, **1998**; b) F. S. Bates, *Science* **1991**, *251*, 898–905.
- [19] a) F. S. Bates, G. H. Fredrickson, *Phys. Today* **1999**, *52*, 32–38; b) T. P. Lodge, *Macromol. Chem. Phys.* **2003**, *204*, 265–273.
- [20] a) G. Glatz, T. Schmalz, T. Kraus, F. Haarmann, G. Motz, R. Kempe, *Chem. Eur. J.* **2010**, *16*, 4231–4238.
- [21] M. Zaheer, G. Motz, R. Kempe, *J. Mater. Chem.* **2011**, *21*, 18825–18831.
- [22] a) R. J. White, R. Luque, V. L. Budarin, J. H. Clark, D. J. Macquarrie, *Chem. Soc. Rev.* **2009**, *38*, 481–494; b) J. Kärger, D. Freude, *Chem. Eng. Technol.* **2002**, *25*, 769–778.
- [23] a) M. Kamperman, A. Burns, R. Weissgraeber, N. van Vegten, S. C. Waren, S. M. Gruner, A. Balkler, U. Wiesner, *Nano. Lett.* **2009**, *9*, 2756–2762.

- [24] M. Zaheer, C. D. Keenan, J. Hermannsdörfer, E. Roessler, G. Motz, J. Senker, R. Kempe, *Chem. Mater.* **2012**, *24*, 3952–3963.

3. Overview of the Thesis

“There are many hypotheses in science which are wrong. That's perfectly all right; they're the apertures to finding out what's right. Science is a self-correcting process. To be accepted, new ideas must survive the most rigorous standards of evidence and scrutiny.”

---Hon. Prof. Carl Sagan.

This chapter describes the overview of following chapters 4-6. The chapter 4 is published in “Chemistry a European Journal” under the title of “Tailored Nano-Structuring of End-Group Functionalized HD-Polyethylene Synthesized via an Efficient Catalytic Version of *Ziegler's* “Aufbaureaktion””. The chapter 5 is published in “Small” under the title of “SiCN nanofibers with a diameter below 100 nm synthesized via concerted block copolymer formation, microphase separation, and crosslinking”. The chapter 6 will be published under the title of “Robustly Supported Porous Au Catalyst for the Selective Oxidation of Alkenes using Air/O₂ as an Oxidant”. In this chapter 3, all the following three chapters will be described by connecting one another by utilization of hydroxyl terminated polyethylene (PE-OH) synthesized via *Ziegler's* “Aufbaureaktion” in 1) the synthesis of porous polyethylene 2) the structuring of SiCN (Fibers, lamellae, and bicontinuous) 3) the synthesis of porous SiCN supported catalysts. The porous polyethylene template was synthesized via three step procedure: 1) synthesis of copolymerization 2) microphase separation 3) selective etching. As a first step towards the synthesis of porous polyethylene template, the copolymers of PE-OH and PL were synthesized (PEOPL) with various ratios using ring-opening polymerization (Figure 3.1). The linear polyethylene block was chosen due to high crystallinity, the presence of reactive hydroxyl end group and can be synthesized with high yield. Polylactide block was chosen due to the amorphous nature that provides good contrast to the crystalline PE-OH block and is compatible with most of the counter blocks.

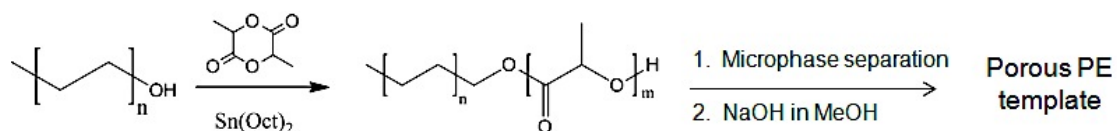


Figure 3.1. Schematic route from hydroxyl terminated polyethylene to porous SiCN.

The PEOPL was synthesized with different ratios (50:50, 70:30 and 90:10) by varying the PL block length. The ratio of the blocks and the covalent link between the blocks were confirmed by ¹H NMR. Also, the mass ratio of the blocks was elucidated by thermo gravimetric analysis (TGA), which confirmed the PEOPL with 50:50 and 70:30 with respect to PE:PL. Furthermore, molecular weight of the PE-OH and copolymers were characterized by high-temperature gel permeation chromatography (GPC). After the characterization, the copolymers were then self-assembled using microphase separation technique in the presence of a high boiling solvent. Bicontinuous morphology was obtained from 70:30 copolymer and lamellae morphology was with 50:50 copolymer. The self-assembled morphologies at green-body stage were mainly analysed by Atomic Force Microscopy (AFM). The Small Angle X-ray Scattering (SAXS) patterns were collected for the 50:50 samples to confirm the presence of alternative lamellae block with lattice size of 20 nm. The self-assembled morphologies were then nanostructured by etching out the PL block under mild basic (NaOH/CH₃OH/H₂O) condition. The progress of etching was monitored by Fourier transform infrared spectroscopy (FTIR). After the completion of etching, the resultant nanostructured polyethylene was analysed by scanning electron microscopy (SEM), which showed the polyethylene with bicontinuously structured porous surface. The resultant porous polyethylene was further analysed by N₂ physisorption measurements to confirm the surface area of 19 m²/g and pore size distribution of 30 nm. The synthesized porous polyethylene may potentially be used as template for the preparation of structurally inverted mesoporous SiCN ceramics. After etching the lamellae morphology of PEOPL, the resultant structure was analysed by SEM and characterized as a fiber/ribbon like polyethylene nanostructure. The same PE-OH was also utilized in the synthesis of SiCN materials such as nanofibers, lamellae, and bicontinuous SiCN. A commercially available preceramic polycarbosilazane (HTT1800) was used as a precursor for SiCN. This HTT1800, an inorganic block, can be cross-

linked in the presence of free radical initiators and tend to be in amorphous form after crosslinking. The inexpensive PE-OH was chosen as an organic *porogen* block due to high crystallinity and having reactive hydroxyl end group to link HTT1800 block. The synthesis of lamellae and fiber SiCN ceramics consists of two step process. The first step of synthesis involves a concerted

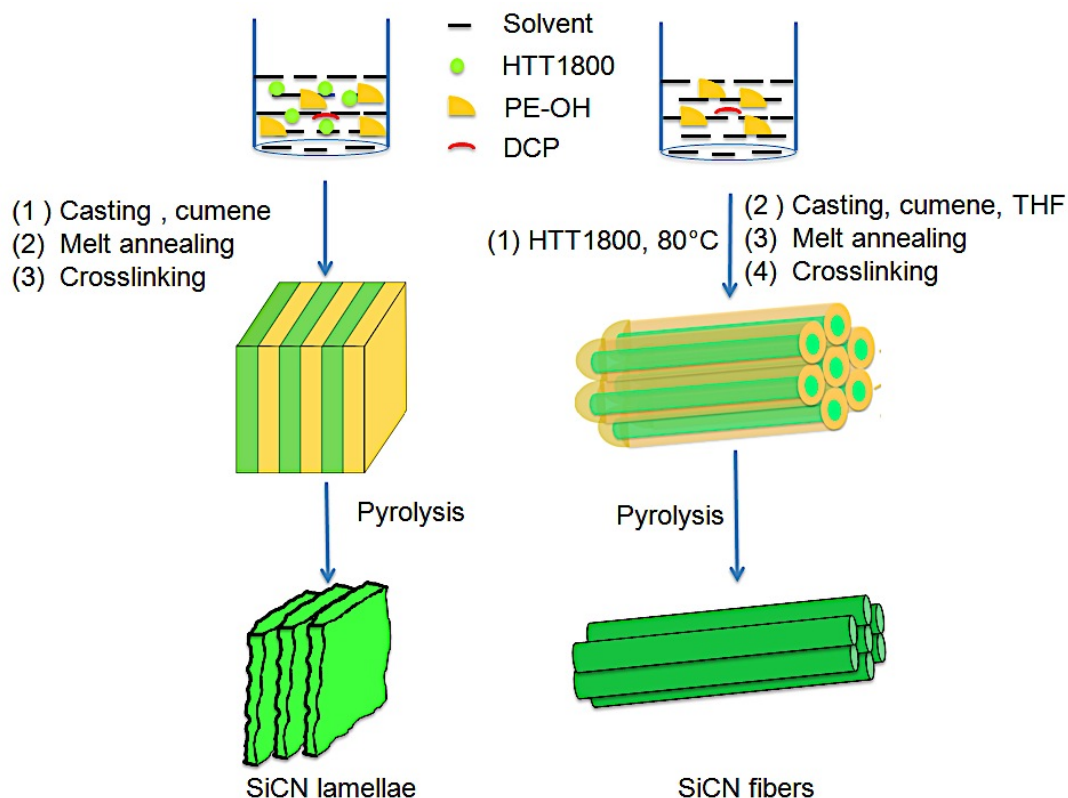


Figure 3.2. Schematic diagram of the synthetic route leading to nano-scaled SiCN lamellae and fibers.

formation of copolymer, microphase separation, and crosslinking. The second step was the pyrolysis of the hybrid material obtained from the concerted first step. The inorganic-organic copolymer (PEOHTT) was linked by the formation of covalent bond between PE-OH and HTT1800 blocks. Due to the rapid crosslinking nature of HTT1800 block, the covalent link of HTT1800 and PE-OH was evidenced by conducting a ^1H NMR study using model compounds. A linear alcohol, $\text{C}_{22}\text{H}_{44}\text{OH}$, and a silylamine, bis((dimethylsilyl)amine), were employed as a mimics to confirm the formation of covalent link between the PE-OH and HTT1800 blocks. The result of the ^1H NMR experiment showed the formation of Si-O-PE link with the evolution of ammonia. The covalently linked PEOHTT was synthesized using equal weight fractions (50:50) of inorganic and organic blocks. Following with microphase separation and

crosslinking, a non-meltable and hardened green-body was obtained. This green-body was then transferred into SiCN ceramics using high temperature pyrolysis programme under inert atmosphere. The PEOHTT was nanostructured into SiCN nanofibers and SiCN lamellae by varying the solvent (Figure 3.2). The lamellae morphology was obtained as a result of microphase separation in the presence of cumene. The lamellae morphology present in the green body stage was confirmed by AFM and TEM. This morphology was pyrolyzed under argon atmosphere for the ceramization and the resultant SiCN was analysed by SEM, which shows the layer like SiCN lamellae structure. The resultant lamellae SiCN was also analysed by FTIR and powder XRD. In the presence of THF and cumene, SiCN nano fibers were synthesized. The green body stage was measured by time dependant Quasi AFM to confirm the presence of core-shell rod like structure, which is consisting of amorphous HTT block as core and polyethylene block as shell. Upon irradiation of laser on the surface of the sample, the shell starts melting and reveals the core with rod like structure. The green-body was then pyrolyzed to get SiCN fiber ceramics and was analysed by SEM, ^{29}Si NMR, Powder XRD, and TEM. The variation in the ratio of inorganic and organic

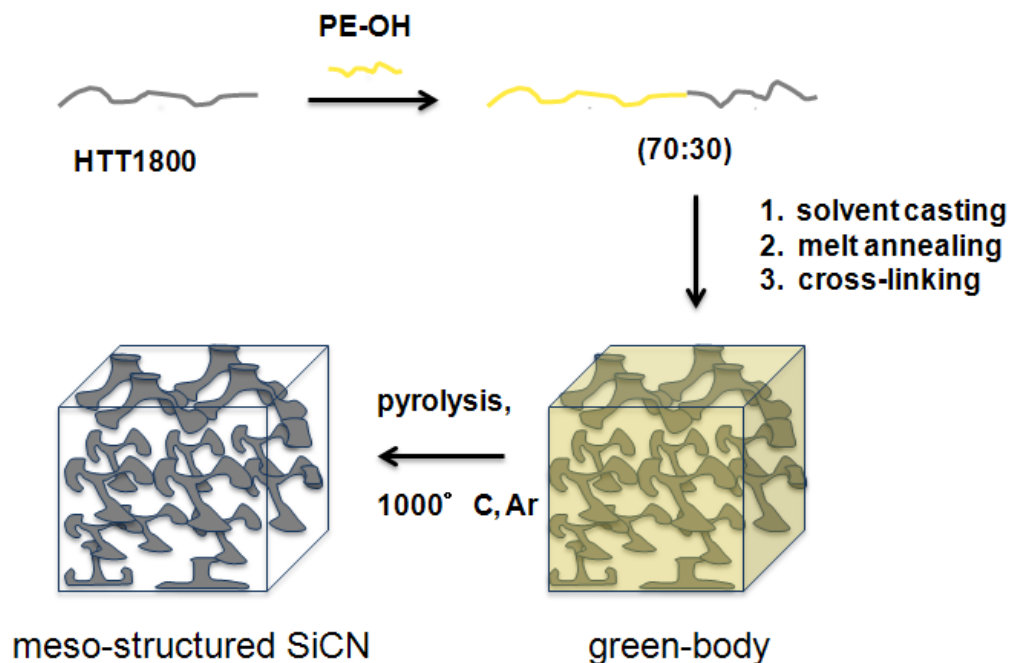


Figure 3.3. Schematic representation of ceramic precursor HTT1800 transferred into disordered bicontinuously porous SiCN via formation of copolymer with PE-OH.

block was also experimented with the addition of 70% of PEOH to 30 % of HTT1800 (Figure 3.3). The same experimental procedure for the synthesis of lamellae SiCN was conducted with a change in the solvent. The resultant self-assembled copolymer was analysed by AFM to see biconteneous structure in the green body stage. Upon pyrolyzing the green body results the mesoporous SiCN with high surface area of $460 \text{ m}^2/\text{g}$ with size of the pores in the range of mesoscale (2-50 nm). The biconteneous structure was analysed by both TEM and SEM. The N_2 adsorption measurements were conducted to calculate surface area and size of the pore size. Due to the high surface area, this biconteneously porous SiCN support was chosen for the synthesis of porous gold catalyst. The gold nanoparticles were introduced to mesoporous SiCN by adding aminopyridinato metal complexes to the mixture of PE-OH (70%) and HTT-1800 (30%). The added aminopyridinato metal complexes prefer to settle on the inorganic carbosilazane block due to the presence of N-H and Si-H functional group (Figure 3.4). These added metal complexes act as mediator for transmetallation reaction via molecular pathway to the HTT1800 block. Pyrolyzing the green-body leads to the porous SiCN supported gold and silver catalysts. Three possible transformations can be taken place during pyrolysis namely i) the formation of metal nanoparticles ii) Pore formation in the place of PE-OH block and iii) ceramization. Figure 3.5 depicts the porous SiCN having molecular network structure with nitrogen

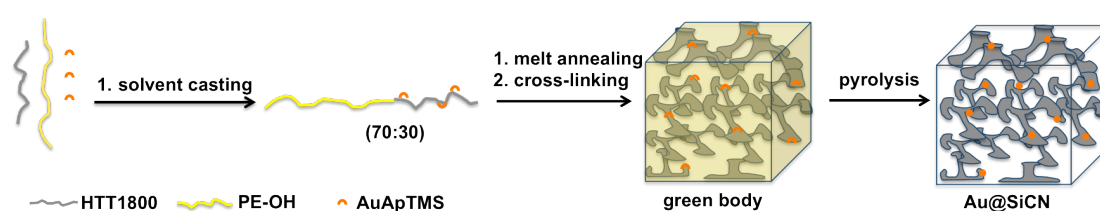


Figure 3.4. Schematic representation of catalyst preparation from ceramic precursor HTT1800, PE-OH, and metal precursor transferred into disordered biconteneously porous Au@SiCN.

function, which might be stabilizing gold nanoparticles. Furthermore, the molecular network of Si-C-N may stabilize the nanoparticles formed at the surface of carbosilazane block. The TEM was used to analyse the presence of nanoparticles as well as the nature of the porous SiCN support. The

porosity was analysed by N_2 adsorption and observed to have the pores in mesoscale range with high surface area. Moreover, solid state NMR experiment was conducted to substantiate the presence of SiCN environment in the sample. The liquid phase oxidation of higher alkenes was conducted with the synthesized Au@SiCN catalyst using air as an oxidant. The Au@SiCN catalyst was active towards oxidation of higher alkenes. In particular, cyclooctene was chosen to perform temperature dependant air oxidation. The inference of the result implies that the conversion increases as the temperature is increased.

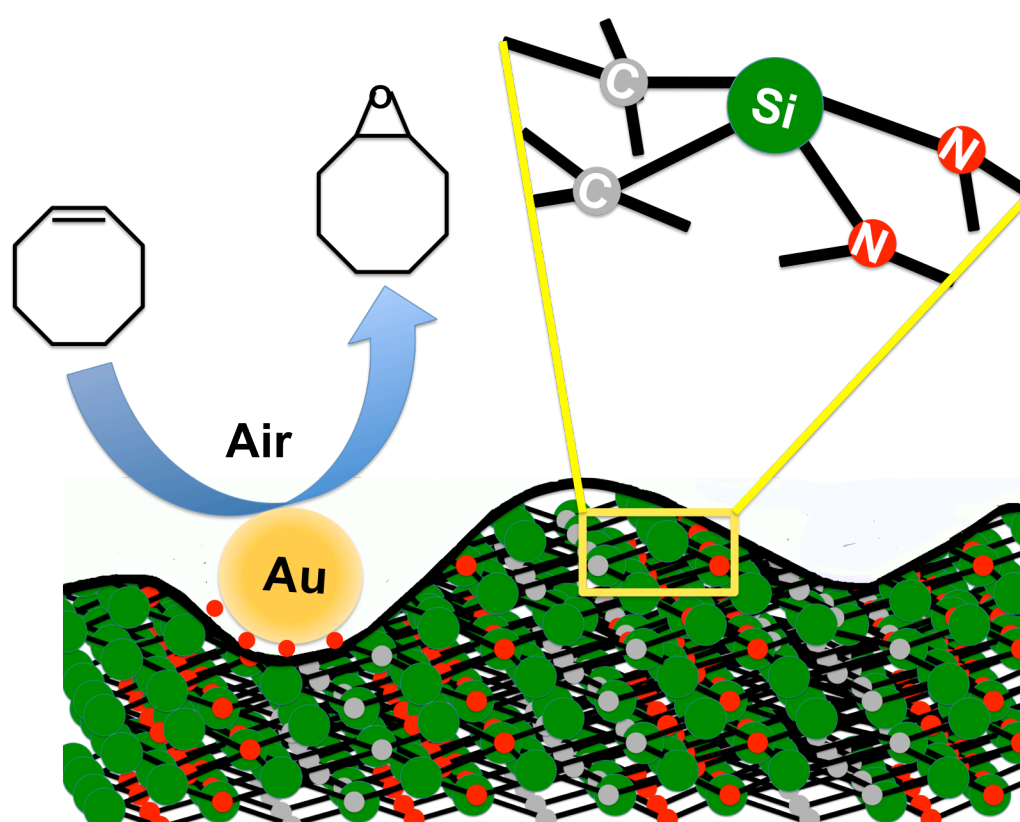


Figure 3.5. Schematic representation of porous SiCN supported gold nanoparticle stabilized by SiCN network structure at the surface.

3.1. Individual Contribution to Joint Publications

The results presented here were obtained in collaboration with co-workers and are published, submitted or to be submitted as indicated below. The individual contributions of all authors are specified. The corresponding author is denoted by an asterisk.

Chapter 4

This work is published in *Chem. Eur. J.*, with the title of

“Tailored Nano-Structuring of End-Group Functionalized HD-Polyethylene Synthesized via an Efficient Catalytic Version of Ziegler’s “Aufbaureaktion””

Saravana K. T. Pillai,^[a] Winfried P. Kretschmer,^[a] Martin Trebbin,^[b] Stephan Förster,^[b] and Rhett Kempe^{*,[a]}

The synthesis of PE-OH part was carried out by Dr. Winfried P. Kretschmer. Copolymerization and nanostructuring part was done by myself, SAXS measurements were carried out by Martin Trebbin and the interpretations were done by both Martin Trebbin and myself. AFM (trained by Markus Hund) and N₂ physisorption measurements were done by myself. The SEM of the samples were analysed by Dr. Christine Denner. DSC measurements were carried out with the help of Dr. Florian Wieberger and TGA with Sandra Ganzleben. All the above-mentioned work was conducted under the super vision of Prof. Dr. Rhett Kempe. Publication, scientific discussions, comments, correction of manuscripts, and preparation of supporting information are done collectively by myself, Dr. Winfried P. Kretschmer, Prof. Stephan Förster and Prof. Dr. Rhett Kempe.

Chapter 5

This work is published in *Small*, with the title of

“SiCN nanofibers with a diameter below 100 nm synthesized via concerted block copolymer formation, microphase separation, and crosslinking”

Saravana K. T. Pillai,^a Winfried P. Kretschmer,^b Christine Denner,^a Günter Motz,^b Markus Hund,^c Andreas Fery,^c Martin Trebbin,^b Stephan Förster,^b and Rhett Kempe^{*,a}

The synthesis of PE-OH part was carried out by Dr. Winfried P.

Kretschmer. SiCN nanofibers synthesis was done by myself. The SEM of the samples were analysed by Dr. Christine Denner. The TEM of the sample was measured by Justus Hermannsdörfer. SAXS pattern was measured by Martin Trebbin and the interpretations were performed by both Martin Trebbin and myself. AFM measurements were carried out by myself. QUASI *in situ* AFM study was conducted by Markus Hund and N₂ physisorption measurements were done by myself. ²⁹Si NMR measurements were conducted by Renee Siegel. DSC measurements were carried out by Dr. Florian Wieberger and TGA by Sandra Ganzleben. All the above-mentioned work were conducted under the super vision of Prof. Dr. Rhett Kempe. Publication, scientific discussions, comments, correction of manuscripts, and preparation of supporting information were done collectively by myself, Dr. Günter Motz and Prof. Dr. Rhett Kempe.

Chapter 6

The following work is “to be submitted”

“Robustly Supported Porous Au and Ag Catalysts for the Selective Oxidation of Alkenes Using air/O₂ as an Oxidant”

Saravana K.T. Pillai,^a Winfried P. Kretschmer,^a Torsten Irrgang,^a Martin Friedrich,^a Justus Hermannsdörfer,^a Günter Motz,^b and Rhett Kempe^{*,a}

The synthesis of PE-OH part was carried out by Dr. Winfried P. Kretschmer. The synthesis of porous SiCN and porous gold and silver catalysts are done by myself. Dr. Torsten Irrgang provided the suggestions on catalysis. Nitrogen physisorption measurements and calculations are done by myself. The TEM of catalysts were analysed by Martin Friedrich and porous SiCN was by Justus Hermannsdörfer. ²⁹Si NMR measurements were conducted by Dr. Yamini Avadhut. The SEM of the samples were analysed by Dr. Christine Denner. AFM measurements were conducted by myself. Powders XRD of the samples were measured with the help of Dr. Wolfgang Milius. All the above-mentioned work were conducted under the super vision of Prof. Dr. Rhett Kempe. Publication, scientific discussions, comments, correction of manuscripts, and preparation of supporting information are done collectively by myself, Dr. Günter Motz and Prof. Dr. Rhett Kempe.

4. Tailored Nano-Structuring of End-Group Functionalized HD-Polyethylene Synthesized via an Efficient Catalytic Version of Ziegler's "Aufbaureaktion"

Saravana K. T. Pillai,^[a] Winfried P. Kretschmer,^[a] Martin Trebbin,^[b] Stephan Förster,^[b] and Rhet Kempe*,^[a]

^[a]Lehrstuhl Anorganische Chemie II, Universität Bayreuth, Universität Bayreuth, 95440 Bayreuth, Germany, E-Mail : kempe@uni-bayreuth.de

^[b]Lehrstuhl Physikalische Chemie I, Universität Bayreuth, Universität Bayreuth, 95440 Bayreuth, Germany.

4.1. Abstract

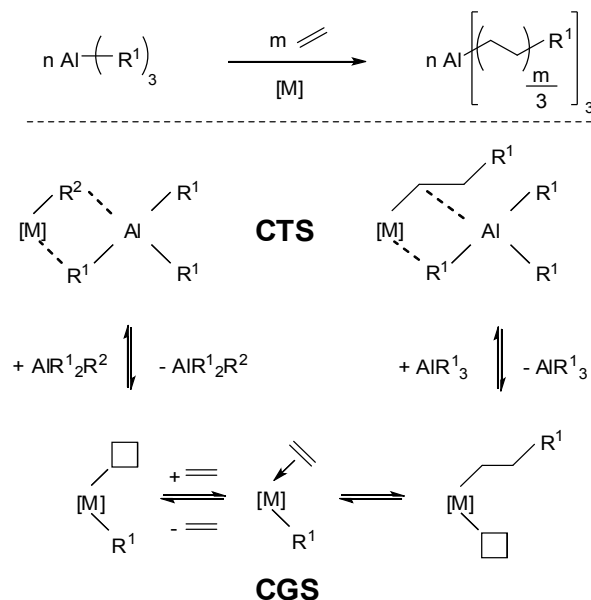
Monoguanidinato titanium complexes are efficient catalysts to make OH end-group-functionalized polyethylene (PE-OH) by a catalyzed version of Ziegler's "Aufbaureaktion". This PE-OH can be structured to mesoporous polyethylene or polyethylene nanofibers/ribbons through diblock copolymer synthesis, microphase separation, and etching of the sacrificial polylactide block.

4.2. Introduction, Results and Discussion

Polyethylene (PE) is the most widely used synthetic polymer and is essential for our modern life style because of its low cost and its broad applicability. Unfortunately, the compatibility with other important polymers or materials is limited. Compatibility agents, having a PE block and a block of that other polymer or a block that is compatible with the material, could solve this problem. Furthermore, PE-based block copolymers may allow to nanostructure PE via microphase separation and enable novel applications of this commodity. Both approaches rely on an efficient synthesis of PE having an end-group that allows the easy introduction of the second polymer block. A polymerization method which produces metal terminated PE that can easily be converted into PE carrying such reactive end-groups is coordinative chain transfer polymerization (CCTP).^{1, 2} Pioneering work was done by Eisenberg and Samsel³ as well as Mortreux and coworkers.⁴ Meanwhile, a few

4. Tailored Nano.Structuring of End-Group Functionalized HD-Polyethylene Synthesized via an Efficient Catalytic Version of Ziegler's "Aufbaureaktion"

ethylene/propylene CCTP catalyst systems using rare earth metals (RE) and transition metals in combination with different chain transfer agents (CTA), like Mg, Zn^{5,6,7} and Al alkyls,^{8,9} are known. Furthermore, enhancements of the CCTP concept like "chain shuttling" and "ternary CCTP"¹⁰ have been developed. A simplified mechanism of CCTP is shown in Scheme 1.



Scheme 4.1. Net reaction and mechanism of CCTP involving aluminum alkyls; top: CTS (chain transfer state); bottom: CGS (chain growing state); [M] = cationic or neutral transition metal or RE complex; R¹, R² = alkyl moiety; n, m = natural numbers.

The chain growing state (CGS) elongates the polymer chain and the chain transfer state (CTS) exchanges the polymer chain between the catalyst and the CTA - here aluminum alkyls. Bochmann and Lancaster reported that the exchange of alkyl chains between group 4 metal cations and Al occurs via bimetallic complexes (CTS).¹¹ Norton and co-workers described a detailed mechanistic picture of a zirconium complex catalyzed chain growth of Al alkyls.^{12,13} The kinetics of chain growth has been studied when catalyzed by [(EBI)Zr(μ-Me)₂AlMe₂][B(C₆F₅)₄] [EBI: ethylene bridged bis(indenyl), Me: methyl]. The reaction is first-order in [olefin] and [catalyst] and inverse first-order in [AlR₃].¹² These inverse first order dependence prohibits the use of high CTA/catalyst ratios. High amounts of CTA result in a poor overall polymerization activity. In consequence, most of the described CCTP catalyst systems work with CTA/catalyst ratios < 500 and become inactive with

significant higher CTA ratios. A possibility to solve this rather fundamental problem is the design of new catalyst systems that undergo fast chain growth in comparison to chain exchange and still suppress β -H elimination/transfer processes. In such a regime, multiple insertions may compensate efficiency loss caused by high CTA/catalyst ratios.¹⁴

Herein, we report on a novel titanium based catalyst system that is highly active in the presence of very high CTA/catalyst ratios and undergoes polyethylenyl chain transfer to triethylaluminum (TEA). No β -hydride elimination/transfer products were observed. This polymerisation process can be viewed as an efficient catalytic version of Ziegler's "Aufbaureaktion". Via oxidation with O₂ and subsequent hydrolytic workup the metallopolymers can be converted to PE-OH. The generated PE-OH was used to synthesize block copolymers having polylactide (PL) as a counter block. Microphase separation yielded different morphologies by varying the PL block length. Etching out of the sacrificial PL block gave rise to meso-porous polyethylene and polyethylene nano-ribbons. Nano-porous "PE" has been generated from hydrogenated 1,4-polybutadiene (hPB). Block copolymers from hPB and polystyrene made via anionic polymerization allow excellent structuring but need rather harsh and difficult to control etching techniques to remove the polystyrene block.¹⁵ Furthermore, polymeric bicontinuous microemulsion templates were generated using hPB and block copolymers carrying a hPB block.¹⁶ Unfortunately, the PE mimic hPB suffers from the unavoidable presence of branches. Ring opening metathesis polymerization of cyclooctene is discussed as an alternative and gave rise to pseudo PE blocks after hydrogenation. Tri-block copolymers carrying such a block were successfully converted into porous "PE".¹⁷ The fabrication of polyethylene nano-ribbons via the block copolymer approach has not been reported yet.^{18,19} A few examples exist in which end group functionalized PE was synthesized via CCTP and used to make block copolymers.²⁰

We recently developed RE based CCTP catalysts²¹ and varied the nature as well as the steric demand of the monoanionic ligand used to stabilize the organo RE cations. In addition, the size of the RE atom was

varied to find a catalyst system that tolerates high CTA/catalyst ratios.²² Unfortunately, these variations did not lead to CTA/catalyst ratios above 500.

Thus we shifted our attention to group 4 metals, especially towards titanium catalysts. Titanium catalysts stabilized by bulky aminopyridinato (Ap) ligands showed attractive polymerization activities but suffered from ligand transfer problems.²³ The Ap ligand is transferred to the CTA (aluminum alkyls) and an increased electron donor ability of the ligand rather increased ligand transfer rates than decreasing them.²⁴ Bulky guanidates²⁵ are chemically related to Ap ligands and were expected to alter ligand transfer rates significantly but may maintain high polymerization activity.

The reaction of amido titanium trichloride complexes²⁶ with N,N'-methanediyldenebis(2,6-diisopropylaniline) leads to the complexes **A**, **B** and **C** via methanediimine insertion into the titanium amide bonds (Figure 4.1). NMR data show a single signal set for the symmetrically substituted complexes **A** and **C**. Signal splitting was observed for complex **B** indicating a dynamic behaviour, presumably rotation around the C-N bond of the non-coordinated nitrogen atom. Variable temperature NMR studies indicate a coalescence temperature of 88 °C for the methine proton signal of the isopropyl groups and a rotation barrier of about 73 kJ/mol. X-ray crystal structure analysis of **A** and **B** reveal mono-guanidinate trichloro complexes and a distorted trigonal bipyramidal coordination of the titanium atoms. The variation of the substituents at the non-coordinated nitrogen atom alters the titanium coordination only slightly (Figure 4.1, bottom).

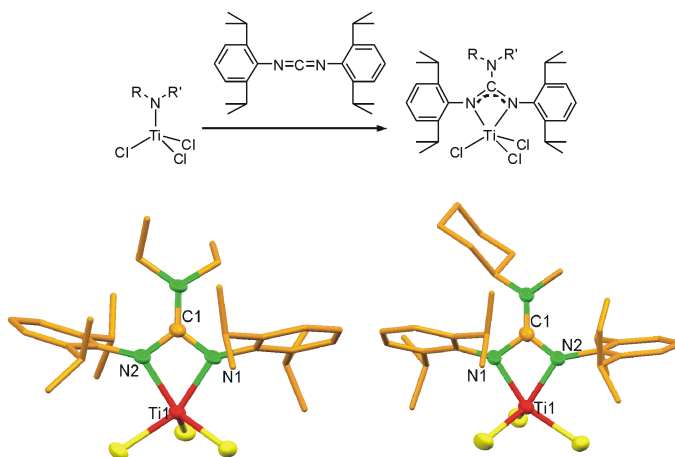


Figure 4.1. Polymerization pre-catalyst synthesis and structure. Top: Synthesis of the complexes **A** (R = R' = ethyl), **B** (R = cyclohexyl, R' = methyl) and **C** (R+R' = pentamethylene). Bottom: Molecular structure of **A** and **B** determined by X-ray single crystal structure analysis (atom colour code: carbon orange, chlorine yellow, nitrogen green and titanium red). Selected bond distances [Å] and angles [°] of **A** (bottom left): N1-Ti1 2.015(3), N2-Ti1 2.027(4), N1-C1-N2 106.0(3); and of **B** (bottom right): Ti1-N1 2.0081(14), Ti1-N2 2.0180(15), N1-C1 N2 106.40(14).

Ethylene polymerization studies using complex **A** as a pre-catalyst and different activation protocols reveal that **A** can be highly active²⁷ if activated with MAO (methyl alumoxanes), d-MAO (dry MAO, free trimethyl aluminum content of MAO was removed) and a combination of aluminium alkyls and perfluoroarylborates (Table 4.1).

Table 4.1. Initial polymerization studies using complex A. Conditions: 2 µmol of A, 2 bar ethylene pressure, 150 ml toluene, 15 min polymerization time, ammonium borate: [R₂N(CH₃)H]⁺[B(C₆F₅)₄]⁻ (R = C₁₆H₃₃ – C₁₈H₃₇), Ti/B = 1/1.1 (TMA = trimethyl aluminum, TiBA = triisobutyl aluminum).

Run	Activator	Temp. [°C]	m _{pol.} [g]	Activity [kgPE mol ⁻¹ h ⁻¹ bar ⁻¹]	Mn [g mol ⁻¹]	Mw/Mn
1	d-MAO ^a	30	3,64	3640	141000	5,9
2	d-MAO ^a	50	1,36	1360	52000	3,2
3	d-MAO ^a	80	1,22	1220	28000	2,7
4	MAO ^b	30	2,82	2820	16000	2,0
5	MAO ^b	50	1,67	1670	8400	2,5
6	MAO ^b	80	0.1	100	7700	4,0
7	TMA/B(C ₆ F ₅) ₄ ^c	50	0,7	700	3900	1,9
8	TEA/B(C ₆ F ₅) ₄ ^c	50	1,62	1620	2200	1,9

4. Tailored Nano.Structuring of End-Group Functionalized HD-Polyethylene Synthesized via an Efficient Catalytic Version of Ziegler's "Aufbaureaktion"

9	TiBA/B(C ₆ F ₅) ₄ ^c	50	1,1	1100	40000	2,0
10	TEA/B(C ₆ F ₅) ₄ ^d	50	1,8	1800	1800	1,9
11	TEA/B(C ₆ F ₅) ₄ ^{d,e}	50	3,7	930	2300	1,7
12	TEA/B(C ₆ F ₅) ₄ ^{d,f}	50	7,0	880	2300	1,7

a) Ti/Al = 1/650, b) Ti/Al = 1/500, c) Ti/Al = 1/500, d) Ti/Al = 1/1000, e) 60 min, f) 120 min

Investigations at different temperatures reveal that the catalyst is stable in the temperature window between 30 and 80 °C. Activation by MAO and d-MAO leads to significant differences of the molecular weight of the polymers indicating a polymeryl chain transfer catalysis to aluminium (Table 4.1, run 1-6). ¹H NMR investigations of the hydrolysed polymers obtained by MAO activation support this hypothesis since no olefinic end-groups were detected. Polymerization reactions using a borate activator and different aluminum alkyls (Table 4.1, run 7-9) indicate that TEA is a better transfer agent than trimethylaluminum (TMA). The polydispersities recorded for all runs listed in Table 4.1 are significantly larger than 1.2. This observation indicates that a classic CCTP mechanism with a very fast chain transfer in comparison to chain growing is not operating. The molecular weight of the polymers does not increase with increased polymerization time, Table 4.1, run 10 to 12. In a time regime from 15 to (60 to) 120 min a larger amount of polymer having essentially the same molecular weight is produced. The number of aluminum alkyl chains extended increases from 17 to (27 to) 50 %, respectively. Control over the molecular weight can be obtained via the catalyst, the temperature and the CTA to catalyst ratio (Table 4.2). The molecular weight of the polymers decreases with CTA/catalyst ratio increasing from 500 to 1000 (Table 4.2).

Table 4.2. Ethylene polymerization studies using complexes **B** and **C**, activation with TEA and ammonium borate. Conditions: pre-catalyst: 2.0 μmol; ammonium borate: 2.2 μmol [R₂N(CH₃)H]⁺[B(C₆F₅)₄]⁻ (R = C₁₆H₃₃ – C₁₈H₃₇), Ti/B = 1/1.1; CTA = TEA; toluene: 150 mL; T = 50 °C, p = 2 bar; t = 15 min.

Run	Pre-cat.	Al/Ti	m _{Pol.}	Activity	M _n	M _w /M _n
-----	----------	-------	-------------------	----------	----------------	--------------------------------

4. Tailored Nano.Structuring of End-Group Functionalized HD-Polyethylene Synthesized via an Efficient Catalytic Version of Ziegler's "Aufbaureaktion"

			[g]	$[\text{kg}_{\text{PE}}\text{mol}_{\text{cat}}^{-1}\text{h}^{-1}\text{bar}^{-1}]$	$[\text{gmol}^{-1}]$	
1	B	500	1.70	1700	2800	2.2
2	B	750	1.75	1750	2100	2.0
3	B	1000	1.80	1800	1600	2.0
4	C	500	1.40	1400	3100	2.4
5	C	750	1.40	1400	2700	2.4
6	C	1000	1.55	1550	2500	2.3

Furthermore, different catalysts have different insertion rates leading to different molecular weights of the polymers at the same CTA/catalyst ratio (Table 4.2). Polymerization runs with very high CTA/catalyst ratios were performed and subsequently oxidized using air as an oxidant to produce PE-OH (Table 4.3).

Table 4.3. Ethylene polymerization studies using complex A, activation with TEA and ammonium borate and subsequent oxidation by air. Conditions: ammonium borate: $[\text{R}_2\text{N}(\text{CH}_3)\text{H}]^+[\text{B}(\text{C}_6\text{F}_5)_4]^-$ ($\text{R} = \text{C}_{16}\text{H}_{33} - \text{C}_{18}\text{H}_{37}$), Ti/B = 1/1.1; CTA = TEA; toluene: 150 mL; $p = 5$ bar; $t = 60$ min.

Run	A [μmol]	Al/Ti	T [$^{\circ}\text{C}$]	$m_{\text{Pol.}}$ [g]	Activity $[\text{kg}_{\text{PE}}\text{mol}_{\text{cat}}^{-1}\text{h}^{-1}\text{bar}^{-1}]$	M_n [gmol^{-1}]	M_w/M_n
1	4 ^a	2500	70	44.0	5500	1700	1.8
2	2	5000	70	47.0	4700	2100	1.9
3	0.6	17000	65	28.4	9470	2500	1.8
4	0.4	25000	60	32.0	16000	3300	1.9
5	0.3	33000	65	24.4	16300	2500	1.9
6	0.2	50000	60	16.7	16700	2900	1.9

a) 2 bar

The ^1H NMR spectra of the polymer obtained from run 2, Table 4.2 is shown in Figure 2. Important regions are expanded (insets). Remarkably, the catalyst based on **A** shows activities of around $16.000 \text{ kg}_{\text{PE}}\text{mol}_{\text{cat}}^{-1}\text{h}^{-1}\text{bar}^{-1}$ in the presence of 25.000, 33.000 or 50.000 equivalent of TEA. The catalyst performance decreases slightly during the last 45 min of the one hour polymerisation experiments indicating a good stability of the catalyst

4. Tailored Nano.Structuring of End-Group Functionalized HD-Polyethylene Synthesized via an Efficient Catalytic Version of Ziegler's "Aufbaureaktion"

system at 60 to 70 °C. Oxidation of the aluminum terminated PE leads to PE-OH (after hydrolytic workup). The PE-OH produced in run 4, Table 3 was used for diblock copolymer synthesis. It contains 80% hydroxyl group functionalized PE as determined by NMR spectroscopy. PL was chosen as sacrificial counter block because it can predominately adopt an amorphous form which is in good contrast to the crystalline nature of linear PE.²⁸ Moreover, PL can be etched out under mild basic conditions without disrupting the PE structure of the microphase separated diblock copolymer. Tin(II) 2-ethylhexanoate [Sn(Oct)₂] was used as a catalyst to polymerize a PL block onto PE-OH. Different amounts of *rac*-lactide gave rise to PE-O-PL diblock copolymers having different PL block lengths [PEOPL(1) and (2)]. The diblock copolymers were characterized by high temperature GPC, NMR, TGA, DSC and IR.

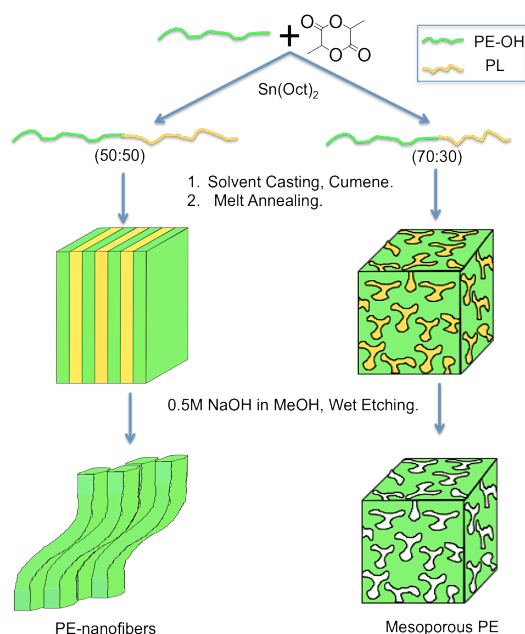


Figure 4.2. Schematic representation of the synthesis of meso-porous polyethylene and polyethylene nano-ribbons.

Different morphologies of PEOPL(1) and (2) via microphase separation were accomplished in cumene (Figure 4.3). The diblock copolymers were dissolved in cumene at 152 °C followed by slow solvent casting at 140 °C oil bath temperature.

Table 4.4. Summary of the characterization data of the diblock copolymers.

4. Tailored Nano.Structuring of End-Group Functionalized HD-Polyethylene Synthesized via an Efficient Catalytic Version of Ziegler's "Aufbaureaktion"

SampleID	M_n^1 g/mol	Mw/ M_n^1	MW^2 g/mol	f_{PL}^3	T_m^4 °C	T_c^4 °C	ΔH_m^4 J/g	X_E^5 %
PE-OH	3300	1.9			130.0	115.0	252.2	91
PEOPL(1)	4500	1.7	5500	0.44	126.6	113.1	104.3	37
PEOPL(2)	4000	1.6	4400	0.38	127.2	114.0	128.1	46

1) M_n and polydispersity as determined by high temperature gel permeation chromatography (HT GPC). 2) Molecular weight of the diblock copolymer as calculated by 1H NMR spectroscopy using relative intensities of repeating unit signals and end-group signals, and M_n of PE as determined by HT GPC. 3) Weight fraction of PL in the diblock copolymer calculated using NMR spectroscopy and the densities at 25 °C reported for the respective components [PL = 1.25;²⁹ LPE = 0.95 (at 60% crystallinity)³⁰.4) Taken as the peak of the melting endotherm (or the crystallization exotherm) during the heat (or cool) in DSC. 5) Percentage of crystallinity of the diblock copolymers calculated³¹ from $[\Delta H_m/(\Delta H_m^0)] \times 100\%$ with $\Delta H_m^0 = 277 \text{ J g}^{-1}$.

The material was subsequently annealed at this temperature for six hours. Annealing of the melt seems to ensure good segregation of the equilibrated nanostructures. The microphase separated diblock copolymers were investigated by synchrotron Small Angle X-ray Scattering (SAXS) (Figure 4.4) and Atomic Force Microscopy (AFM). AFM, recorded at ambient condition in non-destructive tapping mode, is indicative of a rather well ordered lamellar type of structuring for PEOPL(1) (Figure 4.5a and b) and a less ordered bicontinuous morphology for PEOPL(2) (Figure 4.6a).

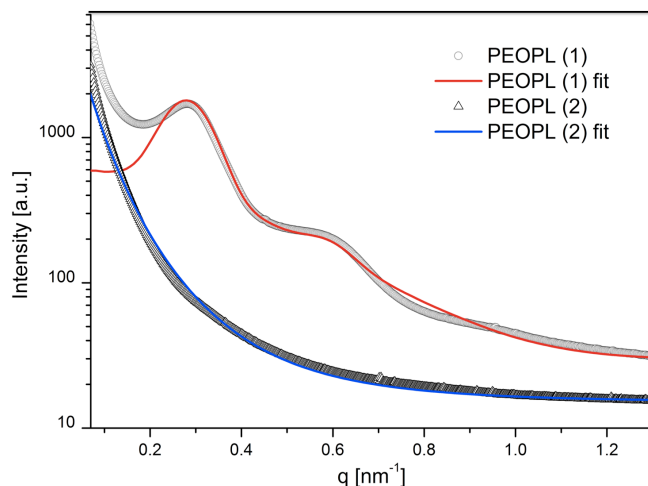


Figure 4.3. Radially averaged synchrotron SAXS patterns for PEOPL(1) and PEOPL(2) indicating a lamellar-type and a disordered bicontinuous morphology, respectively. Colour code: grey measured, red and blue simulated.

Synchrotron SAXS studies are in agreement with these observations (Figure 4.4). The SAXS pattern of PEOPL(1) with three peaks at $q = 0.29$, 0.58 and 0.85 nm^{-1} correspond to the ratio of 1:2:3 which indicates a lamellar structure (Figure 4.4). Calculations using the software Scatter confirm this alternating lamellar lattice with periodic domain spacing (d-spacing) of 20 nm .³² Furthermore, the first order peak at 0.28 nm^{-1} was used to confirm the d-spacing of 22 nm . Observation of such large domain spacing for these lower molecular weight copolymers is due to the polydispersity of PE block and the presence of 20% of the homopolymer in the sample.³³ The SAXS pattern of PEOPL(2) does not show pronounced peaks which would indicate a defined lattice. The fit shown in Figure 4 is based just on a simple sphere particle model.

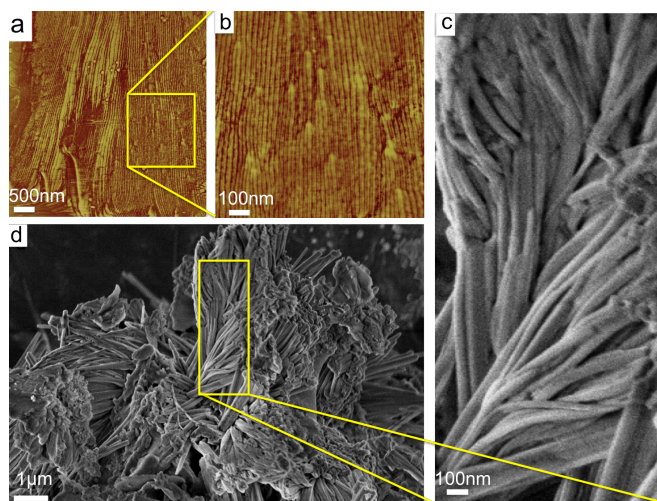


Figure 4.4. Microphase separated PEOPL(1). AFM phase images show a lamella-type morphology (a, b). SEM images of PE nano-ribbons after etching. (c, d)

The microphase separated diblock copolymers were submerged in a NaOH/water/methanol mixture to remove the PL block (Figure 4.3). The completion of the etching process was confirmed by FTIR spectroscopy. Removing the PL block of microphase separated PEOPL(1) afforded a PE material that might be best described as PE nano-fibres as indicated by SEM (Figure 4.5c and d). Microphase separation of PEOPL(2) results disordered bicontinuous morphology. The resultant morphology was mainly driven by both copolymer PEOPL(2) and homopolymer PE present in the sample. Upon etching the lactide block, the PEOPL(2) give rise to a porous PE material with a mean pore size diameter of 30 nm as determined via nitrogen adsorption-desorption studies ((Barrett-Joyner-Helenda method, Figure 4.6). The pore size is in an acceptable agreement with the domain size of microphase separated PEOPL(2) observed by AFM (Figure 4.6a). A surface area of 19 m²/g was calculated for the porous PE using the Brunauer-Emmett-Teller (BET) method. The pores in the range of 10-50 nm contribute mainly to that specific surface. SEM studies (Figure 4.6c and d) support the porous nature of the PE material and the structuring indicated by AFM studies (Figure 4.6a).

4. Tailored Nano.Structuring of End-Group Functionalized HD-Polyethylene Synthesized via an Efficient Catalytic Version of Ziegler's "Aufbaureaktion"

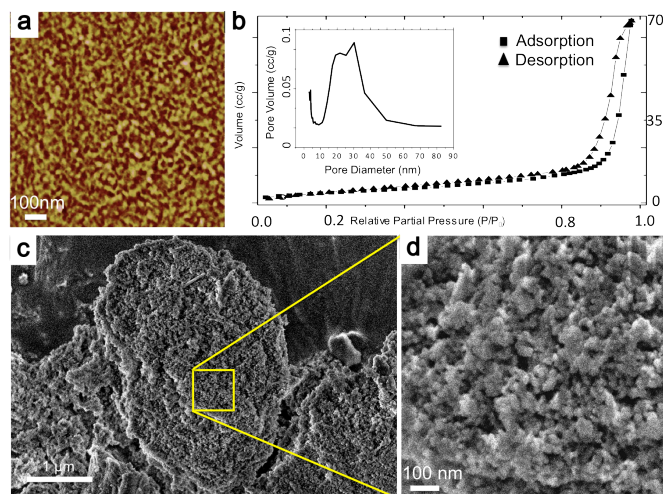


Figure 4.5. Microphase separated PEOP(2). AFM image. Phase image shows the disordered bicontinuous morphology (a). Nitrogen adsorption/desorption studies and inset of the resulting pore size distribution (b). SEM images of porous PE after etching (c, d).

4.3. Conclusion

Two main conclusions can be drawn from this study.

1. Monoguanidinato titanium complexes are efficient catalysts to make OH-endgroup functionalized polyethylene (PE-OH) via a catalyzed version of Ziegler's "Aufbaureaktion".
2. PE-OH can be structured to meso-porous polyethylene and polyethylene nano-ribbons via diblock copolymer synthesis, microphase separation and etching of the sacrificial polylactide block.

4.4. Acknowledgements

This work was supported by the DFG, SFB 840 and Sasol Germany GmbH. We thank Dr. Christine Denner for SEM investigation and Markus Hund for support in the AFM lab.

4.5. References

- [1] R. Kempe, *Chem. Eur. J.* **2007**, *13*, 2764–2773.
- [2] L. R. Sita, *Angew. Chem. Int. Ed.* **2009**, *48*, 2464–2508; *Angew. Chem. Int. Ed.* **2009**, *48*, 2464–2472.
- [3] a) E. G. Samsel, Ethyl Corporation, EP 0539876, **1992**; b) E.G. Samsel, D. C. Eisenberg, Ethyl Corporation, EP 0574854, **1993**.

- [4] a) J.-F. Pelletier, A. Mortreux, X. Olonde, K. Bujadoux, *Angew. Chem. Int. Ed. Engl.* **1996**, *108*, 1980–1982; *Angew. Chem. Int. Ed.* **1996**, *35*, 1854–1856; d) J.-F. Pelletier, K. Bujadoux, X. Olonde, E. Adisson, A. Mortreux, T. Chenal, US 5779942, **1998**; e) T. Chenal, X. Olonde, J.-F. Pelletier, K. Bujadoux, A. Mortreux, *Polymer* **2007**, *48*, 1844–1856.
- [5] a) G. J. P. Britovsek, S. A. Cohen, V. C. Gibson, P. J. Maddox, M. van Meurs, *Angew. Chem.* **2002**, *114*, 507–509; *Angew. Chem. Int. Ed.* **2002**, *41*, 489–491; b) G. J. P. Britovsek, S. A. Cohen, V. C. Gibson, M. van Meurs, *J. Am. Chem. Soc.* **2004**, *126*, 10701–10712; c) M. van Meurs, G. J. P. Britovsek, V. C. Gibson, S. A. Cohen, *J. Am. Chem. Soc.* **2005**, *127*, 9913–9923; d) H. Kaneyoshi, Y. Inoue, K. Matyjaszewski, *Macromolecules* **2005**, *38*, 5425–5435; e) J. O. Ring, R. Thomann, R. Mülhaupt, J.-M. Raquez, P. Degee, P. Dubois, *Macromol. Chem. Phys.* **2007**, *208*, 896–902.
- [6] a) W. Zhang, L. R. Sita, *J. Am. Chem. Soc.* **2008**, *130*, 442–443; b) W. Zhang, J. Wei, L. R. Sita, *Macromolecules* **2008**, *41*, 7829–7833. c) J. Wei, W. Zhang, R. Wickham, L. R. Sita, *Angew. Chem. Int. Ed.* **2010**, *49*, 9140–9144; d) C. Giller, G. Gururajan, L. Wie, W. Zhang, W. Hwang, D. B. Chase, J. F. Rabolt, L. R. Sita, *Macromolecules* **2011**, *44*, 471–482.
- [7] a) D. J. Arriola, E. M. Carnahan, P. D. Hustad, R. L. Kuhlman, T. T. Wenzel, *Science* **2006**, *312*, 714–719; b) P. D. Hustad, R. L. Kuhlman, D. J. Arriola, E. M. Carnahan, T. T. Wenzel, *Macromolecules* **2007**, *40*, 7061–7064; c) P. D. Hustad, R. L. Kuhlman, E. M. Carnahan, T. T. Wenzel, D. J. Arriola, *Macromolecules* **2008**, *41*, 4081–4089; d) R. L. Kuhlman, T. T. Wenzel, *Macromolecules* **2008**, *41*, 4090–4094; e) A. Hotta, E. Cochran, J. Ruokolainen, V. Khanna, G. H. Fredrickson, E. J. Kramer, Y.-W. Shin, F. Shimizu, A. E. Cherian, P. D. Hustad, J. M. Rose, G. W. Coates, *Proc. Natl. Acad. Sci. USA* **2006**, *103*, 15327–15332; f) T. T. Wenzel, D. J. Arriola, E. M. Carnahan, P. D. Hustad, R. L. Kuhlman, *Topics in Organometallic Chemistry*, Vol. 26 (Ed.: Z. Guan), Springer, Berlin, Heidelberg, **2009**, pp. 65–104; g) S. Li, R. A. Register, B. G. Landes, P. D. Hustad, J. D. Weinhold, *Macromolecules*

- 2010**, *43*, 4761–4770; h) P. D. Hustad, G. R. Marchand, E. I. Garcia-Meitin, P. L. Roberts, J. D. Weinhold, *Macromolecules* **2009**, *42*, 3788–3794; i) F. Deplace, Z. Wang, N. A. Lynd, A. Hotta, J. M. Rose, P. D. Hustad, J. Tian, H. Ohtaki, G. W. Coates, F. Shimizu, K. Hirokane, F. Yamada, Y.-W. Shin, L. Rong, J. Zhu, S. Toki, B. S. Hsiao, G. H. Fredrickson, E. J. Kramer, *J. Polym. Sci. B: Polym. Phys.* **2010**, *48*, 1428–1437.
- [8] W. P. Kretschmer, A. Meetsma, B. Hessen, T. Schmalz, S. Qayyum, R. Kempe, *Chem. Eur. J.* **2006**, *12*, 8969–8978.
- [9] a) J. S. Rogers, G. C. Bazan, *Chem. Commun.* **2000**, 1209–1210; b) G. C. Bazan, J. S. Rogers, C. C. Fang, *Organometallics* **2001**, *20*, 2059–2064; c) C. J. Han, M. S. Lee, D.-J. Byun, S. Y. Kim, *Macromolecules* **2002**, *35*, 8923–8925; d) G. Mani, F. P. Gabbai, *Angew. Chem. Int. Ed.* **2004**, *43*, 2263–2316; *Angew. Chem. Int. Ed.* **2004**, *43*, 2263–2266; e) G. Mani, F. P. Gabbai, *J. Organomet. Chem.* **2005**, *690*, 5145–5149; f) C. Döring, W. P. Kretschmer, R. Kempe, *Eur. J. Inorg. Chem.* **2010**, *18*, 2853–2860; g) W. P. Kretschmer, T. Bauer, B. Hessen, R. Kempe, *Dalton Trans.* **2010**, *39*, 6847–6852.
- [10] J. Wei, W. Zhang, L. R. Sita, *Angew. Chem. Int. Ed.* **2010**, *122*, 1812–1816; *Angew. Chem. Int. Ed.* **2010**, *49*, 1768–1772.
- [11] a) M. Bochmann, S. J. J. Lancaster, *J. Organomet. Chem.* **1995**, *497*, 55–59; b) M. Bochmann, S. J. Lancaster, *Angew. Chem.* **1994**, *106*, 1715–1718; *Angew. Chem. Int. Ed. Engl.* **1994**, *33*, 1634–1647.
- [12] R. A. Petros, J. R. Norton, *Organometallics* **2004**, *23*, 5105–5107.
- [13] J. M. Camara, R. A. Petros, J. R. Norton, *J. Am. Chem. Soc.* **2011**, *133*, 5263–5273.
- [14] a) I. Haas, W. P. Kretschmer, R. Kempe, *Organometallics* **2011**, *30*, 4854–4867; b) K. Michiue, R. F. Jordan, *Organometallics* **2004**, *23*, 460–470; c) S. Murtuza, O. L. Casagrande Jr., R. F. Jordan, *Organometallics* **2002**, *21*, 1882–1890.
- [15] a) H. Uehara, T. Yoshida, M. Kakiage, T. Yamanobe, T. Komoto, K. Nomura, K. Nakajima, M. Matsuda, *Macromolecules* **2006**, *39*, 3971–3974; b) H. Uehara, M. Kakiage, D. Sakuma, T. Yamanobe, N. Takano, A. Barraud, E. Meurville, P. Ryser, *ACS Nano* **2009**, *3*, 924–932.

- [16] B. H. Jones, T. P. Lodge, *J. Am. Chem. Soc.* **2009**, *131*, 1676–1677.
- [17] L. M. Pitet, M. A. Amendt, M. A. Hillmyer, *J. Am. Chem. Soc.* **2010**, *132*, 8230–8231.
- [18] F. Cesano, E. Groppo, F. Bonino, A. Damin, C. Lamberti, S. Bordiga, A. Zecchina, *Adv. Mat.* **2006**, *18*, 3111–3114.
- [19] S. Shen, A. Henry, J. Tong, R. Zheng, G. Chen, *Nature Nanotechnology*, **2010**, *5*, 251–255.
- [20] a) H. Kaneyoshi, K. Matyjaszewski, *J. App. Polym. Sci.* **2007**, *105*, 3–13; b) W. Wang, R. Liu, Z. Li, C. Meng, Q. Wu, F. Zhu, *Macromol. Chem. Phys.* **2010**, *211*, 1452–1459.
- [21] For a review please see: R. Kempe, *Z. Anorg. Allg. Chem.* **2010**, *636*, 2135–2147.
- [22] C. Doering, R. Kempe, *Eur. J. Inorg. Chem.* **2009**, *3*, 412–418.
- [23] A. Noor, W. P. Kretschmer, G. Glatz, R. Kempe, *Inorg. Chem.* **2011**, *50*, 4598–4606.
- [24] M. Hafeez, W. P. Kretschmer, R. Kempe, *Eur. J. Inorg. Chem.* **2011**, *36*, 5512–5522.
- [25] C. Jones, *Coord. Chem. Rev.* **2010**, *254*, 1273–1289.
- [26] E. Benzing, W. Kornicker, *Chem. Ber.* **1961**, *94*, 2263–2267.
- [27] Highly active as defined in: G. J. P. Britovsek, V. C. Gibson, D. F. Wass, *Angew. Chem. Int. Ed.* **1999**, *38*, 428–447.
- [28] Y. Wang, M. A. Hillmyer, *J. Polym. Sci part A: Polym. Chem.* **2001**, *39*, 2755–2766.
- [29] D. R. Witzke, J. J. Kolstad, R. Narayan, *Macromolecules* **1997**, *30*, 7075–7085.
- [30] Handbook of Polyethylene, Peacock, A. J. Marcel Dekker, Basel, Switzerland, **2000**.
- [31] R. Wu, T. F. Al-Azemi, K. S. Bisht, *Chem. Commun.* **2009**, 1822–1824.
- [32] S. Förster, L. Apostol, W. Bras, *J. Appl. Cryst.* **2010**, *43*, 639–646.
- [33] a) S. C. Schmidt, M. A. Hillmyer, *J. Poly. Sci. B: poly. Phys.* **2002**, *40*, 2364–2376; b) M. W. Matsen, *Eur. Phys. J.* **2007**, *E 21*, 199–207; c) N. A. Lynd, M. A. Hillmyer, *Macromolecules* **2005**, *38*, 21, 8803–8810.

4.6. Experimental Section (Supporting Information)

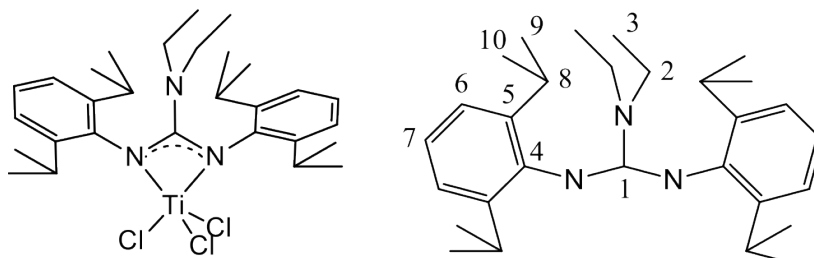
All manipulations, beside microphase separation and etching, were performed with rigorous exclusion of oxygen and moisture in Schlenk type glassware on a dual manifold Schlenk line or in an argon filled glove box (Braun 120-G) with a high-capacity recirculator (<0.1 ppm O₂). Non-halogenated solvents were dried by distillation from sodium wire/benzophenone. N,N-dimethylanilinium tetrakis(pentafluorophenyl)borate ([PhNMe₂H][B(C₆F₅)₄], **abcr GmbH & Co. KG**), N,N,N-trialkylammonium tetrakis(pentafluorophenyl)borate ([R₂NMeH][B(C₆F₅)₄], R = C₁₆H₃₃ – C₁₈H₃₇, 6.2 wt-% B(C₆F₅)₄ in Isopar, DOW Chemicals), trimethyl aluminum (TMA, 2.0 M in toluene, Aldrich), triethyl aluminum (TEA, 25 wt-% in toluene, Aldrich), tri-*iso*-butyl aluminum (TIBA, 25 wt-% in toluene, Aldrich), tri-*n*-octylaluminum (TOA, 25 wt-% in toluene, Aldrich), EURECEN Al 5100-10-toluene (4.9 wt-% in Al, Chemtura Organometallics), bis(2,6-diisopropylphenyl)carbodiimide (TCI Europe) were used as received. The titanium precursors [R'R''NTiCl₃] (R'/R'' = C₂H₅/C₂H₅ or CH₃/C₆H₁₁ or -(CH₂)₅- were synthesized as reported in the literature.^{S1} Cumene was purchased from Aldrich and used as received. D,L-lactide (99%) was purchased from Aldrich and recrystallized from ethyl acetate and dried at 40° C for 24 hrs prior to use. Tin (II) 2-ethylhexanoate [Sn(Oct)₂] from Aldrich was distilled and stored in the glove-box. Deuterated solvents were obtained from Cambridge Isotope Laboratories and were degassed, dried, and distilled prior to use. NMR spectra were recorded with a Varian ARX at 400 MHz or Varian ARX 300 MHz and chemical shifts are reported in ppm relative to the deuterated solvent. Elemental analyses (CHN) were carried out using a Vario EL III instrument. Due to TiC formation, the C value obtained by our analyzer is in average 1% lower in carbon if titanium amides are analyzed. d-MAO was prepared by removal of volatiles from MAO (4.9 wt. % in Al,). The polymer samples for NMR spectroscopic measurements were prepared by dissolving 15 mg of the polymer in 0.5 mL C₂D₂Cl₄ at 100 °C for 3 h before measuring. Gel permeation chromatography (GPC) analysis was carried out on a PL-GPC 220 (Agilent, Polymer Laboratories) high temperature chromatographic unit equipped with a DP and RI detectors and two linear mixed bed columns (Olexis, 13-micron particle size) at 150 °C using 1,2,4-trichlorobenzene as the mobile phase. The samples were prepared by dissolving the polymer (0.05 wt.-%, conc. = 1

mg/mL) in the mobile phase solvent in an external oven and were run without filtration. The molecular weight was referenced to polyethylene ($M_w = 520 - 3200000 \text{ g mol}^{-1}$) and polystyrene ($M_w = 580-2800000 \text{ g mol}^{-1}$) standards. The reported values are the average of at least two independent determinations. X-ray crystal structure analysis was carried out at a STOE IPDS II diffractometer equipped with an Oxford Cryostream low temperature unit. Structure solution and refinement were accomplished using SIR97,^{S2} SHELXL-97^{S3} and WinGX.^{S4} The degradation temperature was determined using thermo gravimetric analysis (TGA) with a TGA/SDTA851e (Mettler Toledo) using a heating rate of 10 K/min under nitrogen flow. Differential scanning calorimetric (DSC) measurements were obtained using a DSC/SDTA 821 calorimeter from MettlerToledo Instruments that was calibrated with an indium standard. Samples were loaded into hermetically sealed aluminum pans prior to analysis. The thermal history of the samples was erased by heating the samples to 250 °C and isothermally annealing for 5 min. The samples were characterized using atomic force microscopy (AFM) under ambient conditions. The images were taken with a commercial AFM (Dimension™ 3100 equipped with a NanoScope® IV and a XY closed-loop scanner (Veeco Instruments Inc., USA). The Data were acquired by scanning areas of 1 $\mu\text{m} \times 1 \mu\text{m}$ with 512 x 512 pixels in TappingMode™ with cantilevers which have a typical spring constant of 42 N/m and a typical resonance frequency of 300kHz (OMCL-AC160TS, Olympus, Japan). The topographic and phase images were flattened and the surface roughness (R_g) was calculated using the NanoScope® Analysis software version XY, Bruker Corporation, USA). Modelling material or fast-drying conductive silver (G3692, Plano GmbH, Germany) was used for sample fixation. Infrared spectra of the materials were recorded using Bruker Vektor 22FT-IR spectrometer. The synchrotron Small Angle X-Ray Scattering (SAXS) measurements were performed at the beamline BW4 at DORIS III (HASYLAB/DESY). The SAXS data was collected using a MarCCD detector with a sample to detector distance of 2.575 m and a wavelength of 0.138 nm. The Scanning Electron Microscopy (SEM) imaging were recorded on a Zeiss LEO 1530 (2kV, 6.4mm) FESEM instrument (Zeiss, Jena, Germany). The samples were sputtered with platinum (2.0 nm) in a Cressington sputter

coater 208HR to enhance conductivity.

4.6.1. Synthesis and Characterization of the Polymerization Catalysts

Synthesis of complex A



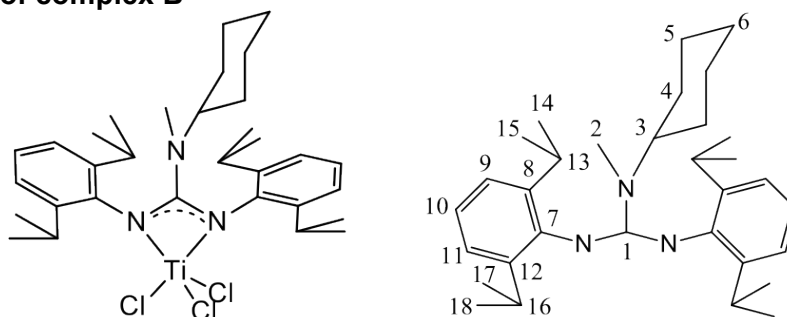
Diethylamidotitanium(VI) chloride (0.50 g, 2.2 mmol) and bis(2,6-diisopropylphenyl) carbodiimide (0.80 g, 2.2 mmol) were subsequently added to a Schlenk flask filled with 25 mL of toluene and stirred at 50 °C. After 24 h the mixture was heated to 110 °C and filtered. Slow cooling to room temperature gives dark red crystals. The supernatant solution was decanted and the titanium complex was dried under reduced pressure (1.05 g, 80 % yield).

Elemental analysis: calcd. C 59.04, H 7.69, N 7.12; found C 57.98, H 7.65, N 7.02.

$^1\text{H-NMR}$ (C_6D_6 , 400 MHz, 298K): δ = 0.36 (t, 6H, CH_2CH_3), 1.15 (d, 12H, $\text{CH}(\text{CH}_3)_2$), 1.52 (d, 12H, $\text{CH}(\text{CH}_3)_2$), 2.52 (q, 4H, CH_2CH_3), 3.57 (m, 4H, $\text{CH}(\text{CH}_3)_2$), 7.0 – 7.11 (m, 6H, C_6H_3).

^{13}C NMR (C_6D_6 , 100.53 MHz, 298K): δ = 12.1 (CH_3^3), 24.4 ($\text{CH}_3^{9,10}$), 25.7 ($\text{CH}_3^{9,10}$), 29.1 (CH^8), 41.5 (CH_2^2), 124.8 (CH^6), 128.6 (CH^7), 143.0 (C^5), 145.0 (C^4), 167.7 (NCN^1).

Synthesis of complex B



Cyclohexyl(methyl)amidotitanium(VI) chloride (0.78 g, 2.93 mmol) and

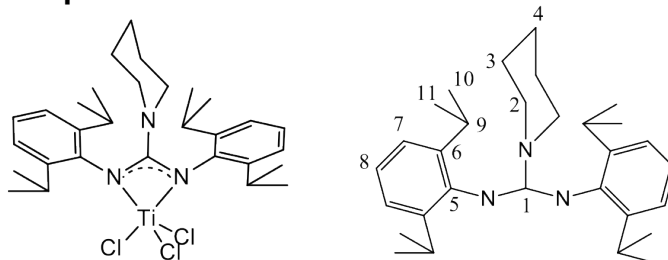
bis(2,6-diisopropylphenyl) carbodiimide (1.06 g, 2.9 mmol) were subsequently added to a Schlenk flask filled with 25 mL of toluene and stirred at 50 °C. After 24 h the mixture was heated to 110 °C and filtered. Slow cooling to room temperature gives dark red crystals. The supernatant solution was decanted and the titanium complex was dried under reduced pressure (0.92 g, 50 % yield).

Elemental analysis: calcd. C 61.01, H 7.84, N 6.67; found C 59.93, H 7.75, N 6.51.

$^1\text{H-NMR}$ (C_6D_6 , 400 MHz, 298K): d = 0.46 (m, 2H, CH_2), 0.71 (m, 4H, CH_2), 1.08 (m, 4H, CH_2), 1.17 (d, 6H, $\text{CH}(\text{CH}_3)_2$), 1.22 (d, 6H, $\text{CH}(\text{CH}_3)_2$), 1.55 (d, 12H, $\text{CH}(\text{CH}_3)_2$), 1.90 (s, 3H, CH_3), 3.33 (m, 1H, $\text{CH}(\text{CH}_2)_2$), 3.49 (m, 2H, $\text{CH}(\text{CH}_3)_2$), 3.75 (m, 2H, $\text{CH}(\text{CH}_3)_2$), 7.04 – 7.14 (m, 6H, C_6H_3).

$^{13}\text{C NMR}$ (C_6D_6 , 100.53 MHz, 298K): d = 23.1 ($\text{CH}_3^{14,15,17,18}$), 24.0 ($\text{CH}_3^{14,15,17,18}$), 24.8 ($\text{CH}_3^{14,15,17,18}$), 25.2 ($\text{CH}_2^{4,5,6}$), 25.8 ($\text{CH}_2^{14,15,17,18}$), 28.9 ($\text{CH}_2^{4,5,6}$), 29.4 ($\text{CH}^{13,16}$), 29.7 ($\text{CH}^{13,16}$), 30.5 (CH_3^2), 58.8 (CH^3), 123.6 ($\text{CH}^{9,11}$), 124.5 ($\text{CH}^{9,11}$), 128.1 (CH^{10}), 143.1 ($\text{C}^{7,8,12}$), 143.2 ($\text{C}^{7,8,12}$), 143.3 (C^7), 167.5 (NCN^1).

Synthesis of Complex C



Piperidin-1-yltitanium(VI) chloride (0.80 g, 3.36 mmol) and Bis(2,6-diisopropylphenyl)carbodiimide (1.22 g, 3.36 mmol) were subsequently added to a Schlenk flask filled with 25 mL of toluene and stirred at 50 °C. After 24 h the mixture was heated to 110 °C and filtered. Slow cooling to room temperature gives dark red crystals. The supernatant solution was decanted and the titanium complex was dried under reduced pressure (1.80 g, 89 % yield).

Elemental analysis: calcd. C 59.86, H 7.54, N 6.98; found C 58.03, H 7.50, N 6.87.

$^1\text{H-NMR}$ (C_6D_6 , 400 MHz, 298K): d = 0.71 (m, br, 6H, $(\text{CH}_2)_3$), 1.17 (d, 12H, $\text{CH}(\text{CH}_3)_2$), 1.53 (d, 12H, $\text{CH}(\text{CH}_3)_2$), 2.56 (m, br, 4H, NCH_2), 3.63 (m, 4H, $\text{CH}(\text{CH}_3)_2$), 7.05 – 7.14 (m, 6H, C_6H_3).

^{13}C NMR (C_6D_6 , 100.53 MHz, 298K): δ = 22.6 ($\text{CH}_3^{9,10}$), 24.1 (CH_2^4), 24.5 (CH_2^3), 25.7 ($\text{CH}_3^{9,10}$), 29.1 (CH^8), 48.1 (CH_2^2), 124.8 (CH^6), 128.3 (CH^7), 143.0 (C^5), 144.8 (C^4), 166.5 (NCN^1).

CCDC-885210 and CCDC-885211 contain the supplementary crystallographic data for complex **A** and **B**. These data can be obtained free of charge from The Cambridge Crystallographic Data Centre via www.ccdc.cam.ac.uk/data_request/cif.

4.6.2. Ethylene Polymerization Studies

Description of ethylene polymerization experiments (Runs 1-28)

The catalytic ethylene polymerization reactions were performed in a 250 mL glass autoclave (Buechi) in semi-batch mode (ethylene was added by replenishing flow to keep the pressure constant). The reactor was ethylene flow controlled and equipped with separated toluene, catalyst and co-catalyst injection systems. During a polymerization run the pressure and the reactor temperature were kept constant while the ethylene flow was monitored continuously. In a typical semi-batch experiment, the autoclave was evacuated and heated for 1h at 80 °C prior to use. The reactor was then brought to desired temperature, stirred at 1000 rpm and charged with 150 mL of toluene. After pressurizing with ethylene to reach 2 bar total pressure the autoclave was equilibrated for 10 min. Successive co-catalyst solution, activator, and 1 mL of a 0.002 M pre-catalyst stock solution in toluene was injected, to start the reaction. After 15 min reaction time the reactor was vented and the residual aluminum alkyls were destroyed by addition of 50 mL of ethanol. Polymeric product was collected, stirred for 30 min in acidified ethanol and rinsed with ethanol and acetone on a glass frit. The polymer was initially dried on air and subsequently in vacuum at 80°C.

Description of ethylene polymerization experiments (Runs 29-37)

The catalytic ethylene polymerization reactions were performed in a stainless steel 800 mL autoclave (Buechi) in semi-batch mode (ethylene was added by replenishing flow to keep the pressure constant). The reactor was pressure, temperature, stirrer speed, and ethylene flow controlled and

equipped with separated toluene, catalyst and co-catalyst injection systems. During a polymerization run the pressure and the reactor temperature were kept constant while the ethylene flow, inner and outer temperature, and stirrer speed were monitored continuously. In a typical semi-batch experiment, the autoclave was evacuated and heated for 1 h at 130 °C prior to use. The reactor was then brought to desired temperature, stirred at 600 rpm and charged with 250 mL of toluene. After pressurizing with ethylene to reach the desired total pressure the autoclave was equilibrated for 10 min. Successive co-catalyst solution, activator, and pre-catalyst stock solution in toluene (0.002 M) was injected, to start the reaction. After 60 min reaction time the reactor was vented and slowly pressurized with dry oxygen to reach 2 bar total pressure. After 15 min 1 mL of titanium(VI)isopropoxide in toluene (1 M) was injected and the autoclave was heated to reach 90°C inside. After four hours the residual aluminum alkyls were destroyed by addition of 50 mL of ethanol. Polymeric product was collected, stirred for 30 min in acidified ethanol and rinsed with ethanol and acetone on a glass frit. The polymer was initially dried on air and subsequently in vacuum at 80°C.

Table SI 4.2.1. Ethylene polymerization with MAO and d-MAO cocatalysts.^a

Entry	Preca	Cocat.	T	m _{Pol.}	Activity	M _n	M _w /M _n
	t.		[°C]	[g]	[kg _{PE} mol _{cat} ⁻¹ h ⁻¹ bar ⁻¹]	[kgmol ⁻¹]	
1	A	MAO	30	2.82	2820	15.9	2.0
2	A	MAO	50	1.67	1670	8.4	2.5
3	A	MAO	80	0.10	100	7.6	4.0
4	B	MAO	30	1.91	1910	13.2	4.8
5	B	MAO	50	4.20	4200	6.5	2.5
6	B	MAO	80	0.95	950	3.3	2.0
7	C	MAO	50	4.50	4500	6.2	3.0
8	A	d-MAO	30	3.64	3640	829.2	5.9
9	A	d-MAO	50	1.36	1360	172.5	3.3
10	A	d-MAO	80	1.22	1220	75.6	2.7
11	B	d-MAO	30	9.30	9300	104.1	4.0
12	B	d-MAO	50	1.92	1920	85.3	2.8
13	B	d-MAO	80	1.08	1080	34.7	2.5

4. Tailored Nano.Structuring of End-Group Functionalized HD-Polyethylene Synthesized via an Efficient Catalytic Version of Ziegler's "Aufbaureaktion"

14 **C** d-MAO 50 3.35 3350 111.6 5.7

^aPrecatalyst: 2.0 μmol; cocatalyst: 1.0 mmol (Ti/Al = 1/500); toluene: 150 mL;
p = 2 bar; t = 15 min.

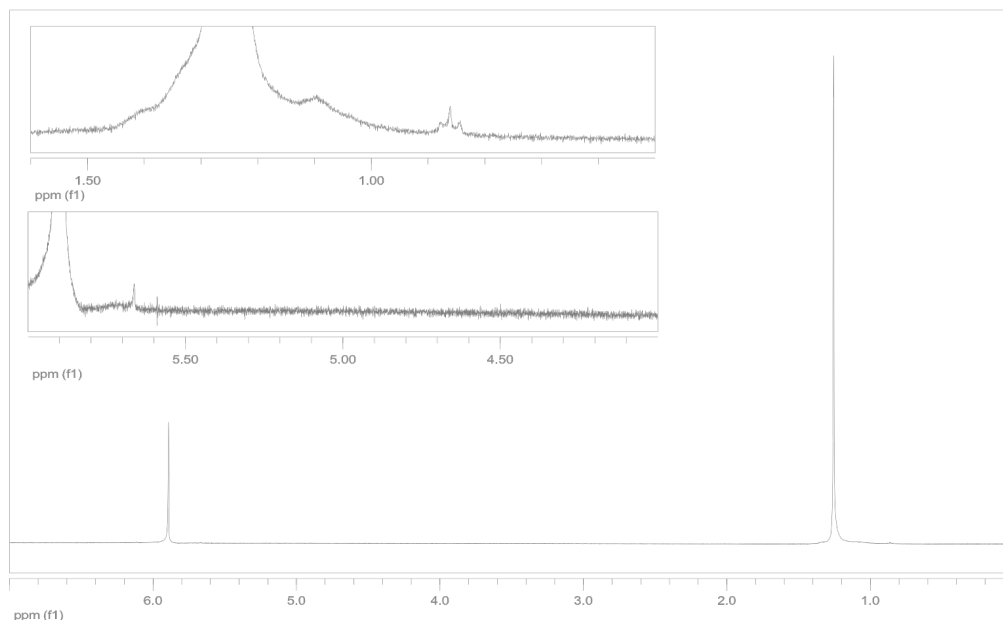


Figure 4.2.1. ¹H NMR spectrum (C₂Cl₄D₂, 120°C) of PE obtained with the A/MAO system catalyst after acidic workup (entry 3).

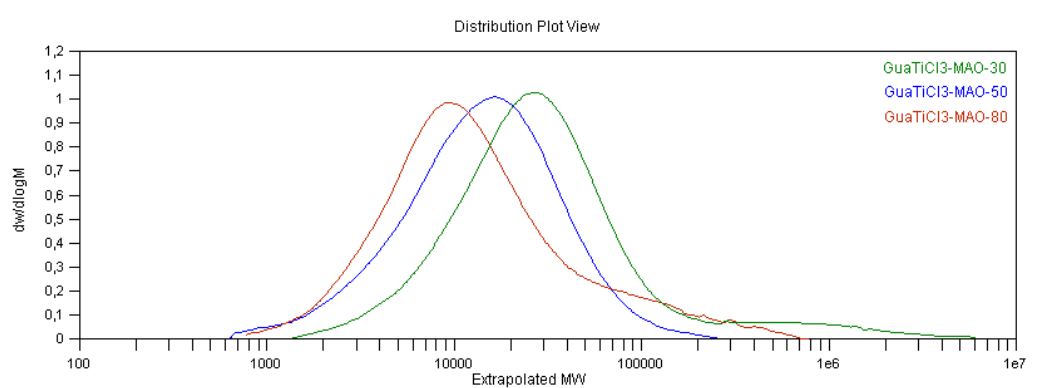


Figure 4.2.2. Molecular-weight distribution (SEC) of the polymerization experiments listed in Table 4.2.1, entries 1 - 3.

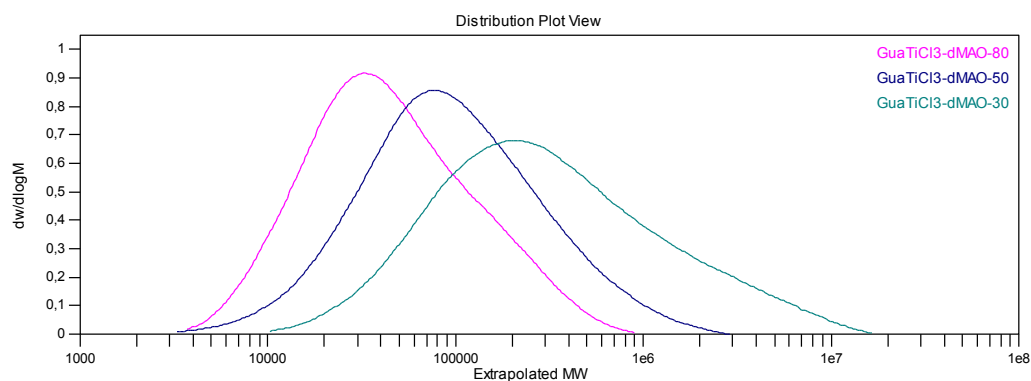


Figure 4.2.3. Molecular-weight distribution (SEC) of the polymerization experiments listed in Table 4.2.1, entries 8 - 10.

Table 4.2.2. Ethylene polymerization with trialkylaluminum cocatalysts and perfluorophenylborate activators.^a

Entry	Preca t.	Cocat.	Al/Ti	m _{Pol.} [g]	Activity [kg _{PE} mol _{cat} ⁻¹ h ⁻¹ bar ⁻¹]	M _n [kgmol ⁻¹]	M _w /M _n
15	A	TEA	250	1.50	1500	2.9	2.3
16	A	TEA	500	1.62	1620	2.2	1.9
17	A	TEA	750	1.53	1530	2.1	2.4
18	A	TEA	1000	1.80	1800	1.8	1.9
19	A	TMA	500	0.70	700	3.9	1.9
20	A	TIBA	500	1.10	1100	40.4	2.0
21	B	TEA	250	0.92	920	3.9	2.5
22	B	TEA	500	1.70	1700	2.8	2.2
23	B	TEA	750	1.75	1750	2.1	2.0
24	B	TEA	1000	1.80	1800	1.6	2.0
25	C	TEA	250	1.50	1500	3.3	2.6
26	C	TEA	500	1.40	1400	3.1	2.4
27	C	TEA	750	1.40	1400	2.7	2.4
28	C	TEA	1000	1.55	1550	2.5	2.3

^aPrecatalyst: 2.0 μmol; ammonium borate: 2.2 μmol [R₂N(CH₃)H]⁺[B(C₆F₅)₄]⁻ (R = C₁₆H₃₃ – C₁₈H₃₇), Ti/B = 1/1.1; toluene: 150 mL; T = 50°C, p = 2 bar; t = 15 min.

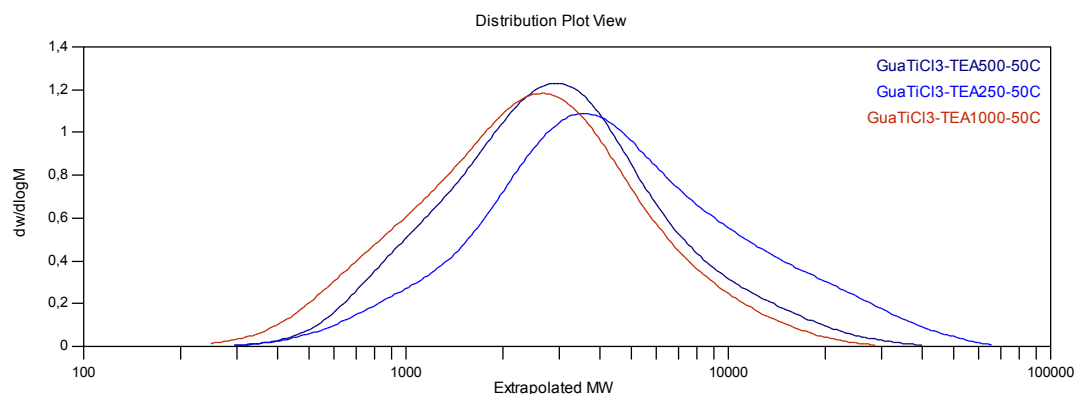


Figure 4.2.4. Molecular-weight distribution (SEC) of the polymerization

4. Tailored Nano.Structuring of End-Group Functionalized HD-Polyethylene Synthesized via an Efficient Catalytic Version of Ziegler's "Aufbaureaktion"

experiments listed in Table 4.3.2, entries 15, 16 and 18.

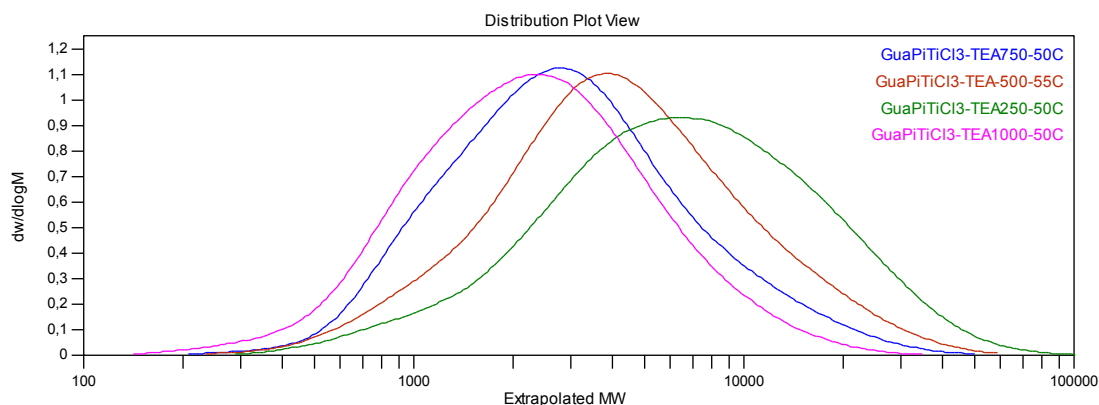


Figure 4.2.5. Molecular-weight distribution (SEC) of the polymerization experiments listed in Table 4.2.2, entries 25 - 28.

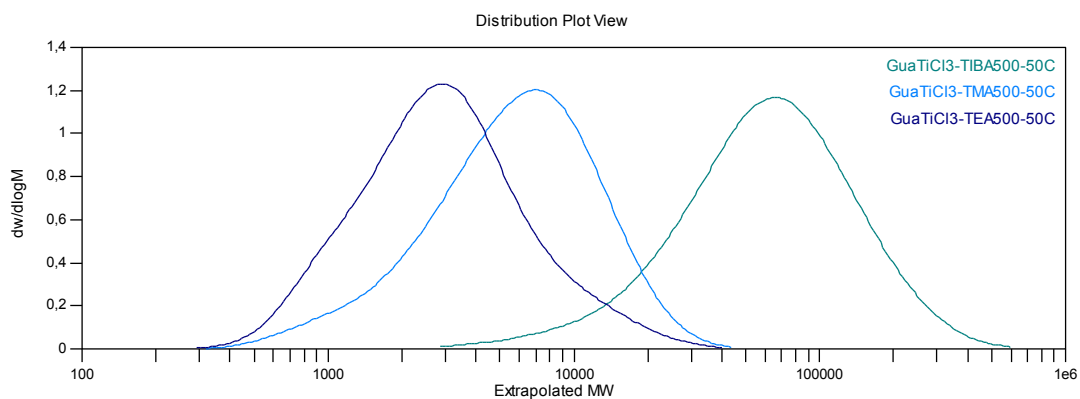


Figure 4.2.6. Molecular-weight distribution (SEC) of the polymerization experiments listed in Table 4.2.2, entries 16, 19 - 20.

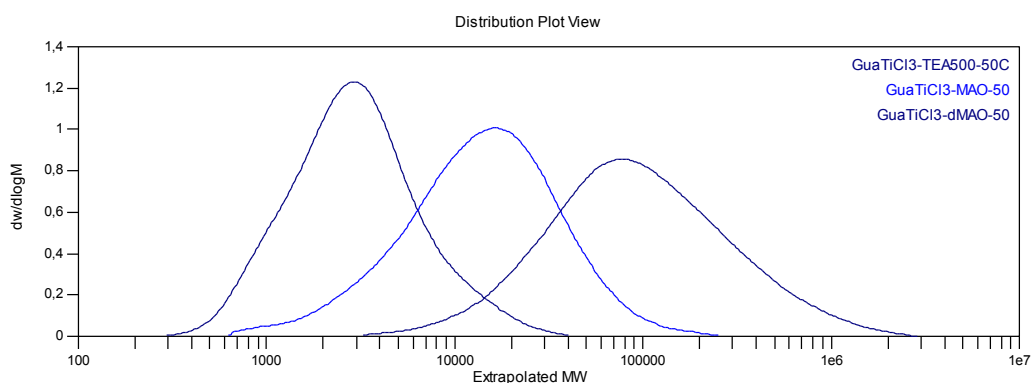


Figure 4.2.7. Molecular-weight distribution (SEC) of the polymerization experiments listed in Table 4.2.1 and 4.2.2, entries 2, 9 - 16.

Table 4.2.3. Ethylene polymerization with trialkylaluminum cocatalysts and perfluorophenylborate activators and subsequent oxidation.

4. Tailored Nano.Structuring of End-Group Functionalized HD-Polyethylene Synthesized via an Efficient Catalytic Version of Ziegler's "Aufbaureaktion"

Entry	Precat.	Cocat.	Al/Ti	T	m _{Pol.}	Activity	M _n	M _w /M _n	
		[μmol]		[°C]	[g]	[kg _{PE} mol _{cat} ⁻¹ h ⁻¹ bar ⁻¹]	[kgmol ⁻¹]		
29	A	4	TEA	2500	70	44.0	5500	1.7	1.8
30	A^b	2	TEA	5000	70	47.0	4700	2.1	1.9
31	A^b	0.6	TEA	17000	65	28.4	9470	2.5	1.8
32	A^b	0.4	TEA	25000	60	32.0	16000	3.3	1.9
33	A^b	0.3	TEA	33000	65	24.4	16300	2.5	1.9
34	A^b	0.2	TEA	50000	60	16.7	16700	2.9	1.9
35	C	4	TEA	2500	60	30.2	3780	1.7	2.0
36	C	4	TEA	2500	65	27.7	3460	1.5	2.0
37	C	4	TEA	2500	75	4.20	525	0.9	1.6

^aAmmonium borate: [R₂N(CH₃)H]⁺[B(C₆F₅)₄]⁻ (R = C₁₆H₃₃ – C₁₈H₃₇), Ti/B = 1/1.1; toluene: 250 mL; p = 2 bar; t = 60 min.

^bp = 5 bar.

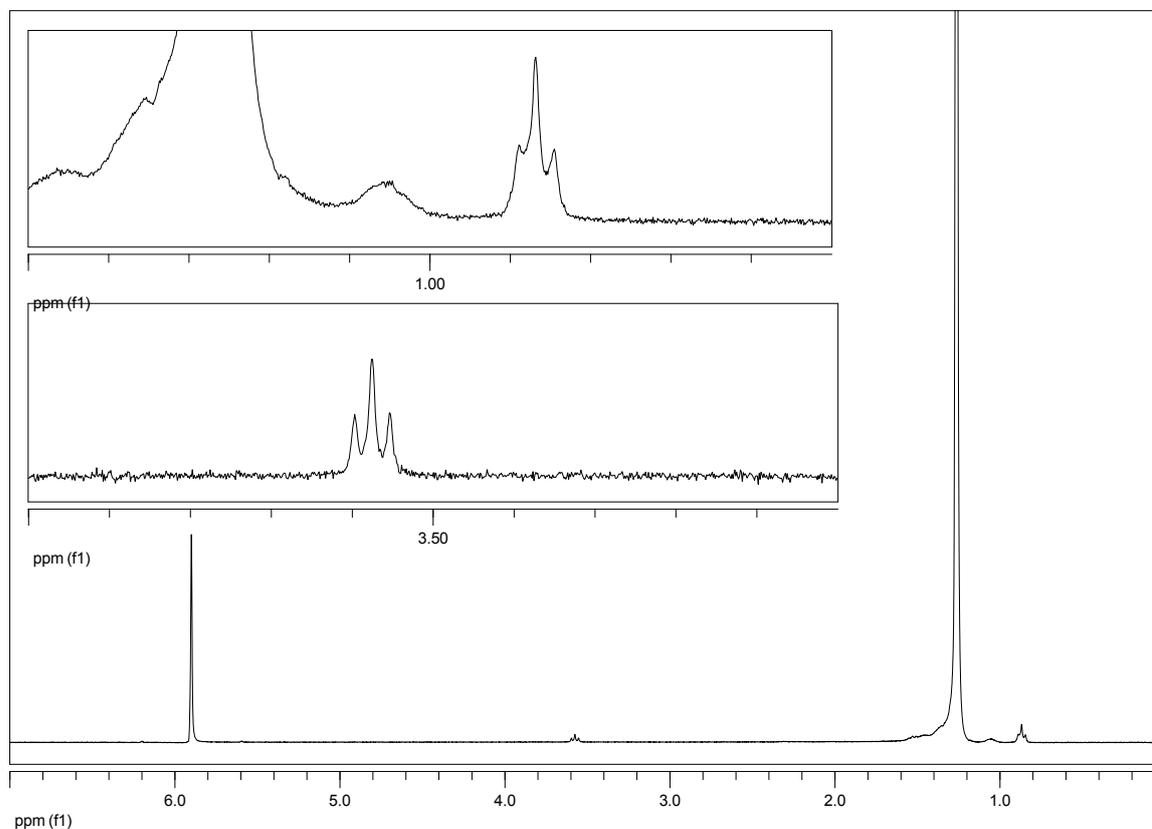


Figure 4.2.8. ¹H NMR spectrum (C₂Cl₄D₂, 120°C) of PE-OH obtained with the **A**/borate catalyst system after oxidative and acidic workup

(entry 30).

4.6.3. General procedure for block copolymer synthesis

PEOPL(1)

Linear hydroxy terminated polyethylene (Mn 3321 g/mol, Mw/Mn 1.9; 2.0 g, 0.6 mmol OH) and rac-lactide (1.6 g, 11.1 mmol) was added in a pressure tube. Sn(Oct)₂ (4.5 mg; 8.5 μmol) and 20ml of dried toluene was transferred to the pressure tube before sealing with Teflon screw-cap fitted with a Viton o-ring seal. The flask was immersed in an oil-bath at 110 °C for 18 h followed by selective precipitation into a tenfold excess by volume of cold methanol. After the filtration, the precipitate was washed with THF prior to dry at 70 °C for 24 h in the conventional oven. The yield of the dried block copolymer was 3.15 g (72% conversion of L-lactide). The resultant diblock copolymer was analyzed using HT GPC, NMR, TGA, DSC and IR.

PEOPL(2)

Linear hydroxy terminated polyethylene (Mn 3321 g/mol, Mw/Mn 1.9; 2.0 g, 0.6 mmol OH) and rac-lactide (0.9 g, 6.24 mmol) was added in a pressure tube. Sn(Oct)₂ (4.5 mg; 8.5 μmol) and 20ml of dried toluene was transferred to the pressure tube before sealing with Teflon screw-cap fitted with a Viton o-ring seal. The flask was immersed in an oil-bath at 110 °C for 18 h followed by selective precipitation into a tenfold excess by volume of cold methanol. After the filtration, the precipitate was washed with THF prior to dry at 70 °C for 24 h in the conventional oven. The yield of the dried block copolymer was 2.72 g (80% conversion of L-lactide). The resultant diblock copolymer was analyzed using HT GPC, NMR, TGA, DSC and IR.

PEOPL(3)

Linear hydroxy terminated polyethylene (Mn 3321 g/mol, Mw/Mn 1.9; 2.0 g, 0.6 mmol OH) and rac-lactide (0.6 g, 4.16 mmol) was added in a pressure tube. Sn(Oct)₂ (4.5 mg; 8.5 μmol) and 20ml of dried toluene was transferred to the pressure tube before sealing with Teflon screw-cap fitted with a Viton o-ring seal. The flask was immersed in an oil-bath at 110 °C for 18 h followed by selective precipitation into a tenfold excess by volume of cold methanol.

After the filtration, the precipitate was washed with THF prior to dry at 70 °C for 24 h in the conventional oven. The yield of the dried block copolymer was 2.48 g (79% conversion of L-lactide). The resultant diblock copolymer was analyzed using HT GPC, NMR, TGA, DSC and IR.

4.6.4. Characterization of the diblock copolymers

Table 4.2.4. Summary of the characterization data.

SampleID	M_n^1 g/mol	M_w/M_n^1	MW^2 g/mol	f_{PL}^3	T_m^4 °C	T_c^4 °C	ΔH_m^4 J/g	X_E^5 %
PE-OH	3300	1.9			130.0	115.0	252.2	91
PEOPL(1)	4500	1.7	5500	0.44	126.6	113.1	104.3	37
PEOPL(2)	4000	1.6	4400	0.38	127.2	114.0	128.1	46
PEOPL(3)	3500	1.8	3900	0.17	128.3	114.6	185.3	66

- 1) M_n and polydispersity as determined by gel permeation chromatography.
- 2) Molecular weight of the diblock copolymer as calculated by 1H NMR spectroscopy using relative intensities of repeating unit signals and end-group signals and M_n of PE as determined by HT GPC.
- 3) Weight fraction of PL in the diblock copolymer calculated using NMR spectroscopy and the densities at 25 °C reported for the respective components [PL = 1.25;^{S5} LPE = 0.95 (at 60% crystallinity)^{S6}].
- 4) Taken as the peak of the melting endotherm (or the crystallization exotherm) during the heat (or cool) in DSC.
- 5) Percentage of crystallinity of the diblock copolymers calculated from $[\Delta H_m / (\Delta H_m^0 \cdot)]$ with $\Delta H_m^0 = 277 \text{ J g}^{-1}$

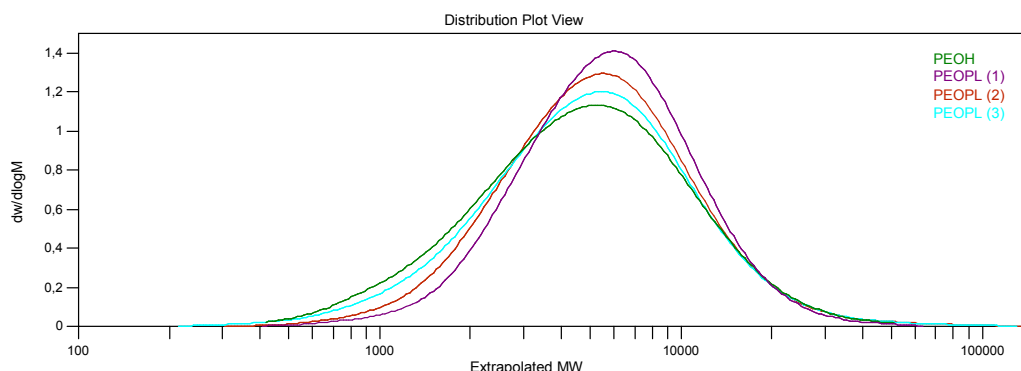


Figure 4.2.9. Molecular weight distribution of different diblock copolymers.

4. Tailored Nano.Structuring of End-Group Functionalized HD-Polyethylene Synthesized via an Efficient Catalytic Version of Ziegler's "Aufbaureaktion"

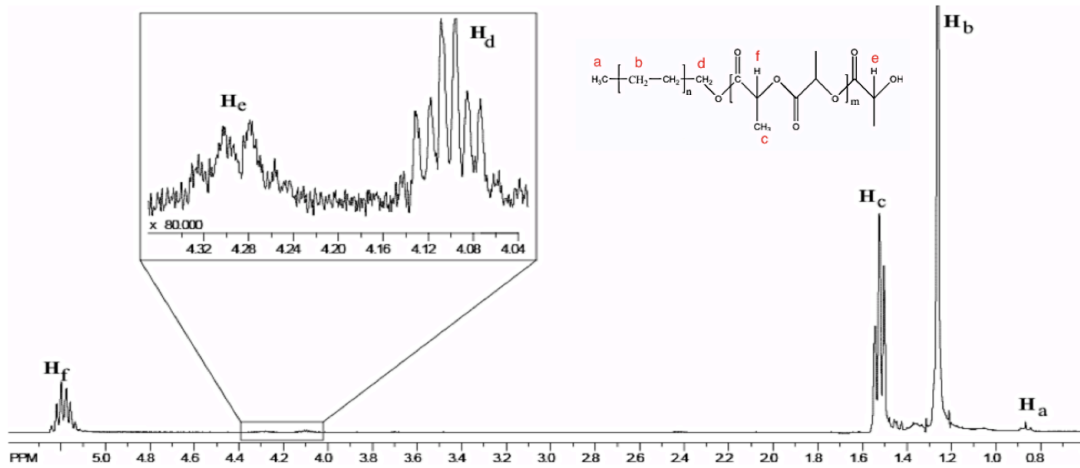


Figure 4.2.10. ^1H NMR spectrum of block polymer PEOPL(1) measured in $\text{C}_2\text{D}_2\text{Cl}_4$ at 120°C with the inset showing a magnified portion that accentuates the methylene protons at the junction between the two components [Hd; $-\text{CH}_2-\text{CH}_2-\text{O}-\text{C}(\text{O})-\text{CH}(\text{CH}_3)-$] and the PLA end-group methine protons [He- $\text{O}-\text{C}(\text{O})-\text{CH}(\text{CH}_3)-\text{OH}$].

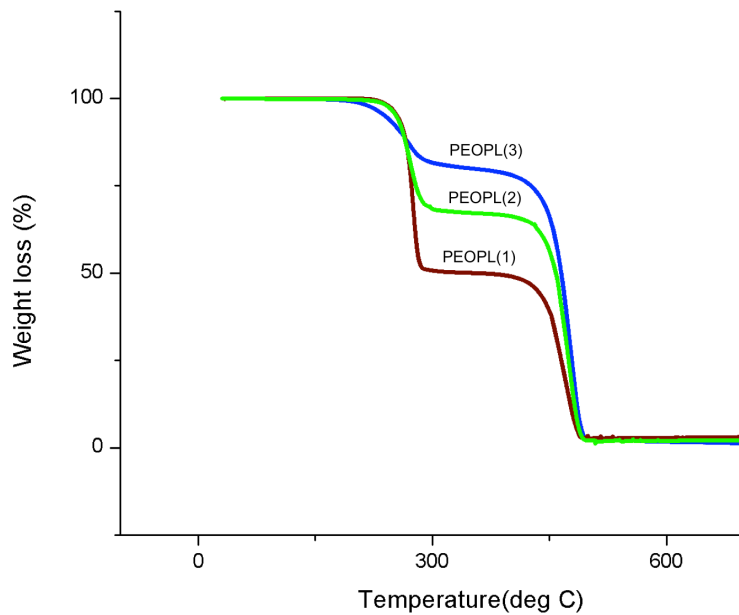


Figure 4.2.11. Thermo gravimetric curve of PEOPL(1), PEOPL(2), and PEOPL(3). The mass loss below 300°C corresponds to PL decomposition and that above 450°C to PE decomposition.

4. Tailored Nano.Structuring of End-Group Functionalized HD-Polyethylene Synthesized via an Efficient Catalytic Version of Ziegler's "Aufbaureaktion"

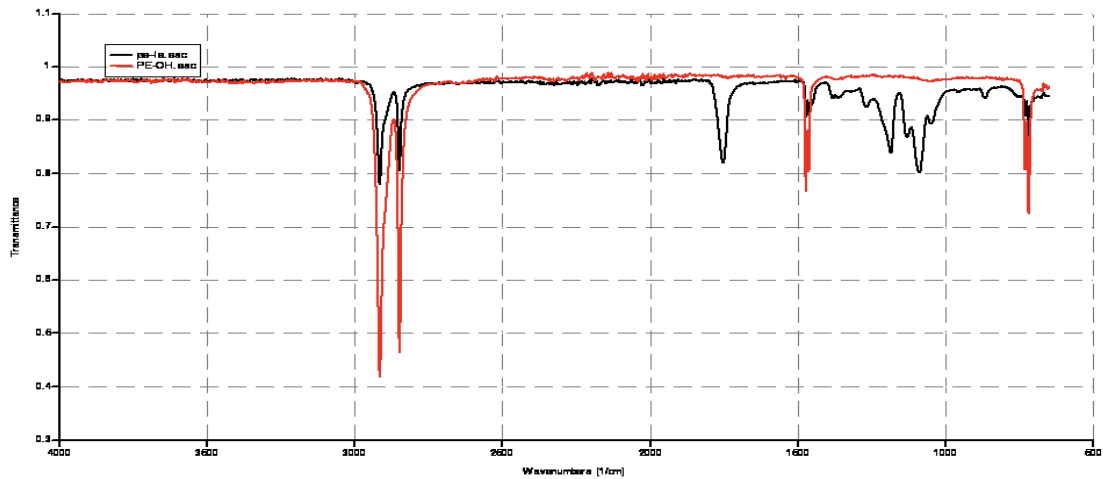


Figure 4.2.12. FTIR-spectra of starting PEOH (red) and synthesized PEOPH copolymer (black).

4.6.5. Microphase separation of PEOPH

PEOPL(1), PEOPL(2), and PEOPL(3) (200mg) were dissolved in 8mL of cumene in a glass vials at 152°C. After slow evaporation of solvent at 140°C (oil bath temperature), the melt morph was annealed for six hours at the same temperature prior to bring the melt morph to room temperature. The resultant phase separated morphologies were analyzed using AFM.

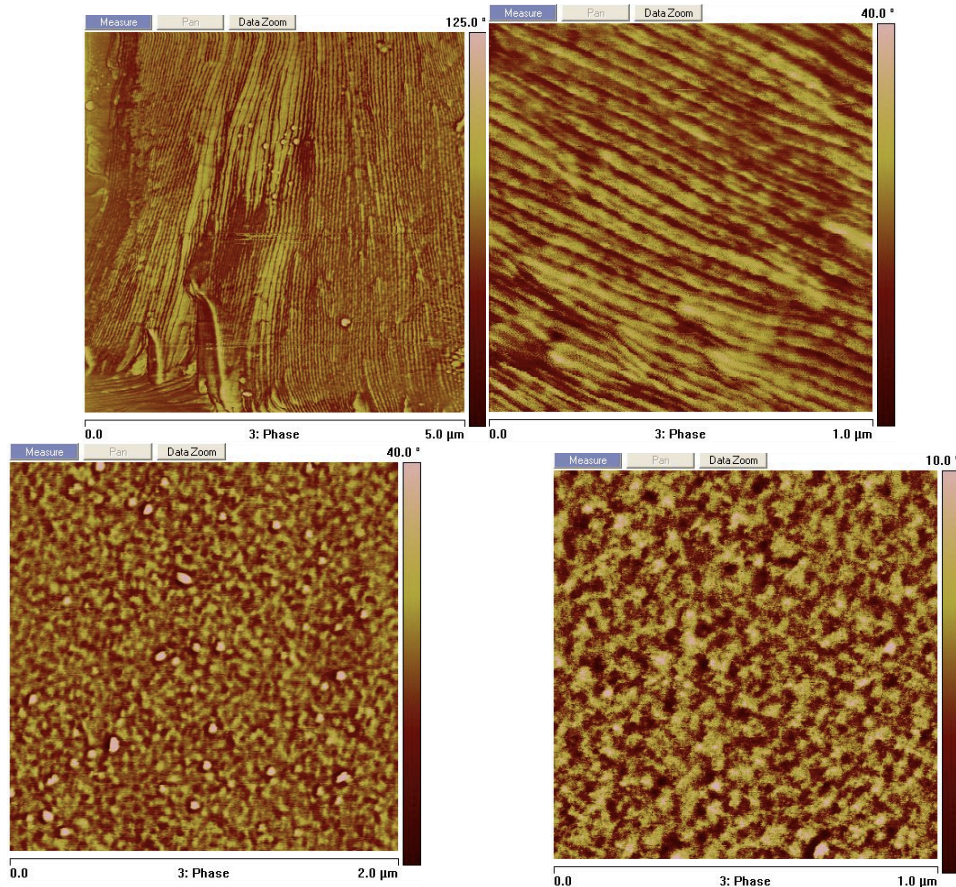


Figure 4.2.13. Top row. AFM images of synthesized copolymers in different scales. Top: phase image of PEOPL(1) showing a lamellar morphology. **Below row:** phase images of PEOPL(2) shows a disordered bicontinuous morphology. All of the AFM images were recorded at non-contact mode and all of them were flattened at first order execution.

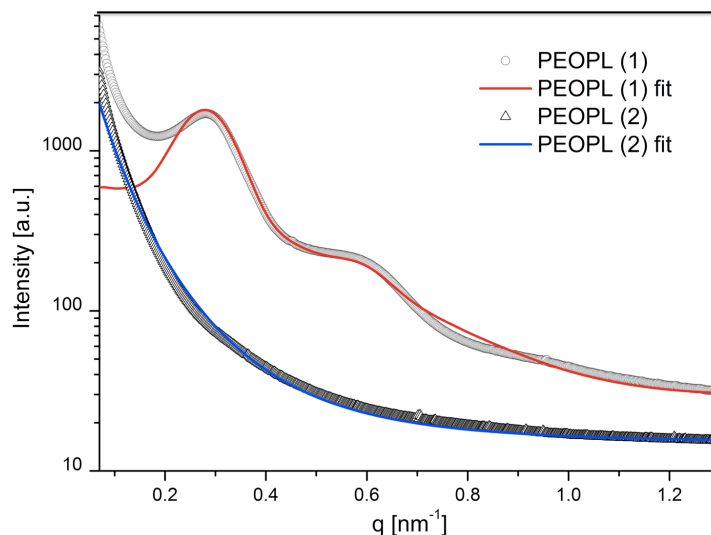


Figure 4.2.14. Radially averaged synchrotron SAXS patterns for PEOPL(1) and PEOPL(2) indicating a lamellar-type and a disordered bicontinuous morphology, respectively.

Table 4.2.5. Simulation parameters (*scattersoftware*)^{S7} used to obtain the fits 5 shown in figure 4.2.14.

Parameter	PEOPL(1)	PEOPL(2)
Lattice	Lamellae	Form factor
Unit cell [nm]	20.2	
Domain size [nm]	48.7	
Displacement [nm]	4.2	
Peak shape	Gaussian	
Particle	Disk	Sphere
Thickness [nm]	4.5	
Radius [nm]	300	8.2
Sigma	0.098	0.523

Etching of the PL block

The microphase separated diblock copolymer was submerged in NaOH/water/methanol mixture (0.5 M NaOH, 40% MeOH) for 3 days at 70°C. The completion of the etching process was confirmed by recording FTIR at different times. The resultant PE materials were analyzed using SEM and BET.

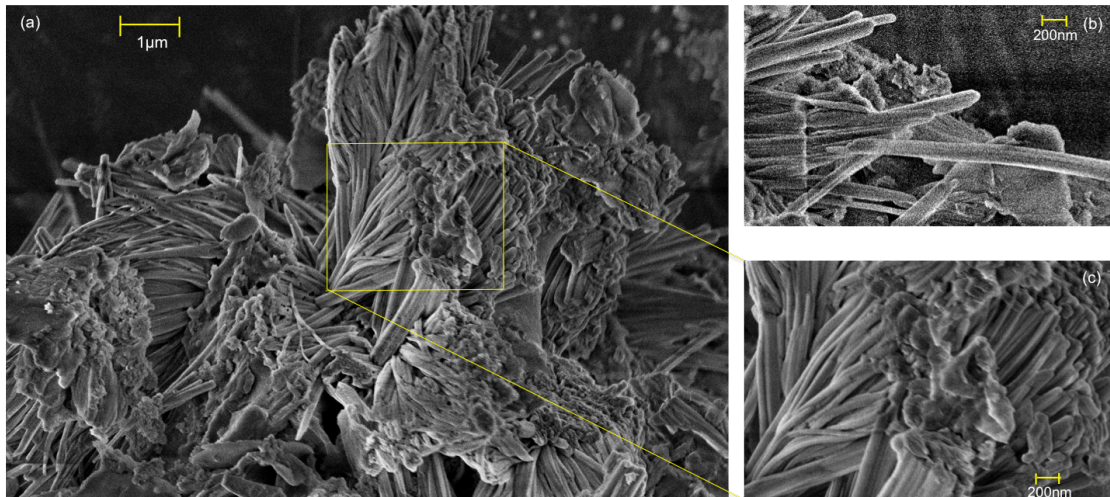


Figure 4.2.15. SEM images PE fibers after removal of the PL block of PEOPL(1) via etching.

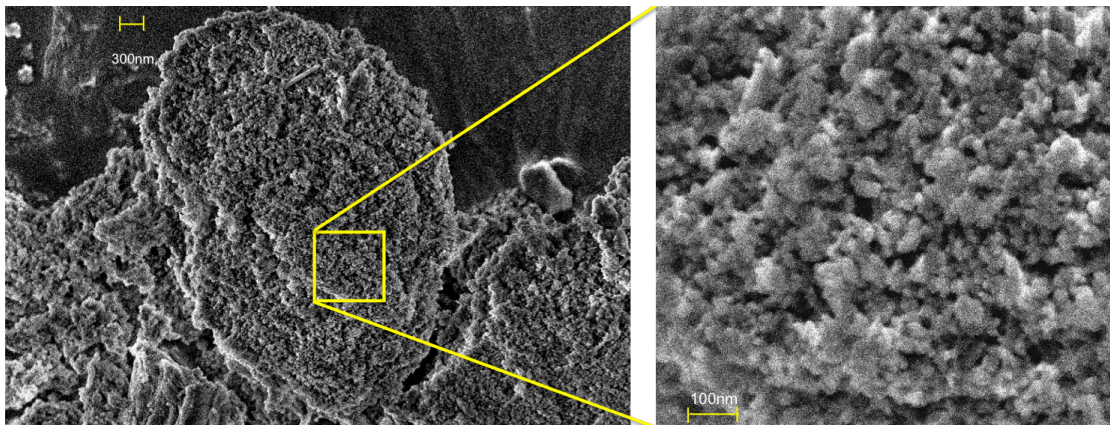


Figure 4.2.16. SEM images of porous polyethylene after removal of the PL block of PEOPL(2).

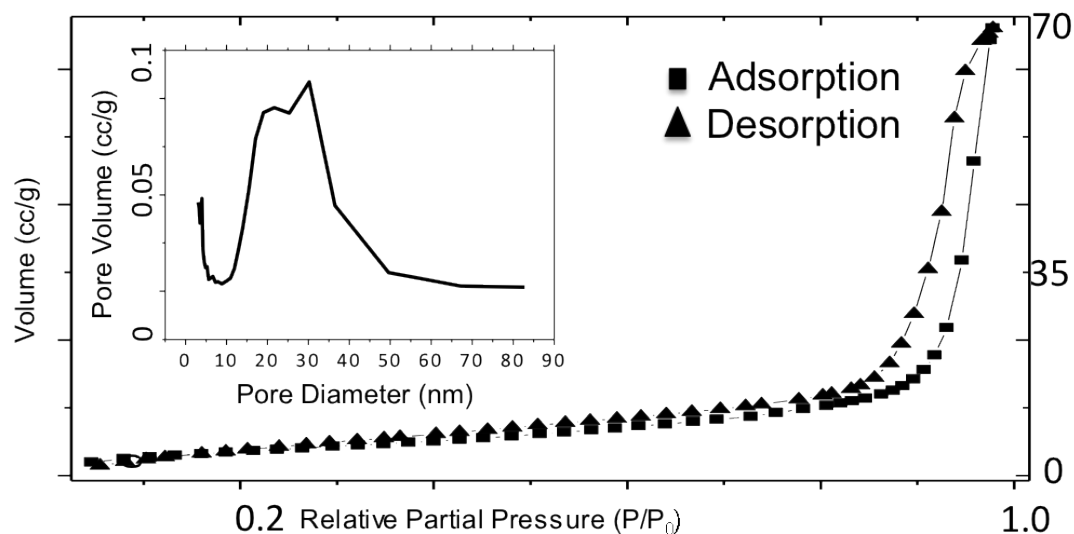


Figure 4.2.17. Nitrogen adsorption-desorption studies of porous polyethylene after removal of the PL block of PEOPL(2). The inset shows the pore size distribution (BJH method). The calculated surface area (BET method) was 19.3 m²/g.

4.7. References (Supporting Information)

- [S1] E. Benzing, W. Kornicker, *Chem. Ber.* **1961**, *94*, 2263–2267.
- [S2] A. Altomare, M. C. Burla, M. Camalli, G. L. Cascarano, C. Giacovazzo, Guagliardi, A. G. G. Moliterni, G. Polidori, R. Spagna, *J. Appl. Crystallogr.* **1999**, *32*, 115–119.
- [S3] G. M. Sheldrick, SHELX-97, Program for Crystal Structure Analysis (Release 97-2), Institut für Anorganische Chemie der Universität, Göttingen, Germany, **1998**.
- [S4] L. J. Farrugia, *J. Appl. Crystallogr.* **1999**, *32*, 837–838.
- [S5] R. Witzke, J. J. Kolstad, R. Narayan, *Macromolecules* **1997**, *30*, 7075–7085.
- [S6] Handbook of Polyethylene, Peacock, A. J. Marcel Dekker, Basel, Switzerland, **2000**.
- [S7] S. Förster, L. Apostol, W. Bras, *J. Appl. Cryst.* **2010**, *43*, 639–646.

5. SiCN nanofibers with a diameter below 100 nm synthesized via concerted block copolymer formation, microphase separation, and crosslinking

Saravana K. T. Pillai,^a Winfried P. Kretschmer,^a Christine Denner,^a Günter Motz,^b Markus Hund,^c Andreas Fery,^c Martin Trebbin,^d Stephan Förster,^d Rhett Kempe^{*a}

^aLehrstuhl Anorganische Chemie II, Universität Bayreuth, Universität Bayreuth, 95440 Bayreuth, Germany, e-mail : kempe@uni-bayreuth.de

^bLehrstuhl Keramische Werkstoffe, Universität Bayreuth, Universität Bayreuth, 95440 Bayreuth, Germany.

^cLehrstuhl Physikalische Chemie I, Universität Bayreuth, Universität Bayreuth, 95440 Bayreuth, Germany.

^dLehrstuhl Physikalische Chemie II, Universität Bayreuth, Universität Bayreuth, 95440 Bayreuth, Germany.

5.1. Abstract

Ultrathin SiCN fibers are produced from inexpensive carbosilazane-polyethylene block copolymers. The two-step synthesis consists of a concerted block copolymer formation, microphase separation and crosslinking step, followed by pyrolysis. The fibers have a mean diameter of 45 nm and an aspect ratio of up to 100. SiCN fibers with a mean diameter of 50 nm and an aspect ratio of up to 100 are produced in a two-step process by R. Kempe and co-workers. The key step to fabricate the longitudinal and cross-sectional views of the mesofibers shown here is a concerted block-copolymer synthesis, microphase separation, and cross linking at 140°C followed by pyrolysis at 1100°C. Inexpensive components like a commercially available silazane and polyethylene are linked. The fibers may find application in electronic devices, as components of ceramic matrix composites, as fiber beds in hightemperature nano-filtering like diesel fine dust removal, or as thermally robust and chemically inert catalyst supports. Furthermore, the SiCN nanofibers introduced on page 984 are a promising alternative to ultrathin carbon fibers, due to their oxidation resistance.

5.2. Introduction, Results and Discussion

1-dimensional nano-materials like rods,^[1] tubes,^[2] and fibers^[3] are of immense interest since they combine small-size relevant properties and a large aspect ratio. Polymer derived amorphous SiCN materials are known for their very high thermal stability and their chemical inertness.^[4] Furthermore, metal modifications significantly extend the application spectrum, for instance, towards catalysis.^[5] The polymeric carbosilazane ceramic precursors (PCCP) are sensitive towards hydrolysis which excludes structuring in the presence of water or even moisture. Despite this sensitivity structuring over multiple length scales under mild conditions is possible.^[6] Structuring in the meso-pore size range (meso-structuring) can be accomplished by the addition of block copolymers to the PCCP as developed by Wiesner and coworkers.^[7] The PCCP components are selectively added to one of the blocks, thereby swelling it. An alteration of the PCCP to block copolymer ratio leads to different morphologies. This structuring concept is meanwhile well established.^[6-8] One could argue that the segments of the block copolymers which are swelled by the PCCP are mostly oxygen rich. The presence of oxygen-containing functional groups may alter the nature of the SiCN material towards higher oxygen contents. The synthesis of meso-structured SiCN precursor ceramics directly from microphase separated block copolymers has been developed by the Kim^[9] as well as the Matsumoto^[10] group and Malenfant *et al.* reported on related boron nitride ceramics.^[11] Organic-inorganic block copolymers in which the inorganic block is the ceramic precursor were synthesized and pyrolyzed. High surface area materials could be obtained by this direct block copolymer approach. Furthermore, block copolymers were synthesized, microphase separated, one of the blocks (polylactide) was etched off and replaced by PCCP.^[12] None of the described block copolymer-based synthetic concepts led to SiCN nanofibers. We have been interested in polymer derived ceramic SiCN (macro) fibers for many years^[13] and describe here the synthesis of fibers having a mean diameter of 45 nm. These ultrathin fibers were made via the direct organic-inorganic block copolymer approach from a commercially available and comparably inexpensive silazane precursor polymer segment and polyethylene. A concerted block copolymer synthesis, microphase separation and

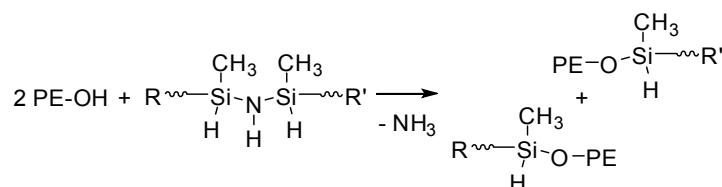
5. SiCN nanofibers with a diameter below 100 nm synthesized via concerted block copolymer formation, microphase separation, and crosslinking

crosslinking process^[14] led to different morphologies (lamellar or cylindrical) by variation of the solvents used (Figure 5.1). The morphologies can be transferred to amorphous SiCN materials via high temperature pyrolysis in an inert atmosphere (Figure 5.1). The commercially available polysilazane HTT1800 (Clariant Advanced Materials, Germany) was chosen as a suitable carbosilazane block since it is rather inexpensive. Amino groups attached to silicon are prone to displacement by hydroxyl groups followed by the evolution of ammonia or silylamines.^[15] Hydroxy-terminated high density polyethylene (PE-OH) was used as counter block. Progress in controlled ethylene polymerization applying a protocol called coordinative chain transfer polymerization (CCTP)^[16] makes PE-OH efficiently available by rare earth and transition metal catalysts transferring the polymeryl chain reversibly to Mg, Zn or Al alkyls.^[17,18,19] PE-OH synthesized via CCTP is inexpensive too and can be highly crystalline. The low cost makes it an attractive sacrificial filler and the highly crystalline nature was expected to give a good segregation contrast to the amorphous carbosilazane block of HTT1800. The resulting nanostructured and crosslinked block copolymer morphology (green body) of PEOHTT-LAM was analyzed using Atomic Force Microscopy (AFM), Transition Electron Microscopy (TEM) (Figure 3a and b), X-ray Powder Diffraction (XRD) and Infrared Spectroscopy (FTIR). The non-crosslinked block copolymers were analyzed by NMR, Thermogravimetric Analysis (TGA) and Differential Scanning Calorimetry (DSC).

A glass vial with 25 mg of PE-OH (M_n of 2500 gmol^{-1} and $M_w/M_n = 1.9$, 80% of the linear PE chains are terminated by hydroxyl group)^[20] in 6 mL of cumene was placed in a flat bottom Schlenk tube (Figure 5. 1). 25 μL of HTT1800 (25 mg) were transferred to the glass vial followed by the addition of dicumylperoxide (DCP; 1 mg, 4 wt% of HTT1800). The Schlenk tube was then placed in a pre-heated oil bath at 160°C to form a homogeneous solution. Cumene is slowly evaporated under anaerobic conditions maintaining an oil bath temperature of 160°C. After the solvent casting, the molten form of the block copolymer was annealed for 24 hours at 140°C to finalize crosslinking of PEOHTT-LAM. PE-OH is linked covalently to the PCCP HTT1800 under these conditions. Nuclear magnetic resonance (NMR) studies using model

5. SiCN nanofibers with a diameter below 100 nm synthesized via concerted block copolymer formation, microphase separation, and crosslinking

silyl amides or DCP-free HTT1800 (crosslinking is very slow then) confirm the linkage of both blocks (Scheme 5. 1). The reaction of C₂₂H₄₅-OH (NACOL 22, SASOL Germany GmbH) with bis(dimethylsilyl)amine at 60°C is 33 times faster (based on the initial rate) than that with bis(dimethyl(vinyl)silyl)amine at the same temperature (and concentration). The difference in reaction rates indicates a preferred reaction of PE-OH with the amines embedded between two methylsilane moieties most likely due to steric reasons. The terminal amine formed during the initial cleavage step immediately reacts with another PE-OH molecule via ammonia elimination. The reaction of C₂₂H₄₅-OH or PE-OH with HTT1800 goes along with a signal shift of the methylene group attached to the OH-group from 3.37 ppm to 3.7 ppm and a peak broadening.



Scheme 5.1. Linkage of the two block copolymer segments (R and R' label the rest of the PCCP HTT1800).

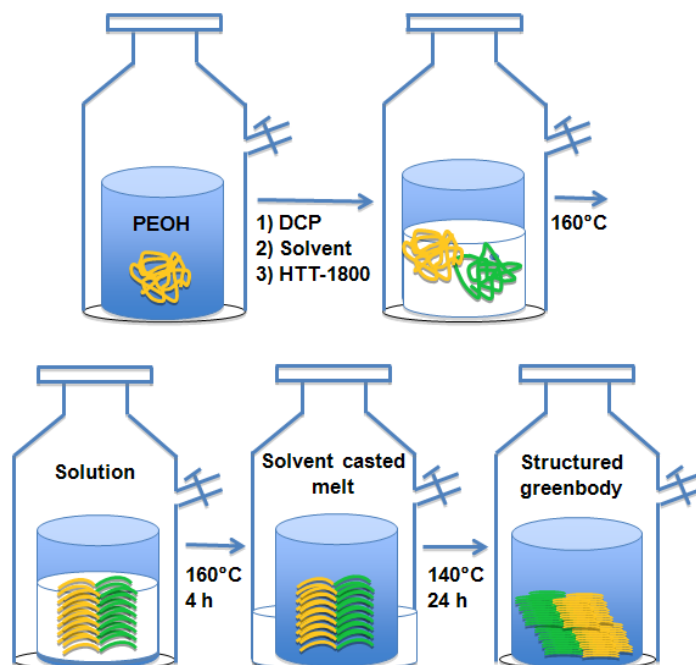


Figure 5.1. Concerted block copolymer formation, microphase separation, and crosslinking leading to PEOHTT-LAM.

To a glass vial with 25 mg of PE-OH 1 mg of dicumylperoxide, 3 mL of

5. SiCN nanofibers with a diameter below 100 nm synthesized via concerted block copolymer formation, microphase separation, and crosslinking

THF and 5 mL of cumene was added and placed in a flat bottom Schlenk tube. The Schlenk tube was heated to dissolve the PEOH. Subsequently, 25 μL of HTT1800 dissolved in 3 mL of THF were added drop by drop to the PE-OH solution. The temperature of the closed Schlenk tube was then heated to 160°C to remove the solvent (about 4 hours of time). Subsequently, the melted form of the block copolymer was annealed for 24 hours at 140°C to finalize crosslinking and microphase separation.

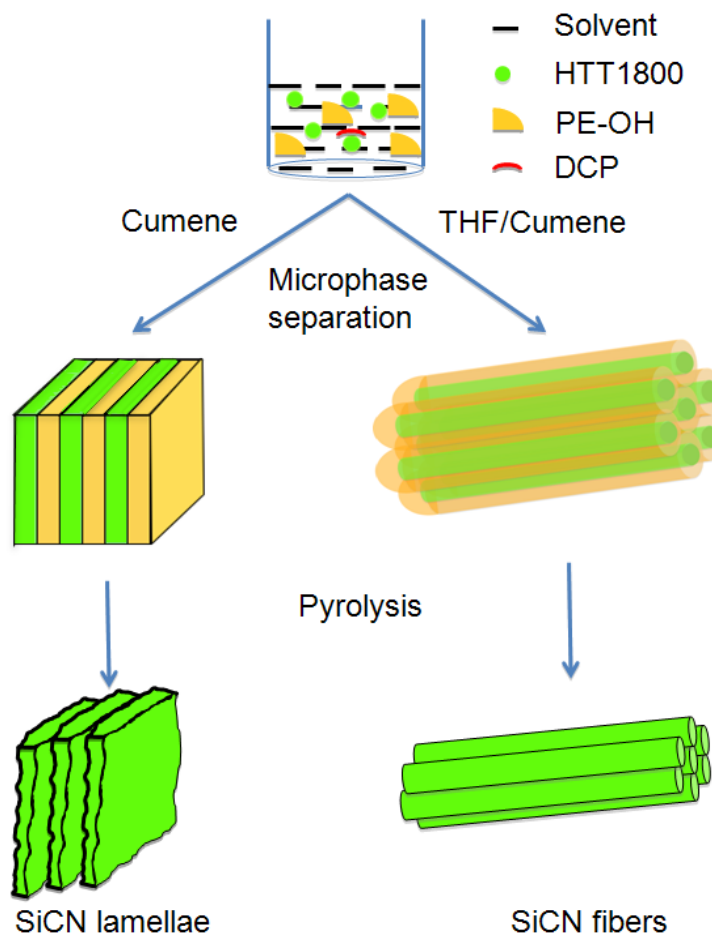


Figure 5.2. Schematic diagram of the synthetic route leading to nano-scaled SiCN lamellae and fibers.

AFM and TEM are indicative of a lamellar structuring (Figure 5. 3. a and b) having uniform domain sizes of about 25 nm. PEOHTT-LAM was pyrolysed under an argon flow: heating of 1 °C per min. to 600°C, holding time 2h at 600°C, heating of 1°C per min. to 1100°C, holding time 2 h at 1100°C, and cooling of 4°C per min. to room temperature. Under these pyrolysis conditions the lamellar structuring could be transferred into an amorphous

5. SiCN nanofibers with a diameter below 100 nm synthesized via concerted block copolymer formation, microphase separation, and crosslinking

SiCN material as indicated by SEM (Figure 5. 3. c), XRD and MAS ^{29}Si NMR (Figure SI 5. 29).

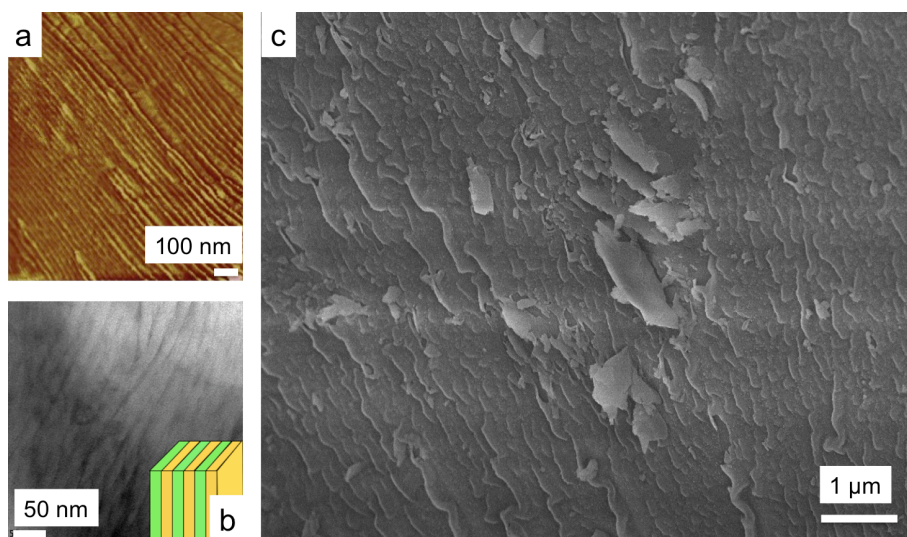
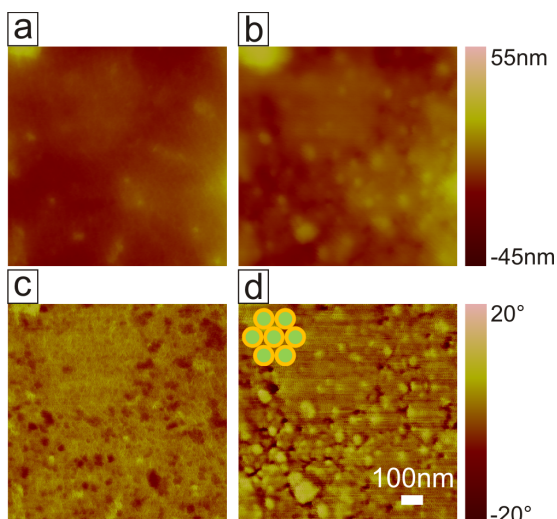


Figure 5.3. Structuring of PEOHTT-LAM. (a) AFM phase image of microphase separated and crosslinked block copolymer indicating a lamellar structure. (b) Corresponding TEM image. (c) SEM image of PEOHTT-LAM after pyrolysis at 1100 °C under an Ar atmosphere.

By changing the reaction conditions and the solvent^[11] used for the concerted block copolymer formation, microphase separation, and crosslinking steps a differently structured green body morphology was obtained (PEOHTT-FIB, see experimental section). AFM analysis of the green body of PEOHTT-FIB (Figure 5. 4) is indicative of a different nano-structuring compared to that of PEOHTT-LAM.



5. SiCN nanofibers with a diameter below 100 nm synthesized via concerted block copolymer formation, microphase separation, and crosslinking

Figure 5.4. Quasi in-situ AFM study of PEOHTT-FIB using successive low pressure plasma treatments. (a) and (b) Tapping Mode™ topography before and after etching (cumulative etch time 50 s). (c) and (d) Corresponding phase images showing rod-like structures. The raw data was acquired with a pixel density of 1024 x 1024 and a constant scan area of 3µm x 3µm (10 process steps).

As can be seen in Figure 4a, a surface rather homogeneously covered by PE is observed in the first place. PE is removed by plasma etching and the number of rod-like structures increases with prolonged etching time (Figure 5.4b and d). We use the quasi in-situ AFM imaging technique^[21] in order to reveal the underlying structures. Series of registered AFM images (topography and phase) indicate that these embeddings are actually cylindrical. They were very hard to be etched off as expected for crosslinked carbosilazanes. The embeddings are below 100 nm in diameter (Figure 5.4d). The PEOHTT-FIB greenbody is a transparent monolith and was synthesized as a tablet having a diameter of about 22 mm and thickness of about 2-3 mm (Figure 5.5).

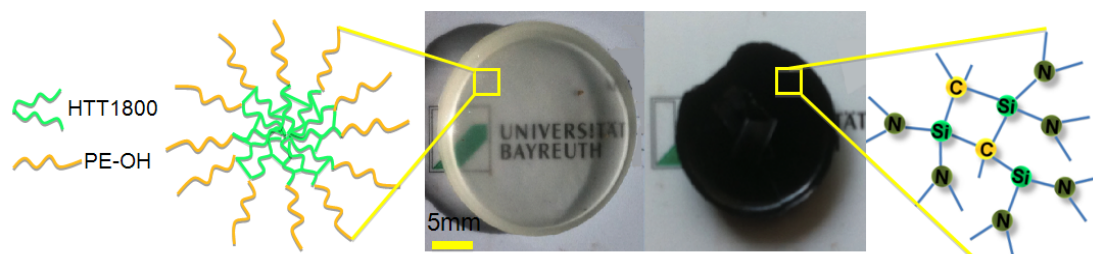


Figure 5.5. PEOHTT-FIB monolith as transparent greenbody and after pyrolysis at 1100 °C.

PEOHTT-FIB was pyrolyzed under an argon flow with a slightly modified program in comparison to PEOHTT-LAM, for details see experimental section. Pyrolysis of PEOHTT-FIB led to a monolith, reduced in size to a diameter of about 19 mm (Figure 5.5), consisting of amorphous SiCN phases as confirmed by XRD and solid state NMR spectroscopy. SEM analysis of the pyrolyzed sample of PEOHTT-FIB indicates that it consists of SiCN nanofibers (Figure 5.6 and 5.7). The fibers have a rather small diameter distribution with a mean diameter of about 45 nm (Figure 5.6c, inset). A cross

5. SiCN nanofibers with a diameter below 100 nm synthesized via concerted block copolymer formation, microphase separation, and crosslinking

section view (Figure 5.7a) indicates a large aspect ratio of the fibers exceeding 100 in the fiber bundles. Furthermore, the fibers seem to partially interpenetrate with each other. The packing of the fibers leads to mesopores. N₂ adsorption/desorption studies of pyrolyzed PEOHTT-FIB indicate a rather narrow pore size distribution with a mean pore size of about 4.5 nm and a surface area of 17 m²/g was calculated using the Brunauer-Emmett-Teller (BET) method. Initial efforts to separate the fibers from the fiber bundle via sonication lead to isolated fibers that were analyzed by TEM (Figure 5.7b).

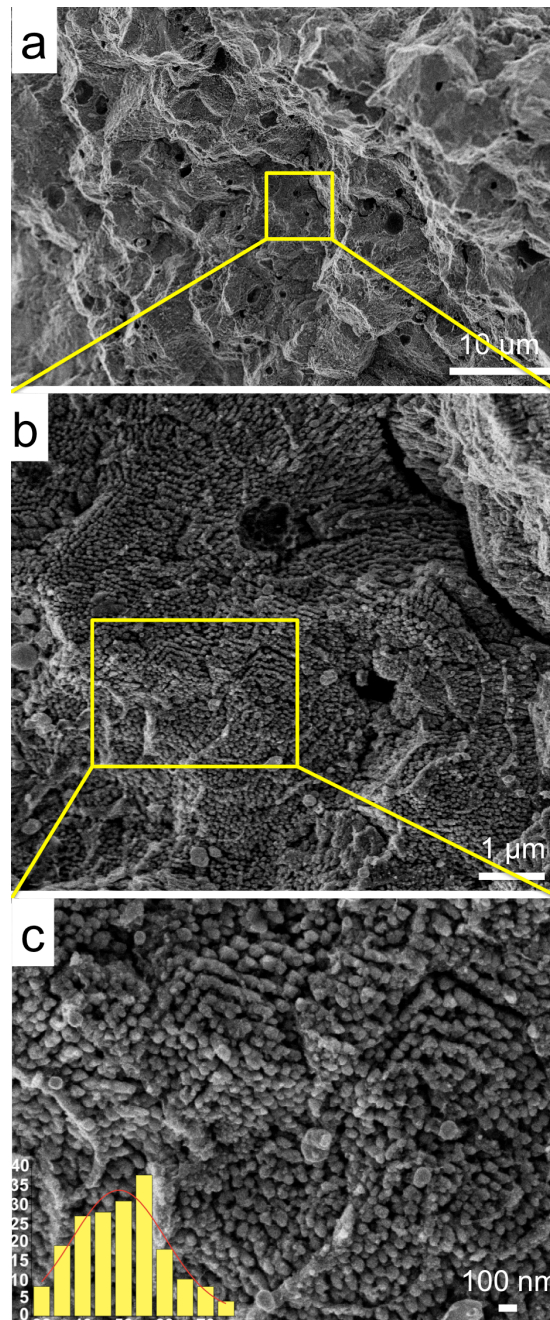


Figure 5.6. SEM image of SiCN fibers. (a) Overview and (b and c) insets with fiber diameter distribution.

5. SiCN nanofibers with a diameter below 100 nm synthesized via concerted block copolymer formation, microphase separation, and crosslinking

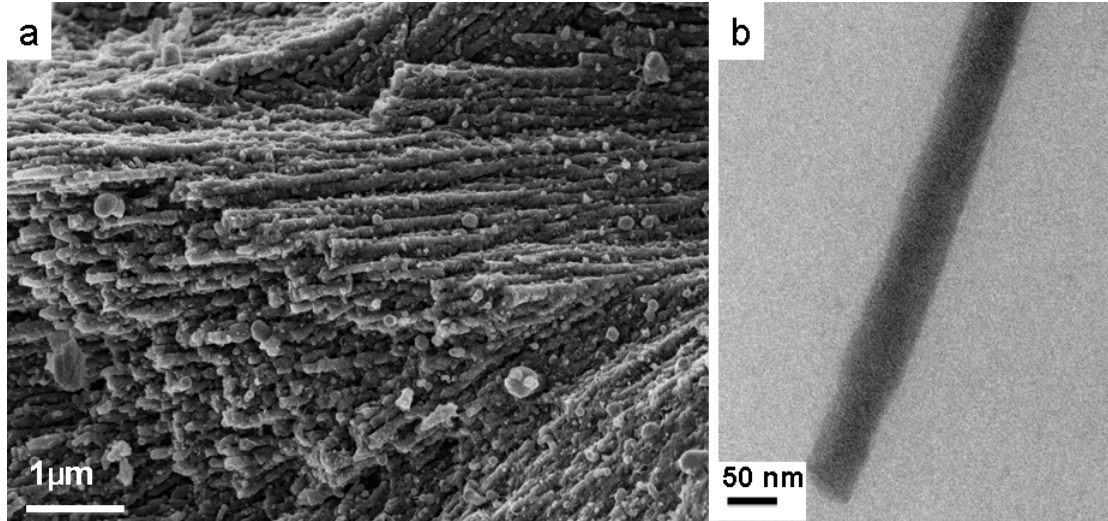


Figure 5.7. Selected additional characterization data of pyrolyzed PEOHTT-FIB. (a) SEM cross-section view indicating the large aspect ratio. (b) TEM of an isolated fiber.

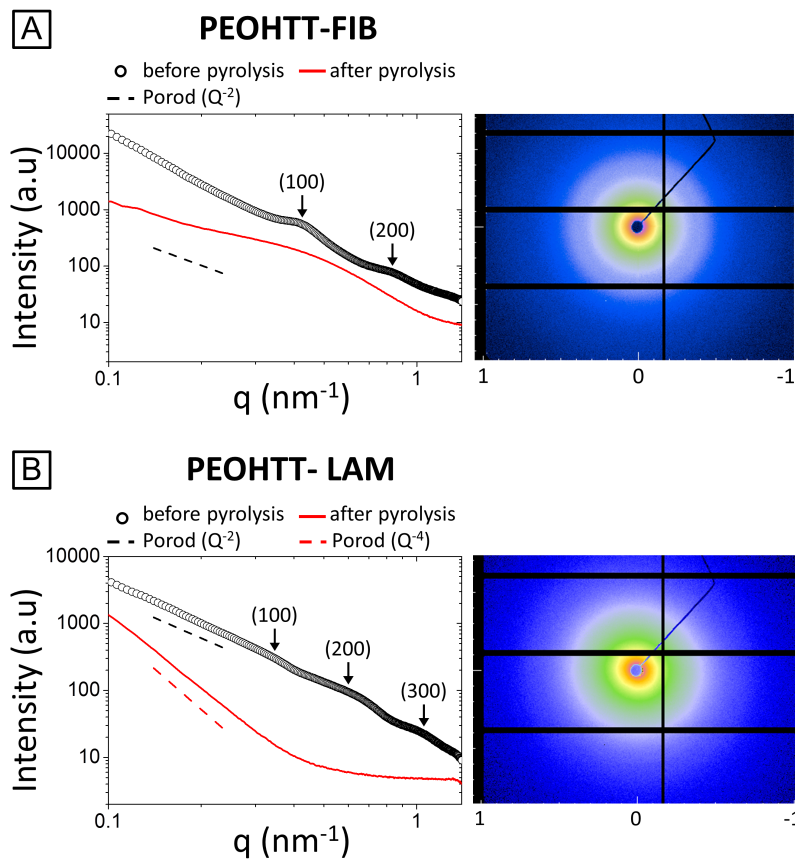


Figure 5.8. a) SAXS patterns for SiCN fibers and PEOHTT-FIB with 2D scattering image of PEOHTT-FIB. b) SAXS patterns for PEOHTT-LAM and SiCN lamellae with 2D scattering image of PEOHTT-LAM.

The SAXS-pattern measured for PEOHTT-FIB before

5. SiCN nanofibers with a diameter below 100 nm synthesized via concerted block copolymer formation, microphase separation, and crosslinking

pyrolysis is dominated by a q^{-2} -scattering typical for layered structures (Figure 5.8). We observe two weak diffraction peaks at $q = 0.42$ and 0.84 nm^{-1} which corresponds to a lamellar lattice structure with a long period (unit cell size) of 15 nm .^[22] A comparison with the SEM-images suggests that the fibers are arranged in layers, rather than in a hexagonal lattice. The SAXS patterns obtained for the SiCN fibers is only weakly structured, with a broad shoulder from 0.2 to 0.8 nm^{-1} . The SAXS patterns of PEOHTT-LAM before pyrolysis is similarly dominated by a q^{-2} - scattering typical for layered structures. We observe weak diffraction peaks at 0.35 , 0.7 and 1.05 nm^{-1} (Figure 5.8) which corresponds to a lamellar lattice structure with a unit cell size of 18 nm .^[22] After pyrolysis, the scattering is dominated by a Porod q^{-4} - surface scattering typical for smooth surfaces in accordance with the SEM-images.

5.3. Conclusion

In summary, the formation of ultrathin SiCN fibers having a large aspect ratio is reported. The fibers were made from inexpensive starting materials, namely a commercially available carbosilazane that is annually produced in ton scale and high density polyethylene carrying an OH-end group. The production process is a one pot synthesis procedure followed by pyrolysis. The first step includes a concerted block copolymer formation, crosslinking, and microphase separation. Despite the concerted nature of the greenbody synthesis and the rather broad polydispersities of the two block copolymer components a good degree of structure control was observed. Variation of the solvent used leads to a differently structured SiCN material. The ultrathin SiCN fibers may find applications in electronic devices, as components of ceramic matrix composites, as fiber beds in high temperature nano-filtering like diesel fine dust removal, or as a thermally robust and chemically inert catalyst support.

5.4. Acknowledgement

Financial support from the Deutsche Forschungsgemeinschaft, SFB 840, is gratefully acknowledged. We also thank Justus Hermannsdörfer for recording the TEM images, Wolfgang Milius for XRD studies and Renee Siegel for recording the MAS NMR spectra. Supporting Information is available online

from Wiley InterScience or from the author.

5.5. References

- [1] a) K. Liu, N. Zhao, E. Kumacheva, *Chem. Soc. Rev.* **2011**, *40*, 656–671; b) H.–G. Liao, L. Cui, S. Whitelam, H. Zheng, *Science* **2012**, *336*, 1011–1014; c) W.–S. Chang, J. W. Ha, L. S. Slaughter, S. Link, *Proc. Natl. Acad. Sci. USA* **2010**, *107*, 2781–2786; d) P. Zijlstra, J. W. M. Chon, M. Gu, *Nature* **2009**, *459*, 410–413.
- [2] a) D. Eder, *Chem. Rev.* **2010**, *110*, 1348–1385; b) K. Otsubo, Y. Wakabayashi, J. Ohara, S. Yamamoto, H. Matsuzaki, H. Okamoto, K. Nitta, T. Uruga, H. Kitagawa, *Nat. Mater.* **2011**, *10*, 291–295; c) F. Xiong, A. D. Liao, D. Estrada, E. Pop, *Science* **2011**, *332*, 568–570; d) J. Foroughi, G. M. Spinks, G. G. Wallace, J. Oh, M. E. Kozlov, S. Fang, T. Mirfakhrai, J. D. W. Madden, M. K. Shin, S. J. Kim, *Science* **2011**, *334*, 494–497.
- [3] a) H. M. T. Galvis, J. H. Bitter, C. B. Khare, M. Ruitenbeek, A. L. Dugulan, K. P. de Jong, *Science* **2012**, *335*, 835–838; b) M. Hasegawa, M. Iyoda, *Chem. Soc. Rev.* **2010**, *39*, 2420–2427; c) S. Shen, A. Henry, J. Tong, R. Zheng, G. Chen, *Nat. Nanotechnol.* **2010**, *5*, 251–255.
- [4] Polymer Derived Ceramics (Eds: P. Colombo, G. D. Sorarú, R. Riedel, A. Kleebe, D. E. Stech), Publications Inc., Lancaster USA **2010**.
- [5] M. Zaheer, T. Schmalz, G. Motz, R. Kempe, *Chem. Soc. Rev.* **2012**, *41*, 5102–5116.
- [6] M. Kamperman, A. Burns, R. Weissgraeber, N. van Vegten, S. C. Warren, S. M. Gruner, A. Baiker, U. Wiesner, *Nano Lett.* **2009**, *9*, 2756–2762.
- [7] a) C. B. W. Garcia, C. Lovell, C. Curry, M. Faight, Y. Zhang, U. Wiesner, *J. Polym. Sci. B: Polym. Phys.* **2003**, *41*, 3346–3350; b) M. Kamperman, C. B. W. Garcia, P. Du, H. S. Ow, U. Wiesner, *J. Am. Chem. Soc.* **2004**, *126*, 14708–14709.
- [8] a) M. Kamperman, P. Du, R. O. Scarlat, E. Herz, U. Werner-Zwanziger, R. Graf, J. W. Zwanziger, H. W. Spiess, U. Wiesner, *Macromol. Chem. Phys.* **2007**, *208*, 2096–2108; b) M. Kamperman, M. A. Fierke, C. B. W. Garcia, U. Wiesner, *Macromolecules* **2008**, *41*, 8745–8752; c) J. L.

5. SiCN nanofibers with a diameter below 100 nm synthesized via concerted block copolymer formation, microphase separation, and crosslinking

- Wan, A. Alizadeh, S. T. Taylor, P. R. L. Malenfant, M. Manoharan, S. M. Loureiro, *Chem. Mater.* **2005**, *17*, 5613–5617; d) J. Wan, P. R. L. Malenfant, S. T. Taylor, S. M. Loureiro, M. Manoharan, *Mater. Sci. Eng. A* **2007**, *463*, 78–88.
- [9] a) Q. D. Nghiem, D. -P. Kim, *Adv. Mater.* **2007**, *19*, 2351–2354; b) C. T. Nguyen, P. H. Hoang, J. Perumal, D. -P. Kim, *Chem. Commun.* **2011**, *47*, 3484–3486; c) N. Q. Dat, N. C. Thanh, D.-P. Kim, *J. Polym. Sci. Part A* **2008**, *46*, 4594–4601.
- [10] K. Matsumoto, J. Nakashita, H. Matsuoka, *J. Polym. Sci. Part A* **2006**, *44*, 4696–4707.
- [11] P. R. L. Malenfant, J. Wan, S. T. Taylor, M. Manoharan, *Nat. Nanotechnol.* **2007**, *2*, 43–46.
- [12] B. H. Jones, T. P. Lodge, *J. Am. Chem. Soc.* **2009**, *131*, 1676–1677.
- [13] a) G. Motz, R. Bordia, Chapter 11: Processing, structure and properties of ceramic fibers in *Handbook of Textile Fibre Structure*, Vol 2 (Eds: S. J. Eichhorn, J. W. S. Hearle, M. Jaffe, T. Kikutani), Woodhead Publishing Ltd., Cambridge UK **2009**, 378–424; b) G. Motz, S. Bernard, Chapter 5.3: Polymer-Derived Ceramic Fibers (PDCFs) in *Polymer Derived Ceramics* (Eds: P. Colombo, G. D. Sorarú, R. Riedel, A. Kleebe, D. E. Stech), Publications Inc., Lancaster USA **2010**, pp. 341–358.
- [14] M. Seo, M. A. Hillmyer, *Science* **2012**, *336*, 1422–1425.
- [15] R. M. Pike, *J. Org. Chem.* **1961**, *26*, 232–236.
- [16] R. Kempe, *Chem. Eur. J.* **2007**, *13*, 2764–2773.
- [17] Based on Mg alkyls: a) J.-F. Pelletier, A. Mortreux, X. Olonde, K. Bujadoux, *Angew. Chem. Int. Ed. Engl.* **1996**, *35*, 1854–1856; b) J.-F. Pelletier, K. Bujadoux, X. Olonde, E. Adisson, A. Mortreux, T. Chenal, US 5779942, **1998**; c) T. Chenal, X. Olonde, J.-F. Pelletier, K. Bujadoux, A. Mortreux, *Polymer* **2007**, *48*, 1844–1856.
- [18] Based on Zn alkyls: a) G. J. P. Britovsek, S. A. Cohen, V. C. Gibson, P. J. Maddox, M. van Meurs, *Angew. Chem., Int. Ed.* **2002**, *41*, 489–491; b) G. J. P. Britovsek, S. A. Cohen, V. C. Gibson, M. van Meurs, *J. Am. Chem. Soc.* **2004**, *126*, 10701–10712; c) M. van Meurs, G. J. P. Britovsek, V. C. Gibson, S. A. Cohen, *J. Am. Chem. Soc.* **2005**, *127*,

5. SiCN nanofibers with a diameter below 100 nm synthesized via concerted block copolymer formation, microphase separation, and crosslinking

- 9913–9923; d) H. Kaneyoshi, Y. Inoue, K. Matyjaszewski, *Macromolecules* **2005**, *38*, 5425–5435; e) J. O. Ring, R. Thomann, R. Mülhaupt, J.–M. Raquez, P. Degee, P. Dubois, *Macromol. Chem. Phys.* **2007**, *208*, 896–902; f) W. Zhang, L. R. Sita, *J. Am. Chem. Soc.* **2008**, *130*, 442–443; g) W. Zhang, J. Wei, L. R. Sita, *Macromolecules* **2008**, *41*, 7829–7833; h) J. Wei, W. Zhang, R. Wickham, L. R. Sita, *Angew. Chem. Int. Ed.* **2010**, *49*, 9140–9144; i) C. Giller, G. Gururajan, L. Wie, W. Zhang, W. Hwang, D. B. Chase, J. F. Rabolt, L. R. Sita, *Macromolecules* **2011**, *44*, 471–482.
- [19] Based on Al alkyls: a) J. S. Rogers, G. C. Bazan, *Chem. Commun.* **2000**, 1209–1210; b) G. C. Bazan, J. S. Rogers, C. C. Fang, *Organometallics* **2001**, *20*, 2059–2064; c) C. J. Han, M. S. Lee, D.–J. Byun, S. Y. Kim, *Macromolecules* **2002**, *35*, 8923–8925; d) G. Mani, F. P. Gabbaï, *Angew. Chem. Int. Ed.* **2004**, *43*, 2263–2266; e) G. Mani, F. P. Gabbaï, *J. Organomet. Chem.* **2005**, *690*, 5145–5149; f) W. P. Kretschmer, A. Meetsma, B. Hessen, T. Schmalz, S. Qayyum, R. Kempe, *Chem. Eur. J.* **2006**, *12*, 8969–8978; g) C. Döring, W. P. Kretschmer, R. Kempe, *Eur. J. Inorg. Chem.* **2010**, *18*, 2853–2860; h) W. P. Kretschmer, T. Bauer, B. Hessen, R. Kempe, *Dalton Trans.* **2010**, *39*, 6847–6852; i) J. Wei, W. Zhang, L. R. Sita, *Angew. Chem. Int. Ed.* **2010**, *49*, 1768–1772; j) I. Haas, W. P. Kretschmer, R. Kempe, *Organometallics* **2011**, *30*, 4854–4867.
- [20] S. K. T. Pillai, W. P. Kretschmer, M. Trebbin, S. Förster, R. Kempe, *Chem. Eur. J.* **2012**, *18*, 13974–13978.
- [21] a) M. Hund, H. Herold, *Rev. Sci. Instrum.* **2007**, *78*, 063703; b) M. Hund, H. Herold, German patent, DE 10 2004 043 191 B4 (**2006**) and US patent 7, 934, 417, (**2011**).
- [22] S. Förster, L. Apostol, W. Bras, *J. Appl. Cryst.* **2010**, *43*, 639–646.

5.6. Experimental Section (Supporting Information)

All manipulations were performed with rigorous exclusion of oxygen and moisture in Schlenk type glassware on a dual manifold Schlenk line or in an argon filled glove box (Braun 120-G) with a high-capacity recirculator (<0.1 ppm O₂). Non-halogenated solvents were dried by distillation from sodium wire/benzophenone.

¹H NMR spectra obtained using C₂D₄Cl₂ as a solvent were measured on a Varian Inova 400 operating at 400 MHz or Varian Inova 300 operating at 300 MHz, with variable temperature capability up to 120°C.

Solid-state NMR spectra of the cross-linked HTT 1800 were acquired on a DSX 400 Bruker Avance Nuclear Magnetic Resonance (NMR) spectrometer using direct-excitation Hahn-echo MAS at a 12.5 kHz rotation frequency. Pyrolyzed samples were characterized by a ramped ²⁹Si{¹H} and ¹³C{¹H} CP/MAS NMR technique and recorded on a commercial Avance II 300 Bruker spectrometer equipped with a standard triple resonance 7-mm MAS probe head.

Gel permeation chromatography (GPC) analysis was carried out on a Polymer Laboratories Ltd. (PLGPC210) chromatograph at 423 K using 1,2,4-trichlorobenzene as the mobile phase. The samples were prepared by dissolving the polymer (0.1% weight/volume) in the mobile phase solvent in an external oven and were run without filtration. The molecular weight was referenced to polyethylene (M_w = 50000 g mol⁻¹) and polystyrene (M_w = 100000–500000 g mol⁻¹) standards. The reported values are the average of at least two independent determinations.

The degradation temperature was determined with a TGA/SDTA851e (Mettler Toledo) using a heating rate of 10 K/min under nitrogen flow.

Differential scanning calorimetric (DSC) measurements were obtained using a DSC/SDTA 821 calorimeter from Mettler Toledo Instruments that was calibrated with an Indium standard. Samples were loaded into hermetically sealed aluminum pans prior to analysis. The thermal history of the samples

5. SiCN nanofibers with a diameter below 100 nm synthesized via concerted block copolymer formation, microphase separation, and crosslinking

was erased by heating the samples to 250°C and isothermally annealing for 5 min. Heating and cooling rate was 10°C per minute.

The phase separated morphology and topography were characterized using atomic force microscopy (AFM) operating in TappingMode™ under ambient conditions. For the quasi in-situ measurements the AFM (Dimension™ 3100 with a NanoScope®IV SPM controller, both from Veeco Instruments Inc., USA) is equipped with a special developed retrofit package. It replaces the original sample holder system and is described in detail in refs. S1 and S2. The image registration of the quasi in-situ data set is described in S2 (see Supporting Information). The used cantilevers from Olympus have a typical spring constant of 42 N/m and a typical resonance frequency of 300 kHz (OMCL-AC160TS). The AFM data passed through standard 2D-image processing tasks like flattening using NanoScope Analysis Software (Bruker Inc., USA). The quasi in-situ plasma etching was performed with a RF power of about 3W at a process pressure of 5 mbar (atmospheric air).

Infrared spectra of the materials were recorded using the Bruker Vektor 22 FT-IR spectrometer/PerkinElmer Spectrum 100 ATR.

The Scanning Electron Microscopy (SEM) imaging were recorded on a Zeiss LEO 1530 (2kV, 6.4mm) FESEM instrument (Zeiss, Jena, Germany). The samples were sputtered with platinum (2.0 nm) in a Cressington sputter coater 208HR to enhance conductivity.

All X-ray powder diffractograms were recorded by using a STOE STADI-P diffractometer (CuK α radiation, 1.54178 Å) in $\theta - 2\theta$ geometry and with a position sensitive detector.

Transmission electron microscopy (TEM) was carried out by using a Varian LEO 9220 (200 kV) instrument. The samples were suspended in chloroform and sonicated for 5 min. Subsequently a drop of the suspended sample was placed on a grid (Plano S 166-3) and allowed to dry.

5. SiCN nanofibers with a diameter below 100 nm synthesized via concerted block copolymer formation, microphase separation, and crosslinking

Nitrogen physisorption measurements were conducted at 77K using Quantachrome Nova 2000e instrument. Specific surface area of the samples were calculated using the Brunauer–Emmet–Teller method (5 points),^{S3} while the pore-size distributions were determined using the Barret–Joyner–Halenda model.^{S4}

5.6.1. Characterization of hydroxyl terminated PE block

The OH group terminated PE was synthesized via Coordinative Chain Trans Polymerization^{S5} and characterized via high temperature GPC and ¹H NMR spectroscopy. The Mn of 2500 gmol⁻¹ and a polydispersity of Mw/Mn = 1.9 was observed. About 80 % of the PE polymer chains carry an OH end group as determined by ¹H NMR spectroscopy.

5.6.2. Characterization of HTT-1800

The ceramic precursor HTT1800 was purchased from Clariant Advanced Materials, GmbH and stored in schlenk flask.

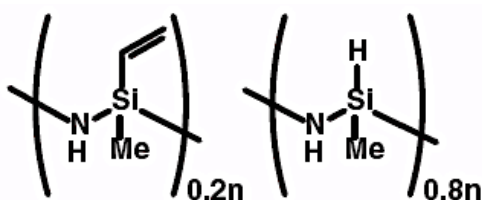


Figure 5.9. The commercially available polysilazane HTT1800 ($M_w=2640\text{gmol}^{-1}$ $M_n=893\text{ gmol}^{-1}$, $d= 1.02\text{ gmL}^{-1}$), is a statistical copolymer with 20% of methyl/vinyl and 80% of methyl/hydride-substituted silazane repeating units. A cross-linked pre-ceramic polymer can be obtained from HTT1800 with a radical initiator, dicumyl peroxide (DCP), upon heating at 130°C.

5. SiCN nanofibers with a diameter below 100 nm synthesized via concerted block copolymer formation, microphase separation, and crosslinking

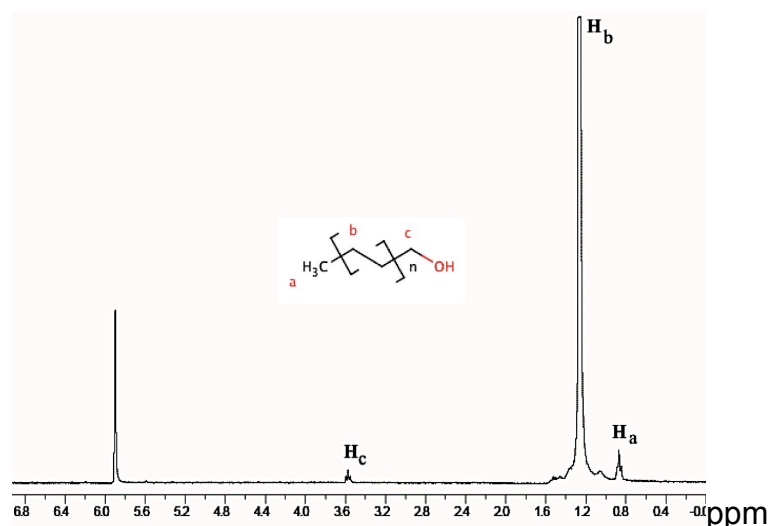


Figure 5.11. ¹H NMR spectrum of hydroxyl terminated polyethylene. Measured in C₂D₂Cl₄ at 120°C.

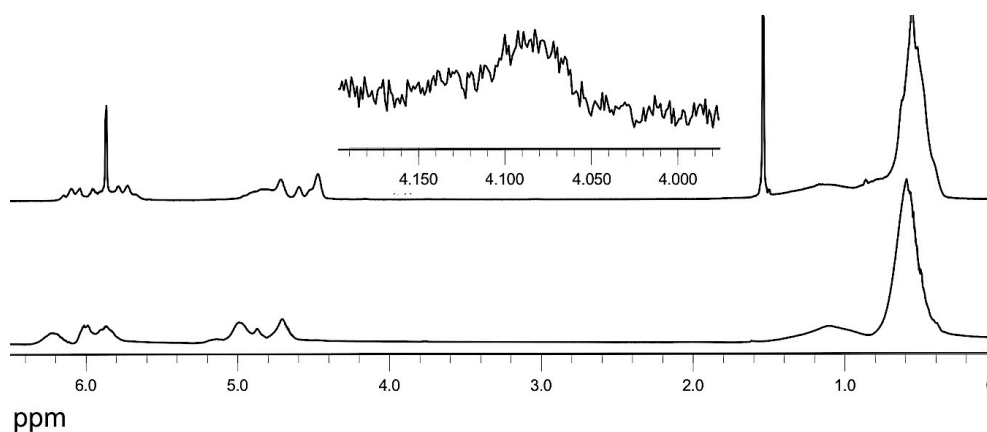


Figure 5.12. ¹H NMR spectrum of hydroxyl terminated polyethylene and HTT1800 measured in C₂D₂Cl₄ at 120°C (top). ¹H NMR spectrum of HTT1800 recorded at room temperature.

5.6.3. Synthesis of SiCN fibers

To a glass vial with 25 mg of PE-OH 1 mg of dicumylperoxide, 3 mL of THF and 5 mL of cumene was added and placed in a flat bottom Schlenk tube. The Schlenk tube was heated to dissolve the PEOH. Subsequently, 25 μ L of HTT1800 dissolved in 3 mL of THF were added drop by drop to the PE-OH solution. The temperature of the closed Schlenk tube was then heated to 160°C to remove the solvent (about 4 hours of time). Subsequently, the melted form of the block copolymer was annealed for 24 hours at 140°C to finalize crosslinking and microphase separation.

5. SiCN nanofibers with a diameter below 100 nm synthesized via concerted block copolymer formation, microphase separation, and crosslinking

PEOHTT-FIB was pyrolysed under an argon flow: heating of 2°C per minute until reaching 6 hrs hold for two hours at 600°C followed by heating up to 1100°C at 5°C per minute. The sample was hold for 2 hours at 1100°C and cooling of 4°C per minute to room temperature.

5.6.4. Characterization of cross-linked “green body”



Figure 5.10. Crosslinked green body of PEOHTT-FIB (left) and SiCN nanofiber monolith (right) after the pyrolysis. Scale bar in the figure is 5mm.

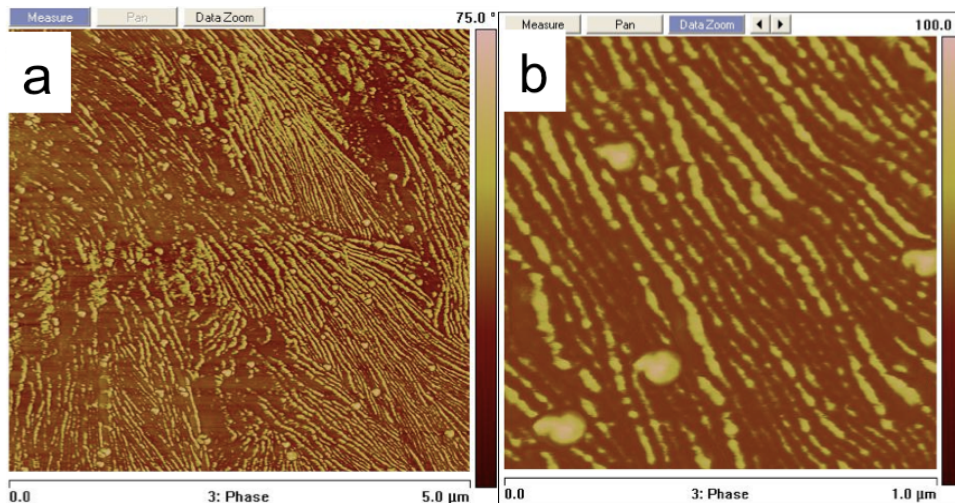


Figure 5.13. AFM phase images of synthesized, microphase separated and cross-linked copolymers PEOHTT-LAM. (a) Scan size of 5 μm x 5 μm) and (b) 1 μm x 1 μm). The phase images shows the lamellar morphology of PEOHTT-LAM.

5. SiCN nanofibers with a diameter below 100 nm synthesized via concerted block copolymer formation, microphase separation, and crosslinking

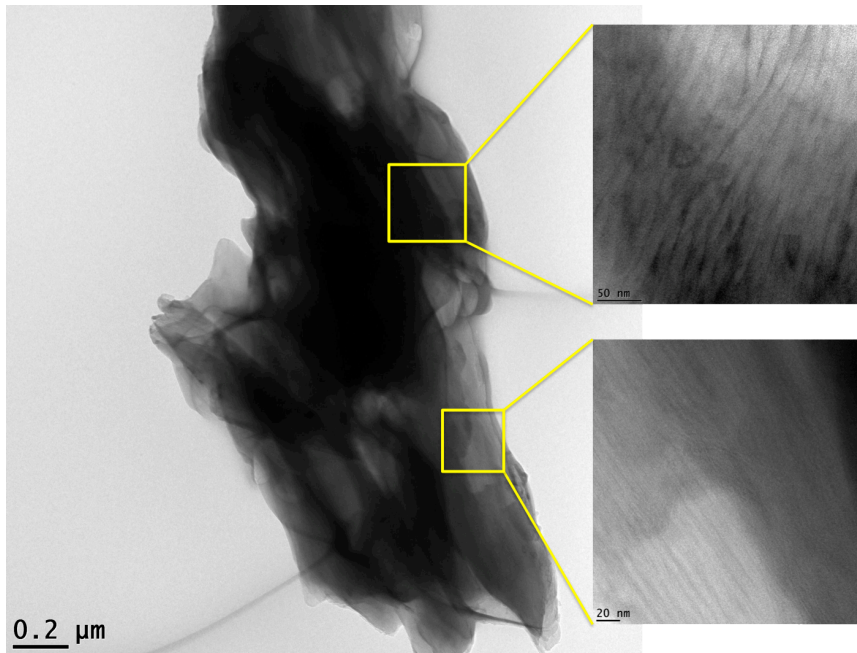


Figure 5.14. TEM image of microphase separated and crosslinked PEOHTT-LAM showing lamellar morphology.

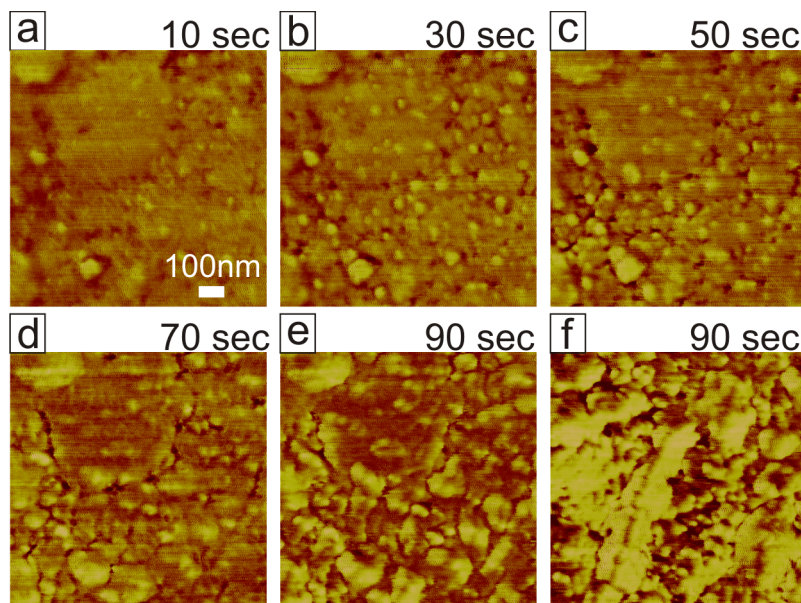


Figure 5.15. Successive low pressure plasma etching of PEOHTT-FIB having with the quasi in-situ AFM (QIS-AFM). The raw data was acquired by scanning areas of $3\mu\text{m} \times 3\mu\text{m}$ with a resolution of 1024×1024 pixels with tapping mode AFM imaging. 5 process steps of the total 10 are shown (crops). (a-e) Series of phase images after prolonged etching. (f) Different crop displaying a longitudinal direction of PEOHTT-FIB. Cumulative etching time as indicated.

5. SiCN nanofibers with a diameter below 100 nm synthesized via concerted block copolymer formation, microphase separation, and crosslinking

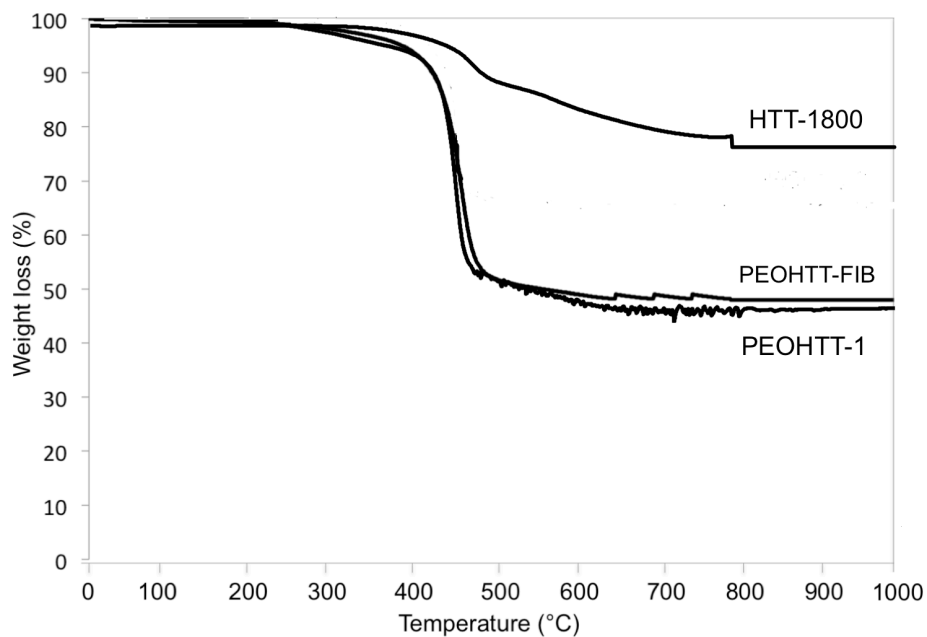


Figure 5.16. TGA of HTT-1800, PEOHTT-FIB and PEOHTT-LAM. Weight loss of 52% (PEOHTT-FIB) and 54% (PEOHTT-LAM) at 480°C correspond to the loss of PE block.

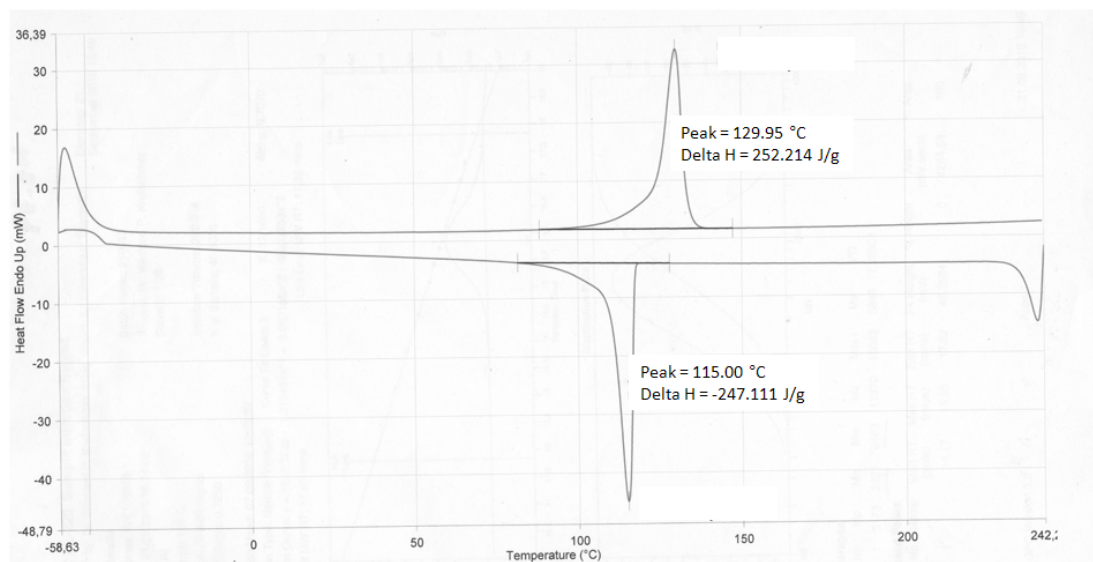


Figure 5.17. DSC of PE-OH.

5. SiCN nanofibers with a diameter below 100 nm synthesized via concerted block copolymer formation, microphase separation, and crosslinking

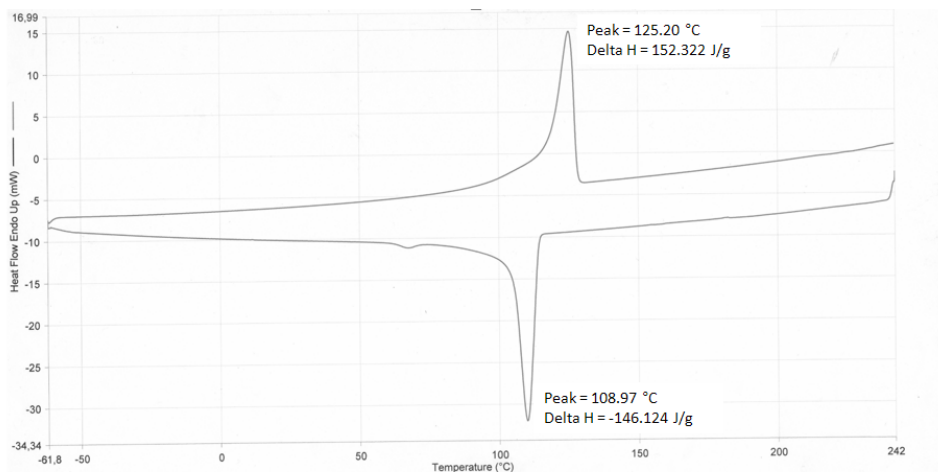


Figure 5.18. DSC of PEOHTT-LAM/FIB without adding DCP. Observation of single peaks for melting (T_m) and cooling (T_c) temperature ensures the formation of a copolymer. Addition of HTT-1800 to PE-OH changes the T_m and T_c of PE-OH confirming the covalent link between HTT1800 and PE-OH under synthesis conditions.

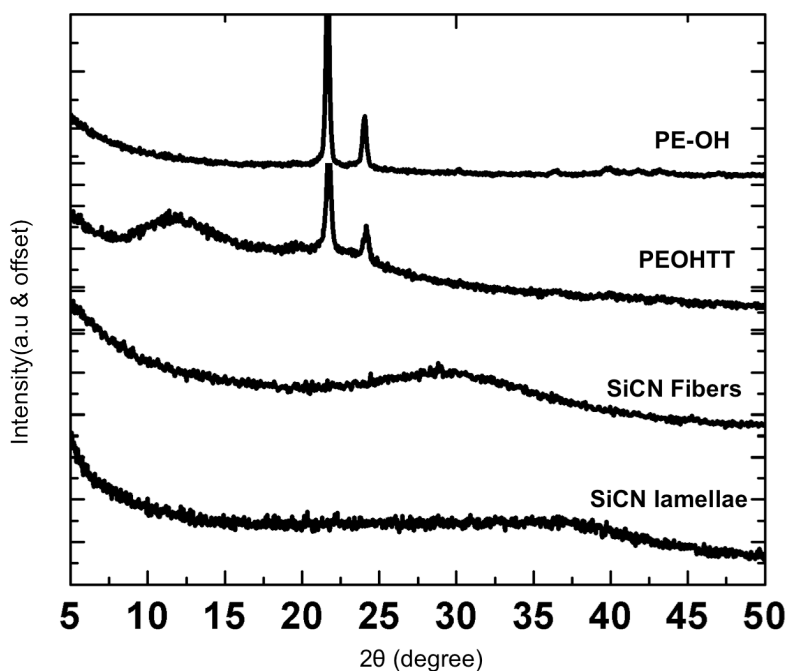


Figure 5.19. Powder XRD pattern of PEOH, PEOHTT and of PEOHTT-FIB as well as PEOHTT-LAM after pyrolysis.

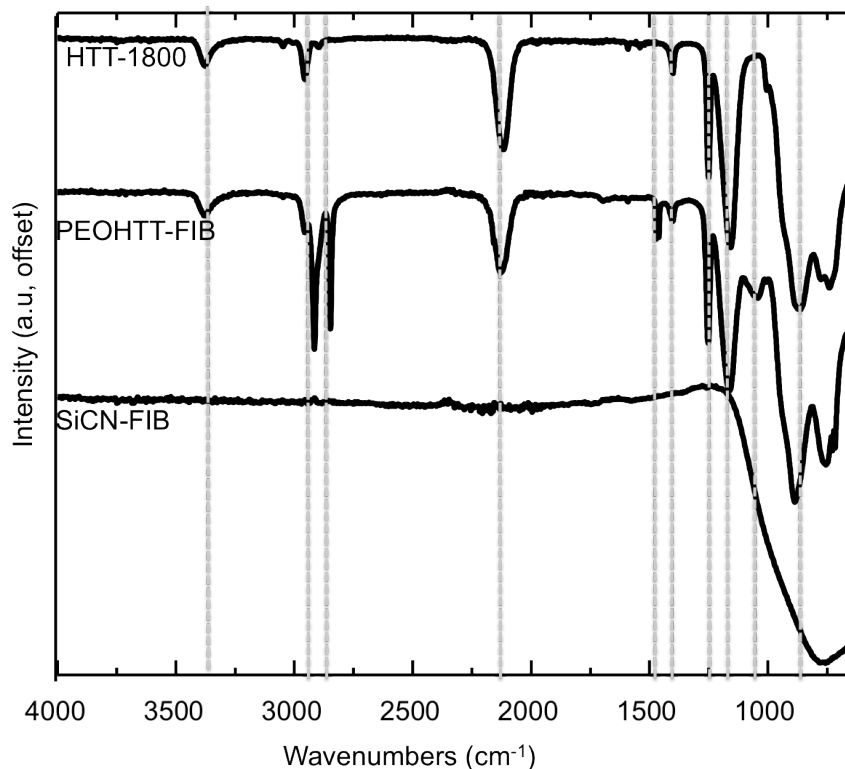


Figure 5. 20. FTIR of the HTT-1800, PEOHTT-FIB before and after pyrolysis.

5.6.5. Pyrolysis of the green body and characterization of the nano-structured SiCN material

PEOHTT-LAM was pyrolysed under argon flow with a heating rate of 1°C per minute until reaching 600°C. The sample was dwelled for two hours at 600°C followed by heating up to 1100°C at 1°C per minute. The sample was hold for 2 hours at 1100°C and then cooled down to room temperature at 4°C per minute.

PEOHTT-FIB was pyrolysed under an argon flow with a heating rate of 2°C per minute until reaching 600°C. The temperature was hold for two hours at 600°C followed by heating up to 1100°C at 5°C per minute. The sample was hold for 2 hours at 1100°C and then cooled down to room temperature at 4°C per minute.

5. SiCN nanofibers with a diameter below 100 nm synthesized via concerted block copolymer formation, microphase separation, and crosslinking

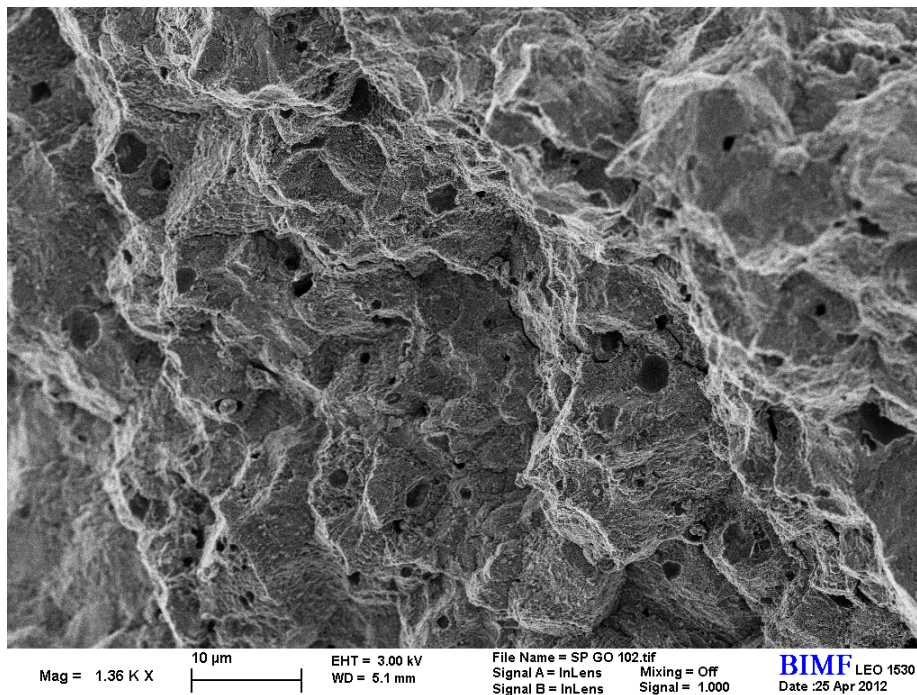


Figure 5. 21. SEM image of PEOHTT-FIB after pyrolysing at 1100°C (overview).

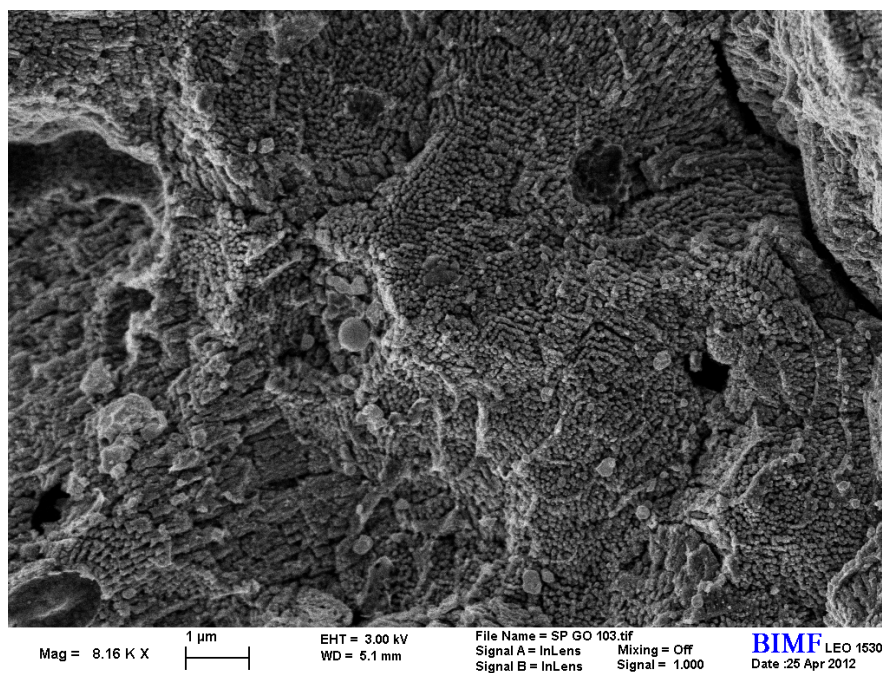


Figure 5. 22. SEM image of PEOHTT-FIB after pyrolysing at 1100°C (top view).

5. SiCN nanofibers with a diameter below 100 nm synthesized via concerted block copolymer formation, microphase separation, and crosslinking

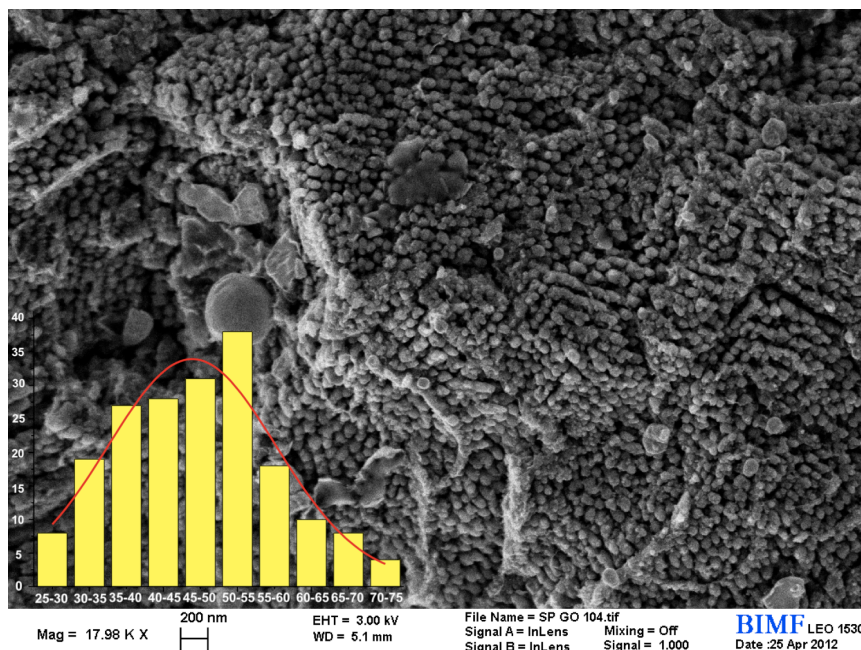


Figure 5. 23. SEM image of PEOHTT-FIB after pyrolysis at 1100°C (top view in detail). The diameter of the synthesized fibers are manually measured from the SEM image. The size distribution curve (inset) shows the range of diameter (x-axis) against the single fiber counts (y-axis).

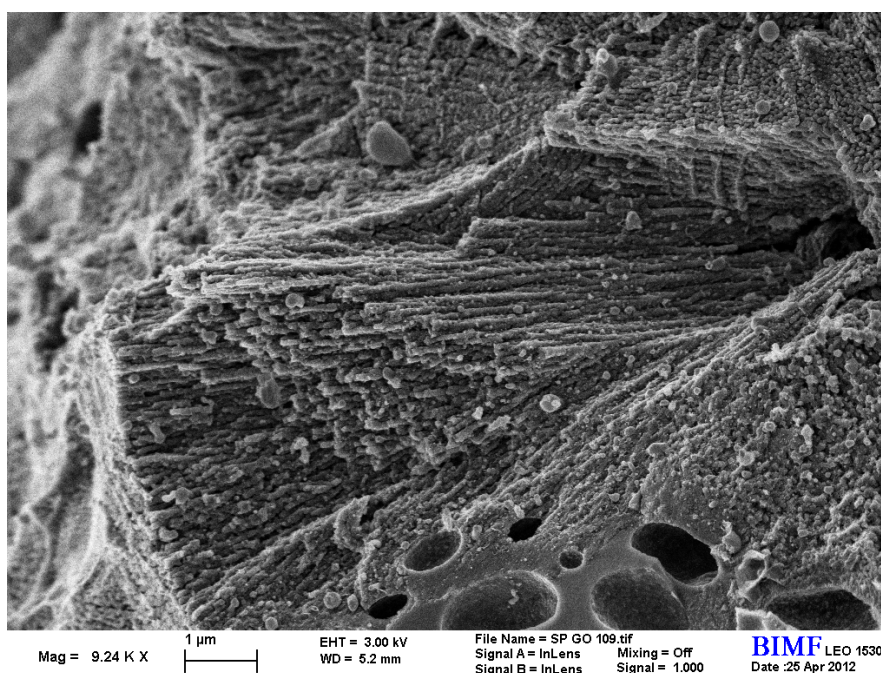


Figure 5. 24. SEM image of PEOHTT-FIB after pyrolysis at 1100°C (side view).

5. SiCN nanofibers with a diameter below 100 nm synthesized via concerted block copolymer formation, microphase separation, and crosslinking

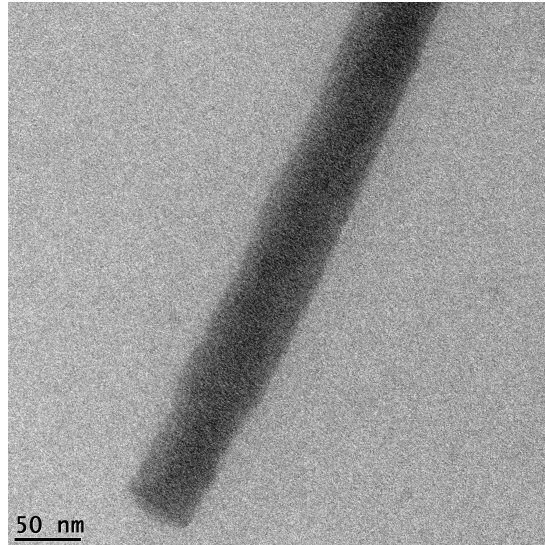


Figure 5. 25. TEM image of separated SiCN fibers. The fibers were dispersed in diethyl ether followed by sonochemical treatment.

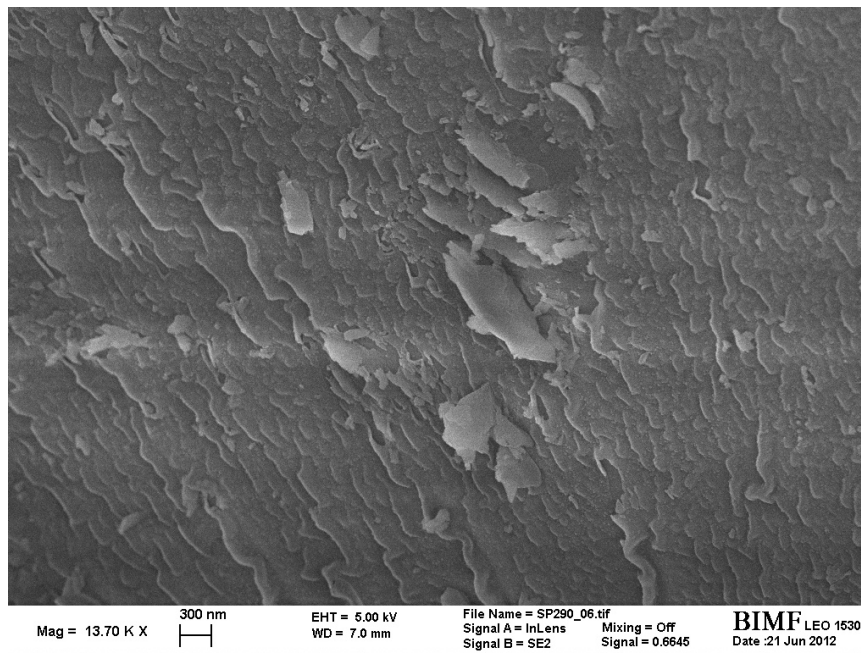


Figure 5. 26. SEM image of PEOHTT-LAM after pyrolysis at 1100°C showing SiCN layers.

5. SiCN nanofibers with a diameter below 100 nm synthesized via concerted block copolymer formation, microphase separation, and crosslinking

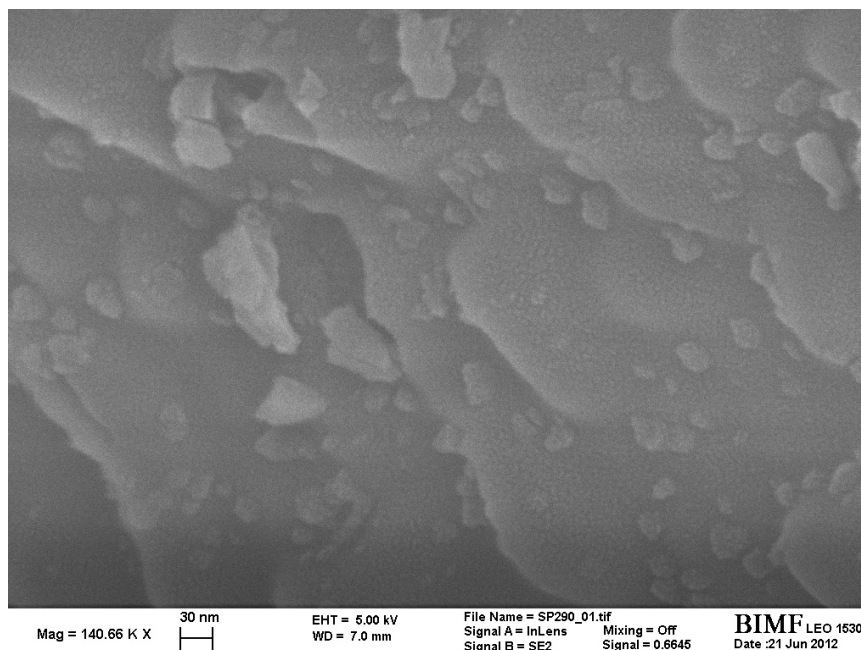


Figure 5. 27. SEM image of PEOHTT-LAM after pyrolysis at 1100°C at a higher resolution.

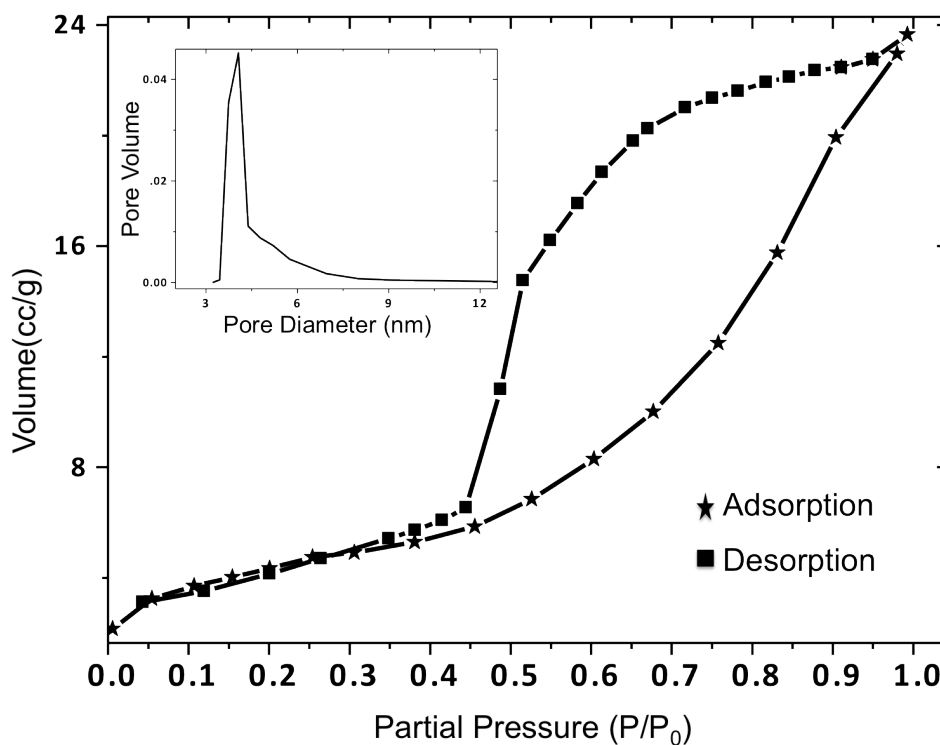


Figure 5. 28. N₂ adsorption and desorption isotherms of the SiCN nanofibers (pyrolyzed PEOHTT-FIB). The inset shows the pore size distribution (BJH method). A specific surface of 17 m²/g (BET method) was observed.

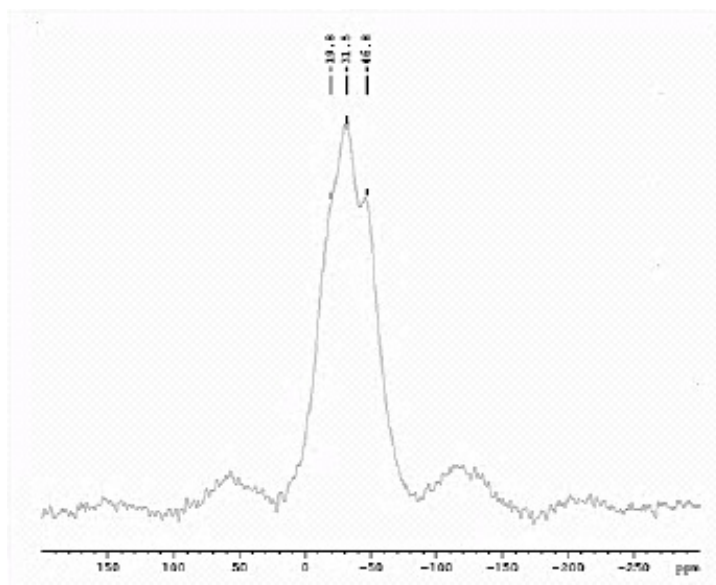


Figure 5. 29. MAS ^{29}Si NMR spectrum of the SiCN material derived from HTT1800-FIBpyrolyzed at 1100°C in an Ar-atmosphere. The main signal at -31.5 ppm is assigned to the formed SiCN₃ environments. Whereas the shoulder at -19.8 ppm and the smaller signal at -46.8 ppm corresponding to SiC₄ and SiN₄ environments, respectively [S6]. The signals and the respective chemical shifts are characteristic for a ceramic material formed from a polymeric SiCN-precursor at temperatures above 1000 °C. An identical NMR spectra is observed for HTT1800-LAM

5.7. References (Supporting Information)

- [S1] a) M.Hund, H.Herold, *Rev. Sci. Instrum.* **2007**, 78, 063703–1–6, b) M.Hund, H.Herold, Germanpatent, DE102004043191 B4 (2006) and U. S. Patent 7, 934, 417 (**2011**).
- [S2] A.Sperschneider, M.Hund, H.G.Schoberth, F.H.Schacher, L.Tsarkova, A.H.E.Müller, A.Böker, *ACS Nano* **2010**, 4, 5609–5616.
- [S3] S. Brunauer, L. S. Deming, W. E. Deming, E. J. Teller, *J. Am. Chem. Soc.* **1940**, 62, 1723–1732.
- [S4] E. P. Barrett, L. G. Joyner, P. P. Halenda, *J. Am. Chem. Soc.* **1951**, 73, 373–380.
- [S5] R. Kempe, *Chem. Eur. J.* **2007**, 13, 2764–2773.
- [S6] a) G. Ziegler, H.–J. Kleebe, G. Motz, H. Müller, W. Weibelzahl, S. Traßl, *Mater. Chem. Phys.* **1999**, 61, 55–63; b) S. Traßl, D. Suttor, G. Motz, E.Rößler, G. Ziegler, *J. Eur. Ceram. Soc.* **2000**, 20, 215–222.

6. Robustly Supported Porous Au Catalyst for the Selective Oxidation of Alkenes using Air/O₂ as an Oxidant

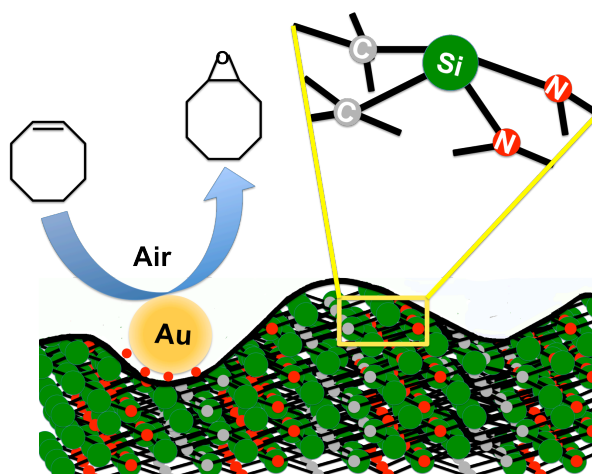
Saravana K.T. Pillai,^a Winfried P. Kretschmer,^a Torsten Irrgang,^a Martin Friedrich,^a Justus Hermannsdörfer,^a Günter Motz,^b and Rhett Kempe^{*,a}

^aLehrstuhl Anorganische Chemie II, Universität Bayreuth, Universität Bayreuth, 95440 Bayreuth, Germany, E-Mail : kempe@uni-bayreuth.de

^bLehrstuhl Keramische Werkstoffe, Universität Bayreuth, Universität Bayreuth, 95440 Bayreuth, Germany.

To be submitted

6.1. Abstract



A general synthetic procedure for mesoporous metal nanoparticles integrated SiCN supports with high surface area has been developed. The synthetic procedure consists of two steps including i) concerted block copolymerization, microphase separation, and cross-linking ii) pyrolysis at 1000°C under inert atmosphere. Hydroxyl terminated polyethylene (PE-OH) and an inexpensive commercially available polymeric carbosilazane precursor were used as organic *porogen* and inorganic ceramic precursor blocks, respectively. The linked hybrid block copolymer is structured using microphase separation in a non-polar solvent. Upon pyrolyzing, the mesostructured organic-inorganic copolymer results in the porous SiCN material with the surface area of 460 m²/g. The synthesis of metal nanoparticles supported mesoporous SiCN

catalysts with bicontinuous morphology was synthesized with surface area of by the addition of aminopyridinato complexes. The synthesized porous Au@SiCN catalysts were characterized by transmission electron microscopy, scanning electron microscopy, atomic force microscopy, powder X-ray diffractometer and nitrogen physisorption techniques. The Au@SiCN is active in oxidation of higher alkenes in the presence of air/O₂ as an oxidant. Selective epoxide formation has been observed for cycloalkenes.

6.2. Introduction

Heterogeneously catalyzed alkene oxidation using molecular oxygen or environmentally benign air as an oxidant is a burgeoning topic of interest in green chemistry/catalysis.¹ Supported gold catalysts have been used as heterogeneous catalysts for the gas phase epoxidation of lower alkenes in the presence of molecular oxygen.² Notably, Hutchings and co-workers have reported liquid phase epoxidation of cyclic alkenes by gold supported on graphite using molecular oxygen under mild and solvent free conditions.³ It is reported that high selectivity for the epoxide can be attainable only by propagating the reaction with a suitable radical initiator/co-catalyst.⁴ Afterwards, Lambert and co-workers have reported the oxidation of styrene by 1.5 nm large Au nanoparticles (generated from a Au₅₅ cluster) in the presence of molecular oxygen. No radical based co-catalyst was needed. Low conversion rates and minor styrene oxide product selectivity were observed.⁵ The olefin oxidation activity without a radical based co-catalyst was explained by the very small size of the Au particles. Styrene was converted to styrene oxide as major product and with high conversion by Choudhary and co-workers.⁶ This study was conducted with gold nanoparticles supported on various oxide supports in the presence of an anhydrous radical initiator. Caps and co-workers reported stereoselective epoxidation of trans-stilbene in methylcyclohexene.⁷ In this study, air was used as source of oxygen and solvent was also oxidized and acts as propagating radical.

Polymer derived amorphous SiCN materials were recently used as extremely robust support for various nanoparticles to study different types of catalysis.⁸ For example, copper containing SiCN catalysts were

synthesized via modification of the preceramic precursor by a copper complex.⁹ This non-porous Cu@SiCN catalyst has shown increase in selectivity for aerobic oxidation of alkanes with increasing copper loading. In another example of non porous SiCN support, palladium silicides at SiCN catalyst was synthesized for the hydrogenation of ketones via modifying precursor ceramic by a palladium complex.¹⁰ Recently, porous ceramic materials have been used as a support because porosity of the support can impact on the performance of catalysts.¹¹ For example, the metal containing macroporous SiCN catalyst for ammonia reformation was reported by Kim and coworkers using two-step synthetic procedure.¹² A macroporous SiCN was fabricated by capillary filling of preceramic polymer followed by the deposition of ruthenium metal. To simplify this two step procedure, Wiesner and co-workers have introduced one pot synthesis of metal nanoparticles supported mesostructured catalysts using block-copolymer as structural directing agent.¹³ Porous SiCN supported platinum nanoparticles have been synthesized via above mentioned approach by copolymer, ceramic precursor, and platinum complex as a part of five component system.¹⁴ The platinum SiCN catalyst synthesized by this approach has shown 44 m²/g of surface area. Recently, microporous SiCN supported nickel catalyst with 400 m²/g for semi hydrogenation of alkynes was synthesized by Kempe and co-workers.¹⁵ Controlled pyrolysis at 600°C is the reason reported for the generation of microporosity in the catalysts.

Recently, copolymers consisting out of an inorganic ceramic precursor block and an organic *porogen* block were used for the synthesis of mesostructured SiCN materials.¹⁶ These inorganic-organic copolymers are a promising tool for direct mesostructuring. Due to the covalent link between the inorganic and the organic block domain size within the mesoscale are favored during phase separation.¹⁷ Furthermore, purely organic block-copolymers have been used as structural directing agents for the synthesis of mesostructured SiCN materials.¹⁸

Herein, we report on the synthesis Au nanoparticles supported on mesoporous SiCN (Au@SiCN) and their catalytic applications in liquid phase

epoxidation of higher alkenes. The catalysts were synthesized via concerted block copolymer formation, microphase separation and cross-linking followed by pyrolysis under inert condition during which metal nanoparticle formation takes place. For the first time, we report on a metal nanoparticle decorated mesoporous SiCN support having a high surface area. Furthermore, we report on a rare example of selective alkene epoxidation with dioxygen (including high conversion) and no need of a radical based co-catalyst.

6.3. Results and Discussion

Recently, the synthesis of SiCN nanofibers adopting concerted copolymer formation, microphase separation, and cross-linking process was communicated as a promising procedure for the synthesis of mesostructured SiCN materials.^{17a} Polyethylene with a hydroxyl end group (PE-OH, Mn = 2500 gmol⁻¹, PDI = 1.9)¹⁹ and commercially available polymeric ceramic carbosilazane precursor (PCCP) were used as organic and inorganic blocks, respectively. Equal weight ratio of PE-OH and PCCP resulted (depending from the solvent used) in strong segregated morphologies such as lamellae and fibrous SiCN (Figure 6.1 a and b).

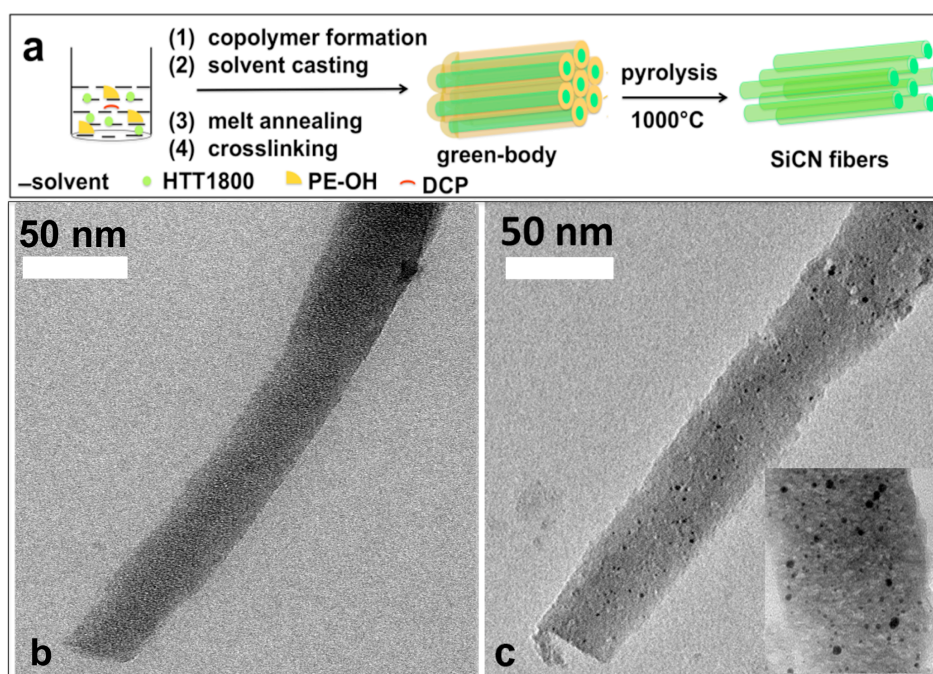


Figure 6.1. a. Schematic representation of the synthetic steps involved in SiCN fibers. b. Representative TEM image of SiCN mesofibers. c. Representative TEM images of gold nanoparticles functionalized SiCN mesofiber with the inset.

The fibrous SiCN was loaded with gold nanoparticles by the addition of a gold aminopyridinato complex (Figure 6.2)²⁰ to the solution of 50% by weight of PE-OH and PCCP. Alkene oxidation (under the conditions listed in Table 6.2) were conducted with the synthesized Au@SiCN fibers. No activity was observed in oxidation of alkenes using dioxygen. It might be due to the low surface area (50 m²/g) of the Au@SiCN fibers and the resulting low active site accessibility of the educts. In consequence, we become interested in morphologies leading to high surface area materials.

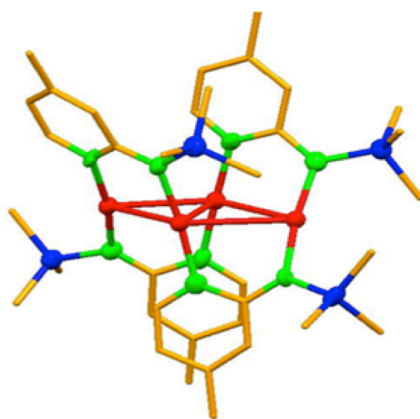


Figure 6.2. Molecular structure of [(Ap^{TMS})₄Au₄], tetrameric aminopyridinato gold (left) complex. Color code: red = gold, green = nitrogen, blue = silicon, orange = carbon.

Weak segregating bicontinuous morphologies can be attained by varying the weight ratio of PE-OH and PCCP copolymer (Figure 6.3). HTT1800 (30% by weight) was added to pore generating PE-OH (70% by weight) to prepare a block copolymer via Si-O-C bond formation. In the presence of PE-OH block selective solvent, this inorganic and organic block copolymer was microphase separated by solvent casting and melt annealing at 140°C. The microphase separated copolymer was crosslinked for 12 hours to obtain the green-body. The structure of self-assembled morphology in the green-body stage was confirmed by AFM measurements and observed to have bicontinuous morphology (Figure 6.3a-b) on the surface. The green-body can be pyrolysed at 1000°C under an argon atmosphere forming a mesoporous SiCN material. The mesoporous SiCN material was examined by transmission electron microscopy (TEM) (Figure 6.3c) and nitrogen

physisorption studies (Table 6.1).

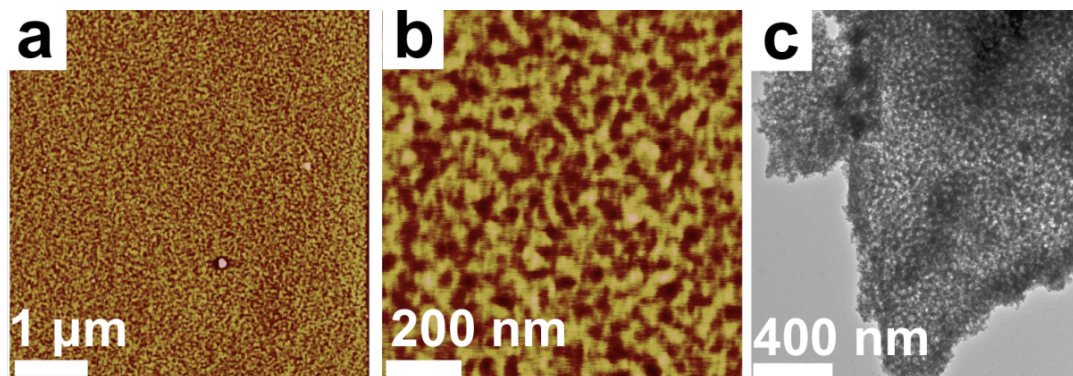


Figure 6.3. a-b. AFM images of cross-linked “green-body” of SiCN sample with surface having bicontinuous morphology. c. TEM images of mesostructured SiCN.

From the N₂ adsorption measurements (Figure 6.4a), the BET (Brunauer-Emmett-Teller) surface area of SiCN support was calculated as 460 m²/g with a mean DFT pore size (Figure 6.4b) of 9 nm (Table 6.1). The surface area is due to the elimination of the *porogen* polyethylene block. In order to calculate the yield of the synthesized SiCN material, thermo gravimetric analysis (TGA) measurements were conducted. A yield of 64% of the PCCP weight contribution was observed. The *vice versa* ratio (30% of PE-OH and 70% of PCCP) were also microphase separated and pyrolysed. The resultant SiCN material was only having a surface area of 117 m²/g and pore volume of 0.124 cc/g, which implies that the higher amount of PE-OH is required to achieve a high surface area.

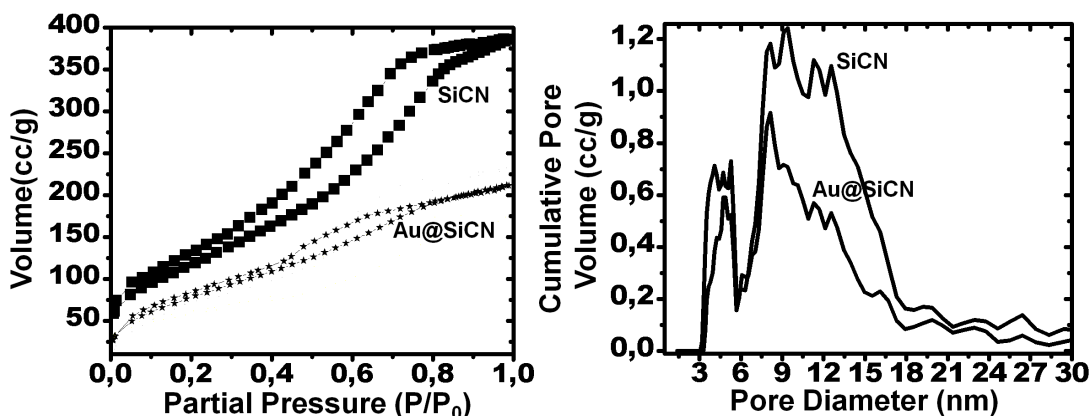


Figure 6.4. a. N₂ physisorption of SiCN and Au@SiCN. b. The pore size distribution curves of SiCN and Au@SiCN.

For the synthesis of SiCN supported metal nanoparticles a 70% of PE-OH / 30% of PCCP ratio was adopted. Following the above described copolymerisation, microphase separation, and cross-linking process, the green-body Au@SiCN was synthesized. Solvent casting was employed with an excess amount of solvent to minimize metal catalyzed cross-linking of the inorganic PCCP block during copolymer formation. The self-assembled and cross-linked green-bodies were pyrolyzed under an inert atmosphere and were characterized by TEM, SEM, TGA, powder X-ray diffraction (XRD), and nitrogen adsorption.

Table 6. 1. Summary of textural properties of synthesized materials.

sample ID	PE-OH : HTT ^a	surface area ^b (m ² /g)	pore volume (cm ³ /g) ^d
SiCN	70 : 30	460	0.553
Au@SiCN	70 : 30	300	0.350

^aWeight ratio, ^bcalculated by BET method, ^cCalculated by density functional theory (DFT), ^d Pore size distribution curve and volume histogram were used.

The yield of Au@SiCN (77% of the PCCP weight contribution) was calculated from TGA measurements (Figure 6.13), which is 13% higher than of porous SiCN (64%). The additional gain of yield Au@SiCN may be due to the contribution from the aminopyridinato complexes. Furthermore, powder XRD analysis was performed. The Au@SiCN catalyst is shown strong reflection ($\theta = 19, 22, 32, 38.5^\circ$) corresponding to the fcc planes [(111), (200), (220), and (331)] of gold nanoparticles immobilized on amorphous SiCN support (Figure 6.5d). The Debye-Scherrer equation was employed to 111 (FWHM = 2.1°) reflection peak for the measurement of an approximate size of 4.1 nm of the Au nanoparticles (Figure 6.15). The porous Au@SiCN catalyst was further analyzed by TEM (Figure 5b). The mean size of the particles measured from TEM image (3 nm) was roughly consisting with the particles size calculated by powder XRD. It is well documented that the sintering of

nanoparticles takes place when reaching the Tammann temperature of gold metal (395°C).²¹ The Au@SiCN catalyst, synthesized at 1000°C, with small particles implies that the sintering of particles has been successfully prevented. This may be due to the stabilization of particles by the N atoms of the Si-C-N network. Nitrogen physisorption measurements were conducted to the synthesized Au@SiCN catalyst (Figure 4a-b). The Au@SiCN catalyst exhibits the surface area of 300 m²/g. Comparing with the surface area of the porous SiCN sample, Au@SiCN is noticed to have a similar pore size distribution and a reduced amount of adsorbed pore volume (0.350 cm³/g) (Table I). The solid-state ²⁹Si NMR study was conducted to confirm Si-C-N phases present in all the samples. The samples are predominantly having SiC₂N₂, SiC₃N, SiCN₃ environments along with shoulder peak of SiO₃C phase which may be due to the contribution from PE-OH block (Figure 6.33).

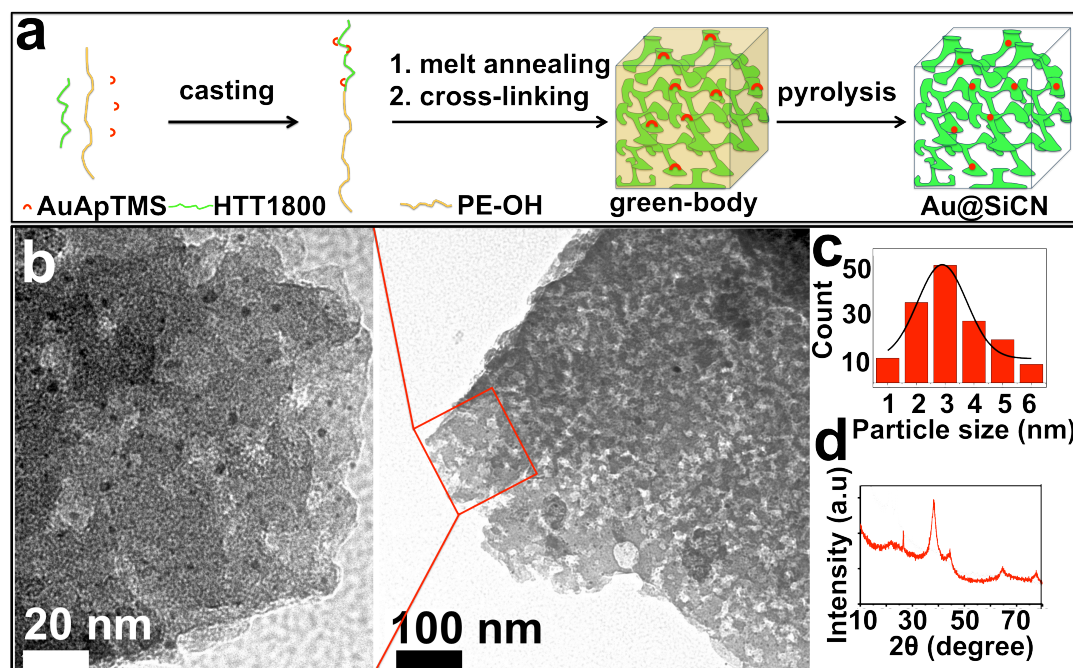


Figure 6.5. a. Schematic diagram depicting the synthesis of bicontinuously porous Au@SiCN. b. Representative TEM image of Au@SiCN. c. Particles size distribution of the gold nanoparticles counted from the TEM image. d. Powder XRD of Au@SiCN catalyst.

Epoxidation of higher alkenes was conducted with the porous Au@SiCN catalyst. Temperature dependent air oxidation was conducted with 9 mmol of cyclooctene at 1 bar with 20 mg of Au@SiCN (Figure 6.6).

Au@SiCN did show conversion at a temperature above 100°C and a selectivity of >99 % towards the epoxide. Since the conversion was maximum at 120°C, The experiment was conducted by changing the condition to high pressure.

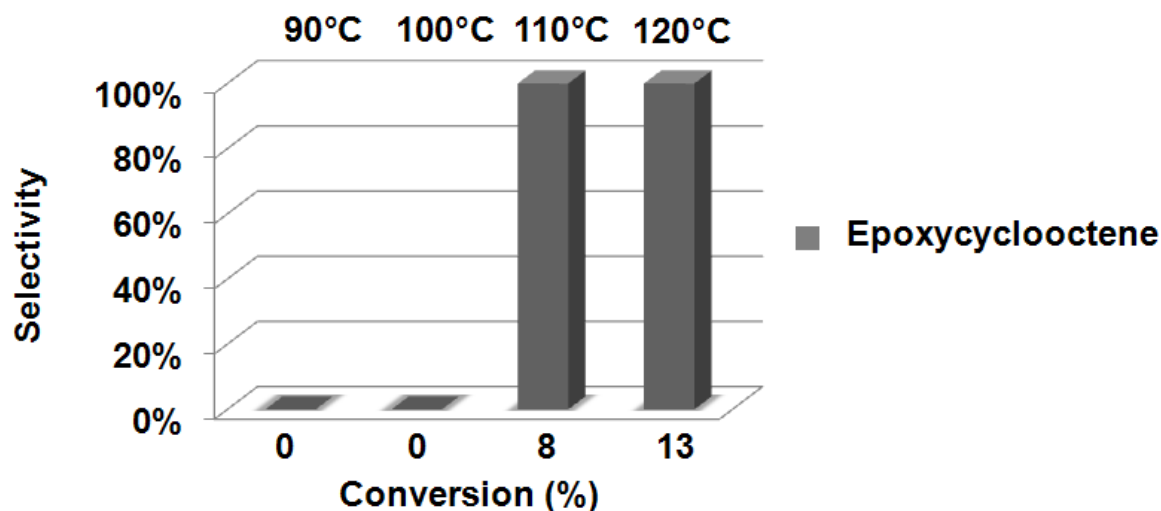


Figure 6.6. Temperature dependent study of the oxidation of cis-cyclooctene using Au@SiCN under air and at atmospheric pressure.

The Au@SiCN catalyst was active for the oxidation of alkenes under 20 bar of air (24 h) and at 120°C. The conversion was observed to be higher with cyclic alkenes than for linear alkenes (Table 6.2). In order to confirm the cyclic ring selectivity, the limonene with both linear and cyclic unsaturated double bond was studied to confirm the selectivity. The catalyst was observed to have selective towards cyclic alkenes over linear alkenes (Table 6.2). The catalyst was washed for the subsequent run with acetone followed by water then dried at 150°C for 12 hours.

Table 6.2. Catalytic results for the epoxidation with M@SiCN

Substrate	Au@SiCN	
	Conversion	Epoxide Selectivity
Cyclooctene	56	>99
Cyclododecene	51	62
Decene	10	84
(-) Limonene	47	>99*

Standard conditions: 3.0 mmol of substrate, 20 mg of catalyst (1/160 of Au/Si. 14 w% of Au). Experimental conditions were 24 hrs, 120°C, 20 bar and 3500 rpm. * cyclic epoxidized product.

6.4. Conclusion

- 1) Bicontinuous morphologies of commercially available silazanes and hydroxyl-terminated polyethylene were synthesized by concerted block copolymer formation, microphase separation, and cross-linking. The resultant morphologies were pyrolysed at 1000°C and mesoporous SiCN with high specific surface area were obtained.
- 2) Mesoporous SiCN supported gold catalyst was synthesized using the same synthetic procedure. Gold aminopyridinato metal complex was used as precursor for gold nanoparticles.
- 3) The catalytic performance of the synthesized catalysts has been demonstrated in the oxidation of cyclic and linear alkenes with air. The gold catalyst was highly selective concerning epoxide formation of cyclic alkenes.

6.5. Acknowledgments

Financial support from the Deutsche Forschungsgemeinschaft, SFB 840, is gratefully acknowledged. We thank Dr. Yamini Avadhut for recording the MAS NMR spectra and Dr. Wolfgang Milius for XRD studies. We also thank Dr. Christene Denner for SEM and Sandra Ganzleben for TGA measurements. Markus Hund is acknowledged for assisting AFM measurements. Authors acknowledge Julia Ewert for the suggestions on the figures. Supporting Information is available online from Wiley Inter Science or from the author.

6.6. References

- [1] a) M. Haruta, *Nature* **2005**, 437, 1098–1099; b) G. J. Hutchings, *Catal. Today* **2007**, 122, 196–200; c) C. H. Christensen, J. K. Norskov, *Science* **2010**, 327, 278–279. d) R. A. Sheldon, *Stud. Surf. Sci. Catal.* **1991**, 66, 33–54.P; e) Gallezot, *Catal. Today* **1997**, 37, 405–418; f) J. R. Monnier, *Appl. Catal. A* **2001**, 221, 73–91.

- [2] a) M. Haruta, *Catal. Today* **1997**, *36*, 153–166; T. Hayashi, K. Tanaka, M. Haruta, *J. Catal.* **1998**, *178*, 566–575; b) B. Chowdhury, J. J. Bravo-Suarez, M. Date, S. Tsubota, M. Haruta, *Angew. Chem.* **2006**, *118*, 426–429; *Angew. Chem. Int. Ed.* **2006**, *45*, 412–415; c) A. K. Sinha, S. Seelan, S. Tsubota, M. Haruta, *Angew. Chem. Int. Edn. Engl.* **2004**, *43*, 1546–1548; d) R. A. Sheldon, *Stud. Surf. Sci. Catal.* **1991**, *66*, 33–54; e) C. D. Pina, E. Falletta, L. Prati, M. Rossi, *Chem Soc Rev.* **2008**, *37*, 2077–2095.
- [3] M. D. Hughes, Y.–J. Xu, P. Jenkins, P. McMorn, P. Landon, D. I. Enache, A. F. Carley, G. A. Attard, G. J. Hutchings, F. King, E. H. Stitt, P. Johnston, K. Griffin, C. J. Kiely, *Nature* **2005**, *20*, 1132–1135.
- [4] a) N. Dimitratos, J. A. Lopez–Sanchez, G. J. Hutchings, *Chem. Sci.* **2012**, *3*, 20–44; b) c) G. J. Hutchings, M. Brust, H. Schmidbaur, *Chem. Soc. Rev.* **2008**, *37*, 1759–1765. d) S. Bawaked, N. F. Dummer, D. Bethell, D. W. Knight, G. J. Hutchings, *Green Chem.* **2011**, *13*, 127–134; e) H. Alshammari, P. J. Miedziak, D. W. Knight, D. J. Willock, G. J. Hutchings, *Catal. Sci. Technol.* **2013**, *3*, 1531–1539.
- [5] M. Turner, V. B. Golovko, O. P. H. Vaughan, P. Abdulkin, A. Berenguer-Murcia, M. S. Tikhov, B. F. G. Johnson, R. M. Lambert, *Nature* **2008**, *454*, 981–984.
- [6] a) N. S. Patil, B. S. Uphade, P. Jana, S. K. Bharagava, V. R. Choudhary, *J. Catal. Commun.* **2010**, *12*, 127–134; b) a) N. S. Patil, B. S. Uphade, P. Jana, S. K. Bharagava, V. R. Choudhary, *Chem. Lett.* **2004**, *33*, 400–401.
- [7] a) P. Lignier, F. Morfin, S. Mangematin, L. Massin, J. L. Rousset, V. Caps, *Chem. Commun.* **2007**, 186–188; b) P. Lignier, F. Morfin, L. Piccolo, J. L. Rousset, V. Caps, *Catal. Today* **2007**, *122*, 284–291.
- [8] M. Zaheer, T. Schmalz, G. Motz, R. Kempe, *Chem. Soc. Rev.* **2012**, *41*, 5102–5116.
- [9] G. Glatz, T. Schmalz, T. Kraus, F. Haarmann, G. Motz, R. Kempe, *Chem. Eur. J.* **2010**, *16*, 4231–4238.
- [10] M. Zaheer, G. Motz, R. Kempe, *J. Mater. Chem.* **2011**, *21*, 18825–18831.
- [11] a) R. J. White, R. Luque, V. L. Budarin, J. H. Clark, D. J. Macquarrie,

- Chem. Soc. Rev.* **2009**, *38*, 481–494; b) J. Kärger, D. Freude, *Chem. Eng. Technol.* **2002**, *25*, 769–778.
- [12] I.–K. Sung, Cristian, M. Mitchell, D.–P. Kim, P. J. A. Kenis, *Adv. Funct. Mater.* **2005**, *15*, 1336–1342.
- [13] a) C. B. W. Garcia, C. Lovell, C. Curry, M. Faught, Y. Zhang, U. Wiesner, *J. Polym. Sci. Part B: Polym. Phys.* **2003**, *41*, 3346–3350; b) M. Kamperman, C. B. W. Garcia, P. Du, H. Ow, U. Weisner, *J. Am. Chem. Soc.* **2004**, *126*, 14708–14709; c) J. Wan, A. Alizadeh, S. T. Taylor, P. R. L. Malenfant, M. Manoharan, S. M. Loureiro, *Chem. Mater.* **2005**, *17*, 5613–5617; d) J. Wan, P. R. L. Malenfant, S. T. Taylor, S. M. Loureiro, M. Manoharan, *Mater. Sci. Eng. A* **2007**, *463*, 78–88; e) M. Kamperman, P. Du, R. O. Scarlat, E. Herz, U. Werner–Zwanziger, R. Graf, J. W. Zwanziger, H. W. Spiess, U. Wiesner, *Macromol. Chem. Phys.* **2007**, *208*, 2096–2108; f) M. Kamperman, M. A. Fierke, C. B. W. Garcia, U. Wiesner, *Macromolecules* **2008**, *41*, 8745–8752.
- [14] M. Kamperman, A. Burns, R. Weissgraeber, N. van Vegten, S. C. Waren, S. M. Gruner, A. Balkler, U. Wiesner, *Nano Lett.* **2009**, *–9*, 2756–2762.
- [15] M. Zaheer, C. D. Keenan, J. Hermannsdörfer, E. Roessler, G. Motz, J. Senker, R. Kempe, *Chem. Mater.* **2012**, *24*, 3952–3963.
- [16] a) Q. D. Nghiem, D. Kim, and D.–P. Kim, *Adv. Mater.* **2007**, *19*, 2351–2354.
- [17] a) S. K. T. Pillai, W. P. Kretschmer, C. Denner, G. Motz, M. Hund, A. Fery, M. Trebbin, S. Förster, R. Kempe, *Small* **2013**, *9*, 984–989; b) M. C. Orilall, U. Wiesner, *Chem. Soc. Rev.* **2011**, *40*, 520–535; c) F. H. Schacher, P. A. Rugar, I. Manners, *Angew. Chem. Int. Ed.* **2012**, *51*, 7898–7921; d) Y. Wang, F. Li, *Adv. Mater.* **2011**, *23*, 2134–2148.
- [18] a) C. B. W. Garcia, C. Lovell, C. Curry, M. Faught, Y. Zhang, U. Wiesner, *J. Polym. Sci. Part B: Polym. Phys.* **2003**, *41*, 3346–3350; b) M. Kamperman, C. B. W. Garcia, P. Du, H. Ow, U. Weisner, *J. Am. Chem. Soc.* **2004**, *126*, 14708–14709; c) J. Wan, A. Alizadeh, S. T. Taylor, P. R. L. Malenfant, M. Manoharan, S. M. Loureiro, *Chem. Mater.* **2005**, *17*, 5613–5617; d) J. Wan, P. R. L. Malenfant, S. T. Taylor, S. M. Loureiro, M. Manoharan, *Mater. Sci. Eng. A* **2007**, *463*, 78–88; e) P. F.

- W. Simon, R. Ulrich, H. W. Spiess, U. Wiesner, *Chem. Mater.* **2001**, *13*, 3464–3486. f) M. Kamperman, P. Du, R. O. Scarlat, E. Herz, U. Werner–Zwanziger, R. Graf, J. W. Zwanziger, H. W. Spiess, U. Wiesner, *Macromol. Chem. Phys.* **2007**, *208*, 2096–2108; g) M. Kamperman, M. A. Fierke, C. B. W. Garcia, U. Wiesner, *Macromolecules* **2008**, *41*, 8745–8752.
- [19] a) R. Kempe, *Chem. Eur. J.* **2007**, *13*, 2764–2773; b) S. K. T. Pillai, W. P. Kretschmer, M. Trebbin, S. Forster, R. Kempe, *Chem. Eur. J.* **2012**, *18*, 13974–13978.
- [20] a) G. Glatz, G. Motz, R. Kempe, *Z. Anorg. Allg. Chem.* **2008**, *634*, 2897–2902; b) R. Kempe, P. Arndt, *Inorg. Chem.* **1996**, *35*, 2644–2649.
- [21] a) M. T. Bore, H. N. Pham, E. Switzer, T. L. Ward, A. Fukuoka, A. K. Datye, *J. Phys. Chem. B* **2005**, *109*, 2873–2880; b) A. Cao, R. Lu, G. Veser, *Phys. Chem. Chem. Phys.* **2010**, *12*, 13499–13510.

6.7. Experimental Section

All the experiments were performed with rigorous exclusion of oxygen and moisture in Schlenk type glassware on a dual manifold Schlenk line or in an argon filled glove box (Braun 120-G) with a high-capacity recirculator (<0.1 ppm O₂). Non-halogenated solvents were dried by distillation from sodium wire/benzophenone. Ligand, 4-methyl-2-((trimethylsilyl)amino)pyridine (Ap^{TMS}H), was synthesised as reported literature procedure.^{S1} Synthesis of [(Ap^{TMS})₄Au₄] was carried out under the exclusion of light and the synthesized complexes were preserved at -30°C wrapping with aluminum foil.^{S2}

6.7.1. General Characterization Methods

¹H NMR spectra obtained using C₂D₄Cl₂ as a solvent were measured on a Varian Inova 400 operating at 400 MHz or Varian Inova 300 operating at 300 MHz, with variable temperature capability up to 120°C. Solid-state NMR spectra of the cross-linked HTT 1800 were acquired on a DSX 400 Bruker Avance Nuclear Magnetic Resonance (NMR) spectrometer using direct-excitation Hahn-echo MAS at a 12.5 kHz rotation frequency. Pyrolyzed samples were characterized by a ramped ²⁹Si{¹H} and ¹³C{¹H} CP/MAS NMR

technique and recorded on a commercial Avance II 300 Bruker spectrometer equipped with a standard triple resonance 7-mm MAS probe head.

Gel permeation chromatography (GPC) analysis was carried out on a Polymer Laboratories Ltd. (PLGPC210) chromatograph at 423 K using 1,2,4-trichlorobenzene as the mobile phase. The samples were prepared by dissolving the polymer (0.1% weight/volume) in the mobile phase solvent in an external oven and were run without filtration. The molecular weight was referenced to polyethylene ($M_w = 50000 \text{ g mol}^{-1}$) and polystyrene ($M_w = 100000\text{--}500000 \text{ g mol}^{-1}$) standards. The reported values are the average of at least two independent determinations.

The degradation temperature was determined with a TGA/SDTA851e (Mettler Toledo) using a heating rate of 10 K/min under nitrogen flow. Differential scanning calorimetric (DSC) measurements were obtained using a DSC/SDTA 821 calorimeter from MettlerToledo Instruments that was calibrated with an indium standard. Samples were loaded into hermetically sealed aluminum pans prior to analysis. The thermal history of the samples was erased by heating the samples to 250°C and isothermally annealing for 5 min. Heating and cooling rate was 10°C per minute.

The phase separated morphology and topography were characterized using atomic force microscopy (AFM) in tapping mode under ambient conditions by silicon cantilevers (Digital Instruments). The analysis were performed with AFM DimensionTM 3100 equipped with a NanoScope[®] IV AFM controller from Veeco Instruments Inc., USA. Silver colloidal solution was used to hold the sample to avoid sample movement while scanning. For each sample, both height and phase images were recorded (5 X 5 μm) with the maximum available number of pixels (1040 X 1040). For image analysis the recorded scans were “flattened” using the *Nanoscope* image processing software. Plasma etching was performed using USB FLECTO-10 Plasma Technology under 0.2mbarr, 100W and air.

Infrared spectra of the materials were recorded using Bruker Vektor 22

FT-IR spectrometer/PerkinElmer Spectrum 100 ATR. The Scanning Electron Microscopy (SEM) imaging were recorded on a Zeiss LEO 1530 (2kV, 6.4mm) FESEM instrument (Zeiss, Jena, Germany). The samples were sputtered with platinum (2.0 nm) in a Cressington sputter coater 208HR to enhance conductivity. All X-ray powder diffractograms were recorded by using a STOE STADI-P-diffractometer (CuK α radiation, 1.54178 Å) in $\theta - 2\theta$ geometry and with a position sensitive detector. Transmission electron microscopy (TEM) was carried out by using a Varian LEO 9220 (200 kV) instrument. The samples were suspended in chloroform and sonicated for 5 min. Subsequently a drop of the suspended sample was placed on a grid (Plano S 166-3) and allowed to dry. Nitrogen physisorption measurements were conducted at 77K using Quantachrome Nova 2000e instrument. Specific surface area of the samples was calculated using the Brunauer–Emmet–Teller (BET) method,^{S3} while the pore-size distributions were determined using the Density of Functional Theory (DFT).^{S4} The compatibility of model was studied using adsorption isotherm to fit with Nonlocal Density Functional Theory (NLDFT)^{S5} function. Gas chromatography (GC) analyses were performed using an Agilent 6890N gas chromatograph equipped with a flame ionization detection (FID) device and an Agilent 19091 J-413 FS capillary column or thermo focus GC/Trace DSQ system equipped with a HP-5MS column (30 m x 0.32 μ m x 0.25 μ m), using decane as an internal standard.

The OH group terminated PE was synthesized via Coordinative Chain Trans Polymerization^{S6} and characterized via high temperature GPC and ¹H NMR spectroscopy. Mn of 2500 gmol⁻¹ and a polydispersity of Mw/Mn = 1.9 was observed. About 80 % of the PE polymer chains carry an OH end group.

6. Robustly Supported Porous Au Catalyst and their Activity in Oxidation of Alkenes using Air/O₂ as an Oxidant

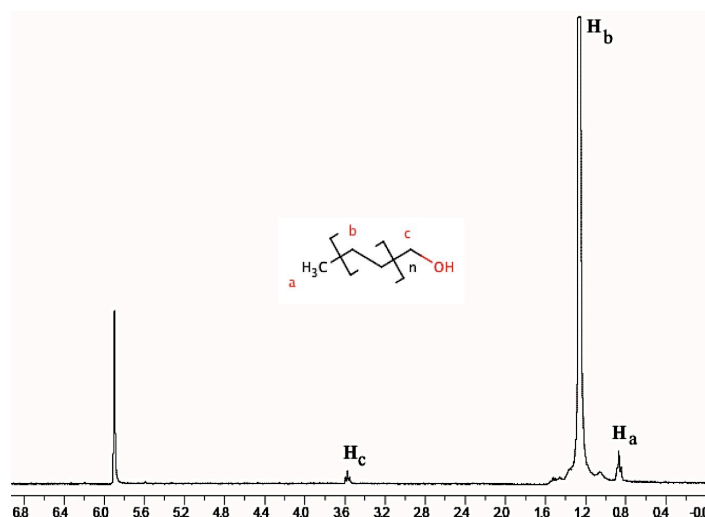


Figure 6.7. ¹H NMR spectrum of hydroxyl terminated polyethylene. Measured in C₂D₂Cl₄ at 120 °C.

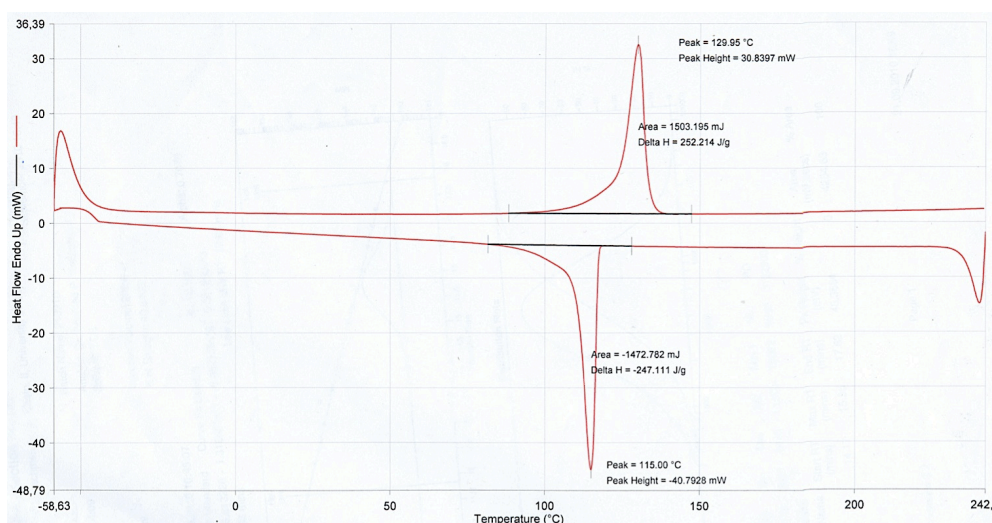


Figure 6.8. DSC result of PE-OH confirms the melting point of 129.95°C and crystallization point of 115.00°C.

The Ceramic precursor HTT1800 was purchased from Clariant Advanced Materials, GmbH and stored in schlenk flask.

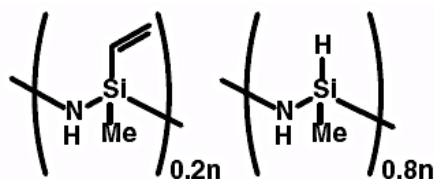


Figure 6.9. Commercially available Polysilazane, grade of HTT1800 (Mw = 2640 gmol⁻¹ Mn = 893 gmol⁻¹, d = 1.02 gmL⁻¹), is a statistical copolymer with 20% of methyl/vinyl and 80% of methyl/hydride-substituted silazane

repeating units. A cross-linked pre-ceramic polymer can be obtained from HTT1800 with a radical initiator, dicumyl peroxide (DCP), upon heating at 130°C.

6.7.2. Synthesis of SiCN and Au@SiCN

6.7.2.1. Synthesis of SiCN (30% VL-20)

To a glass vial with 200 mg of PE-OH, 4 mg of dicumylperoxide, and 8mL of toluene is added and placed in a flat bottom Schlenk tube. The Schlenk tube was heated to 140°C to dissolve the PEOH. Subsequently, 85 μL of HTT1800 was added drop by drop to the PE-OH solution. The temperature of the closed Schlenk tube is then heated to 160°C to cast the solvent (about 4 hours of time). After the solvent casting, the melt was annealed for 24 hours at 140°C to crosslinking the block copolymer. The resultant cross-linked copolymer morphology was analyzed using AFM and TEM.

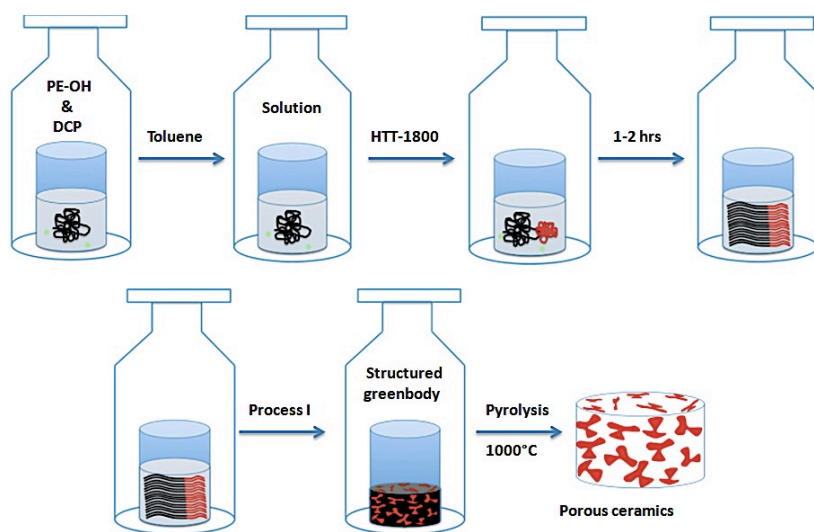


Figure 6.10. Scheme of the synthesis of the cross-linked microphase separated PE-OH-HTT1800 block copolymer (Process I = solvent casting, melt annealing, and crosslinking).

6.7.2.2. Synthesis of SiCN (70% VL-20)

To a glass vial with 85 mg of PE-OH, 4 mg of dicumylperoxide, and 8mL of toluene is added and placed in a flat bottom Schlenk tube. The Schlenk tube was heated to 140°C to dissolve the PEOH. Subsequently, 200 μL of HTT1800 was added at once to the PE-OH solution and waited to

see HTT1800 is well dispersed in the solution. Metal precursor was injected drop by drop to the above solution. The temperature of the closed Schlenk tube is then heated to 160°C to cast the solvent (about 4 hours of time). After the solvent casting, the melt was annealed for 24 hours at 140°C to crosslinking the block copolymer. The resulted cross-linked copolymer morphology was analyzed using AFM and TEM.

6.7.2.3. Synthesis of Au@SiCN

To a glass vial with 200 mg of PE-OH, 4 mg of dicumylperoxide, and 8mL of toluene is added and placed in a flat bottom Schlenk tube. The Schlenk tube was heated to 140°C to dissolve the PEOH. Subsequently, 85 μL of HTT1800 was added drop by drop to the PE-OH solution following with the injection of 30 mg of gold aminopyridinato caomplex dissolved in 1 ml of dry toluene. The temperature of the closed Schlenk tube is then heated to 160°C to cast the solvent (about 4 hours of time). After the solvent casting, the melt was annealed for 24 hours at 140°C to crosslinking the block copolymer. The resultant cross-linked copolymer morphology was analyzed using AFM and TEM.

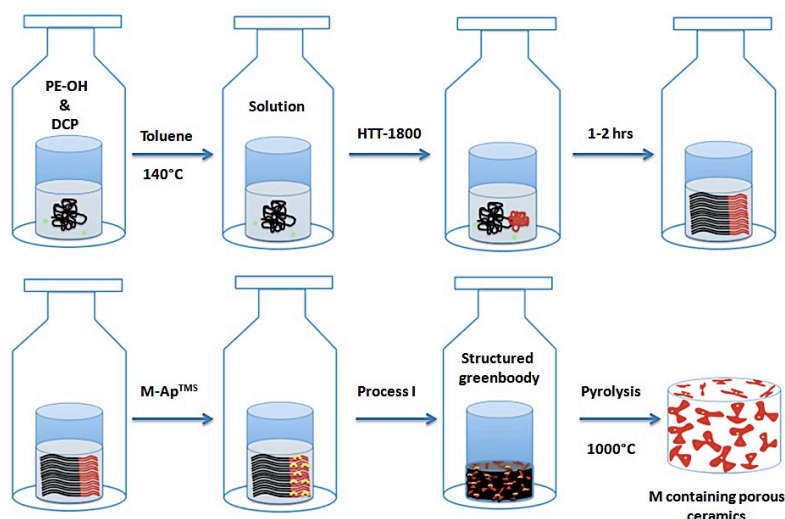
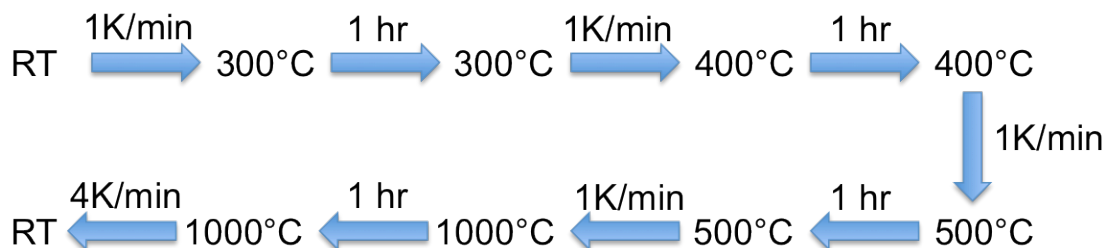


Figure 6.11. Scheme of the synthesis of the cross-linked microphase separated PE-OH-HTT1800 block copolymer (Process I = Solvent casting, Melt annealing, and Crosslinking)

SiCN and Au@SiCN was pyrolysed by the following programme.



Programme 6.1. Pyrolysis programme of Au@SiCN catalyst

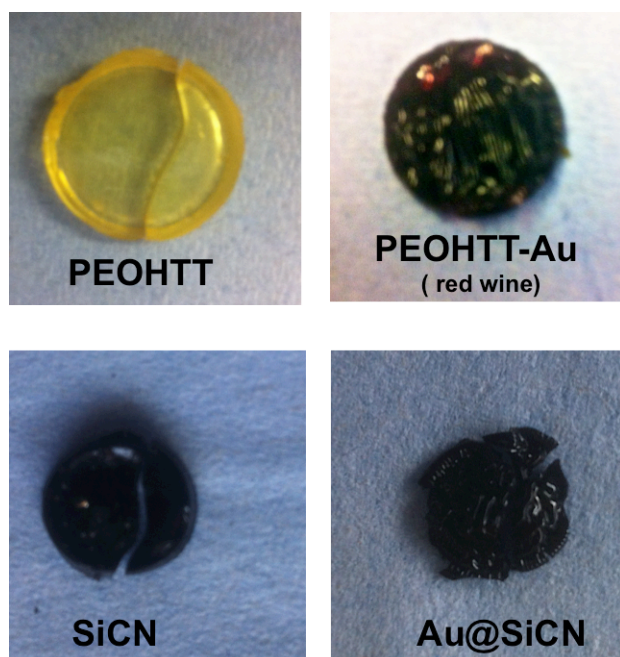
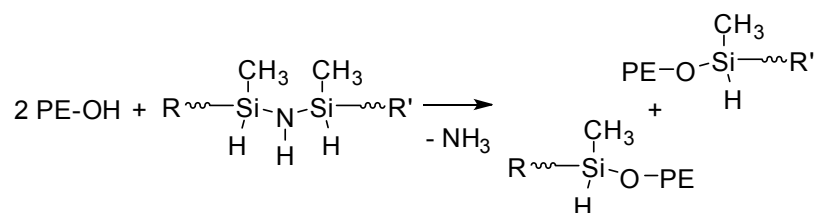


Figure 6.12. Top row. Solvent casted, melt annealed and crosslinked green bodies. Bottom row. Pyrolysed green bodies (images not to scale).

6.7.3. Characterization of SiCN, Au@SiCN, and Ag@SiCN

6.7.3.1. Characterisation of PEOHTT copolymer

The reaction of C₂₂H₄₅OH or PE-OH with HTT1800 goes along with a signal shift of the methylene group attached to the OH-group from 3.37 ppm to 3.7 ppm and a peak broadening.



Scheme 6.1. Linkage of the two-block copolymer segments (R and R' label the rest of the PCCP HTT1800).

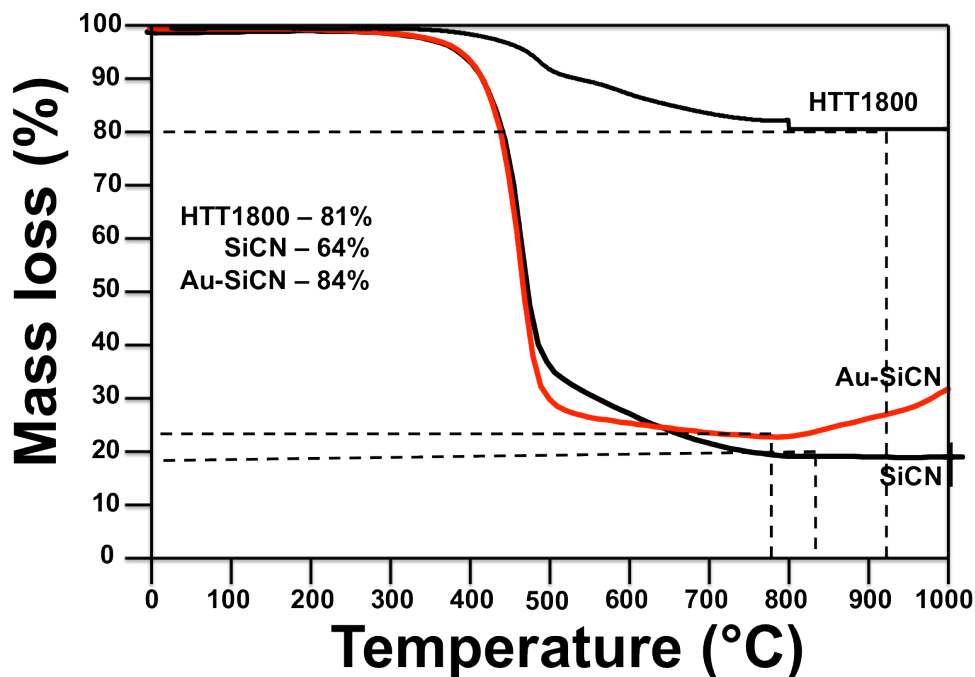


Figure 6.13. Thermo gravimetric analysis curves of as synthesized materials. Weight loss at 480 °C to 520°C correspond to the loss of PE and other organic moieties. The yield of the ceramics was calculated from the amount of VL-20 and subtracted contribution of PE towards the formation of SiCN. The yield of the SiCN afterpyrolysis was in the range of 79-82 in every run. The weight gain after 800°C may be due to the deposition of carbon.

6.7.3.2. Characterization of pyrolysed SiCN, Au@SiCN, and Ag@SiCN

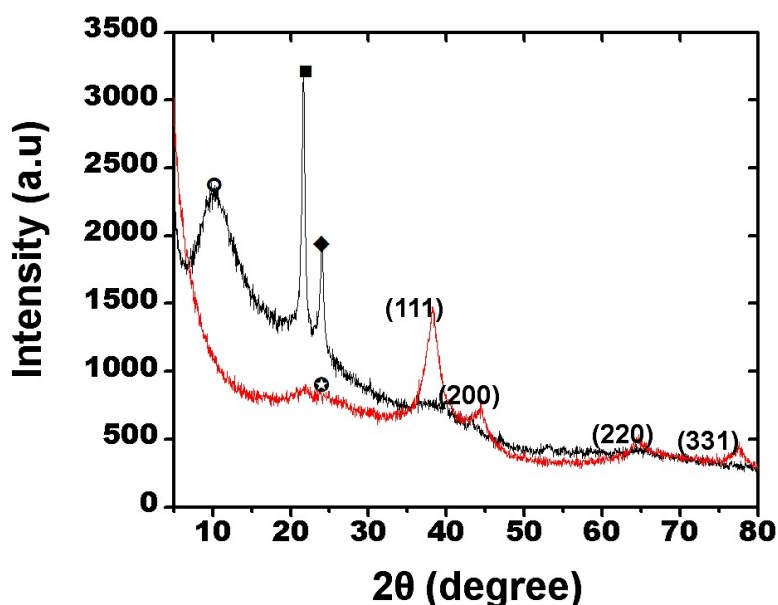
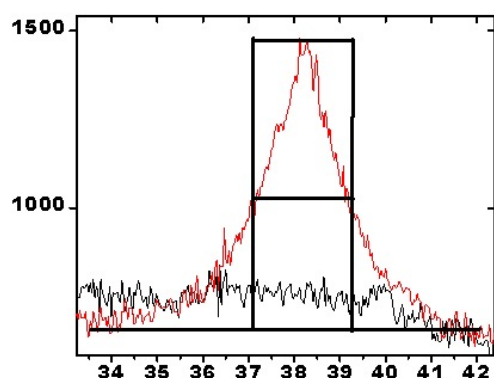


Figure 6.14. WXR D of both green body and pyrolysed Au@SiCN. Greenbody is with amorphous peak (○) of PCCP block and crystalline peaks (◆)

of PE block. Gold nanoparticles supported amorphous SiCN was confirmed by observing typical fcc reflections. Presence of graphitic phase in the sample is highlighted by □.



$$B(2\theta) = \frac{K\lambda}{L \cos \theta}$$

$$2\theta = 38.2^\circ ; \theta = 19.10^\circ ; \cos (19.10) = 0.945$$

$$2.10^\circ = (2.10 \times 2 \times 3.14) / 360 = 0.0366 \text{ radians}$$

$$L = \frac{0.94 \times 0.154}{0.0366 \times 0.948} \approx 4.1 \text{ nm}$$

Figure 6.15. Reflection (111) of (Figure 6.13) was used for the calculation of particle size by Debye-Scherrer.

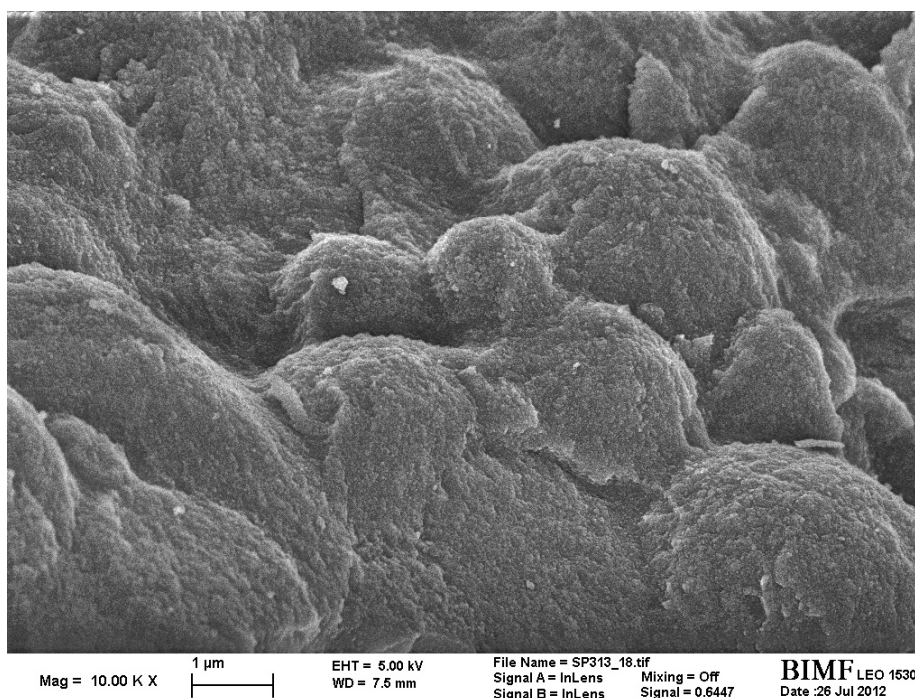


Figure 6.16. SEM image of SiCN after pyrolysing at 1000°C (detailed view)

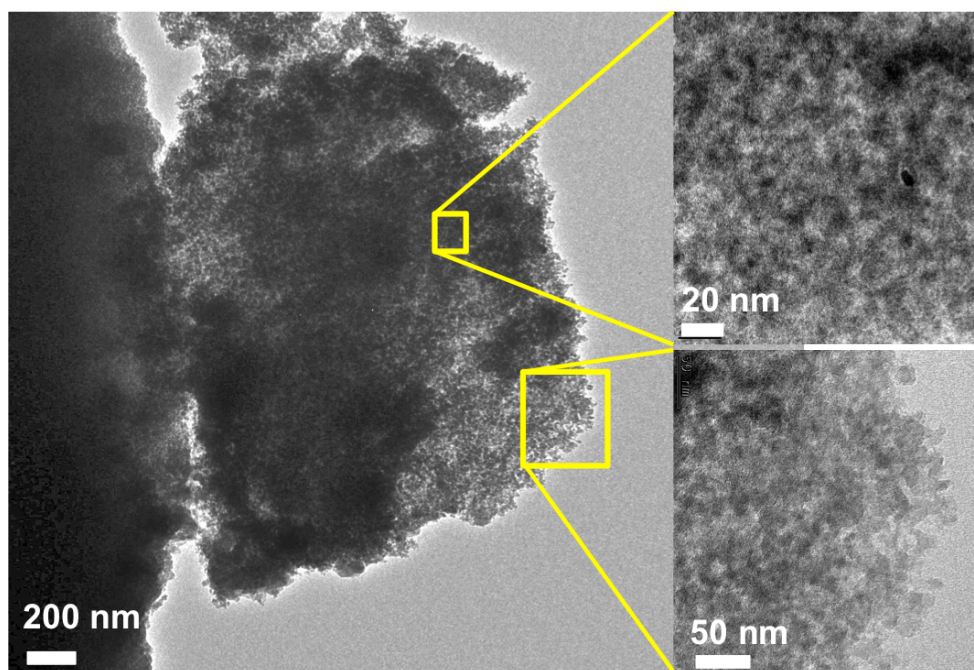


Figure 6.17. Detailed morphological view of the SiCN-2 sample analyzed by TEM.

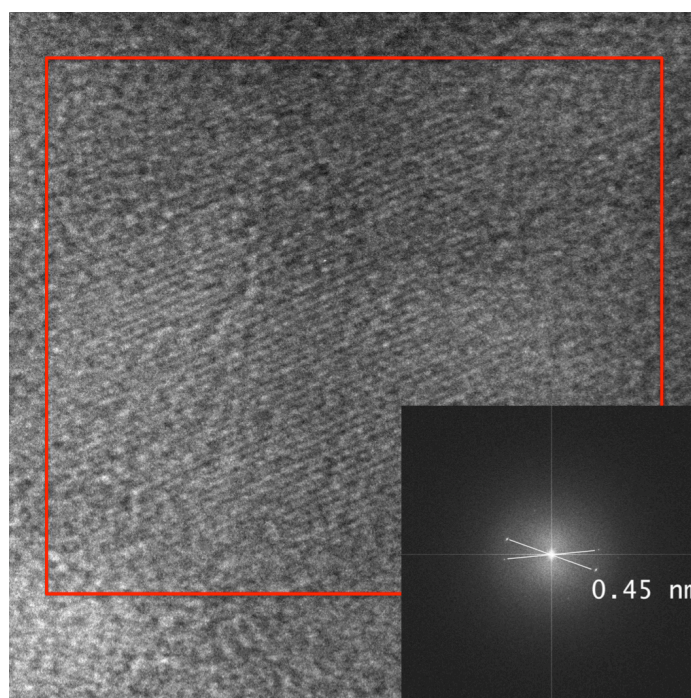


Figure 6.18. Presence of graphitic phase in Au@SiCN sample with inter planar distance of 0.45 nm highlighted with inset of diffractogram plane image.

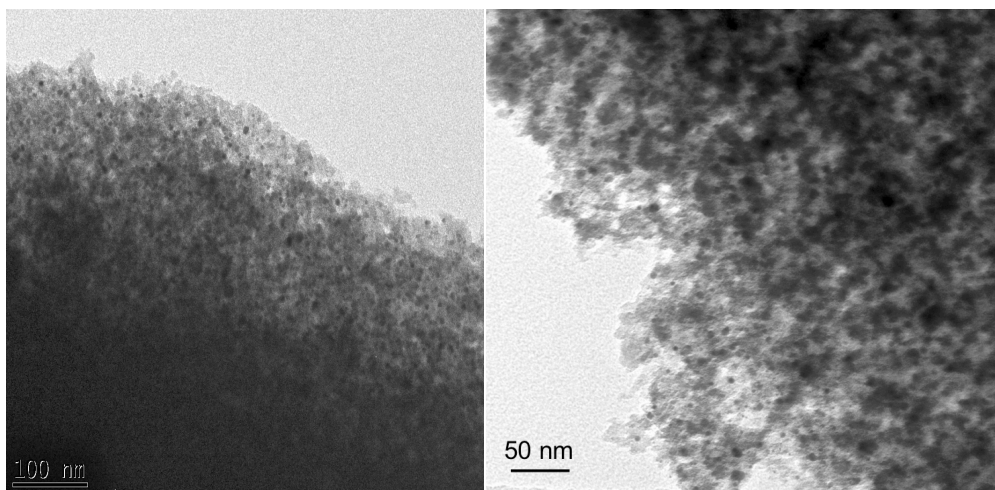


Figure 6.19. TEM image of pyrolysed Au@SiCN sample at 1000°C assisting the presence of bicontinuous porous SiCN supported gold nanoparticles.

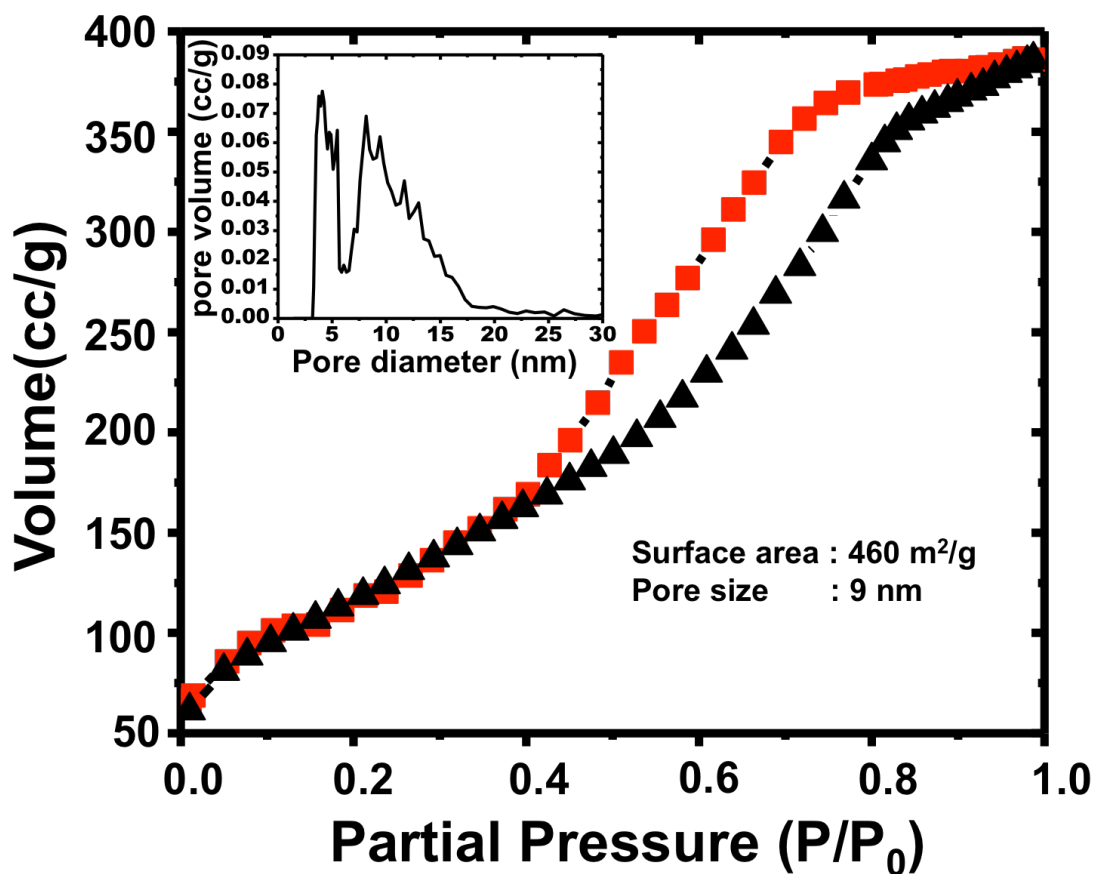


Figure 6.20. Hysteresis of SiCN Sample with inset of corresponding pore size distribution plot.

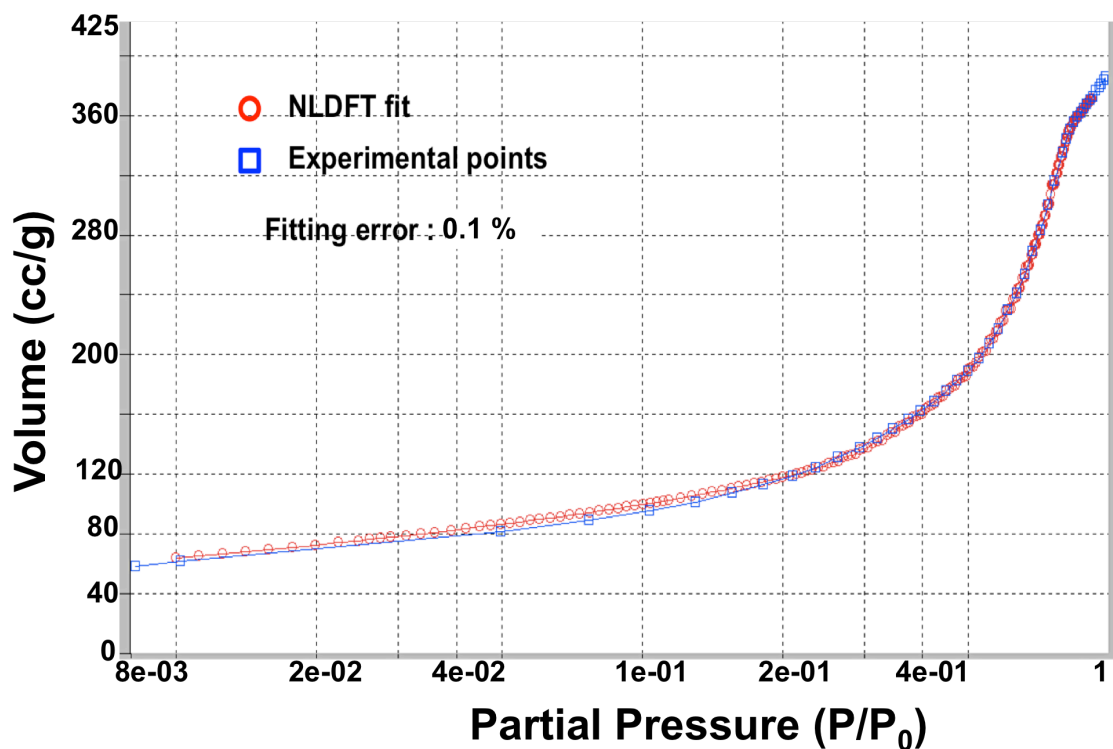


Figure 6.21. Experimental isotherm of SiCN and fit from NLDFT cylinder/sphere adsorption model.

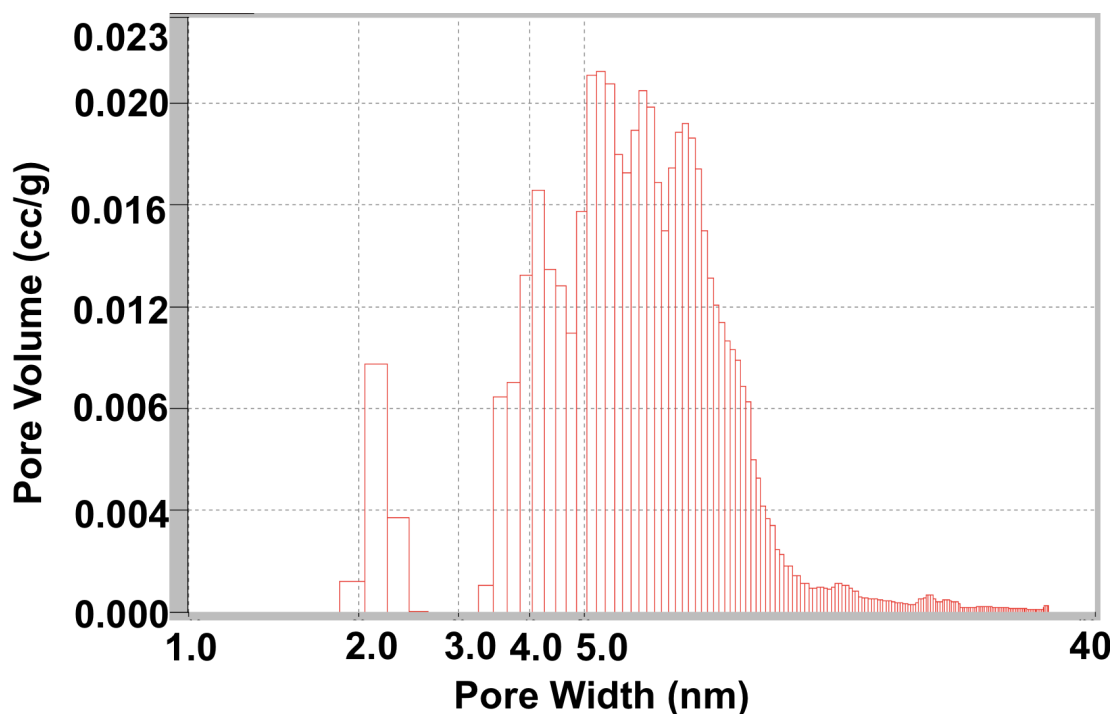


Figure 6.22. Volume histogram of SiCN sample matching the pore size distribution of 9 nm.

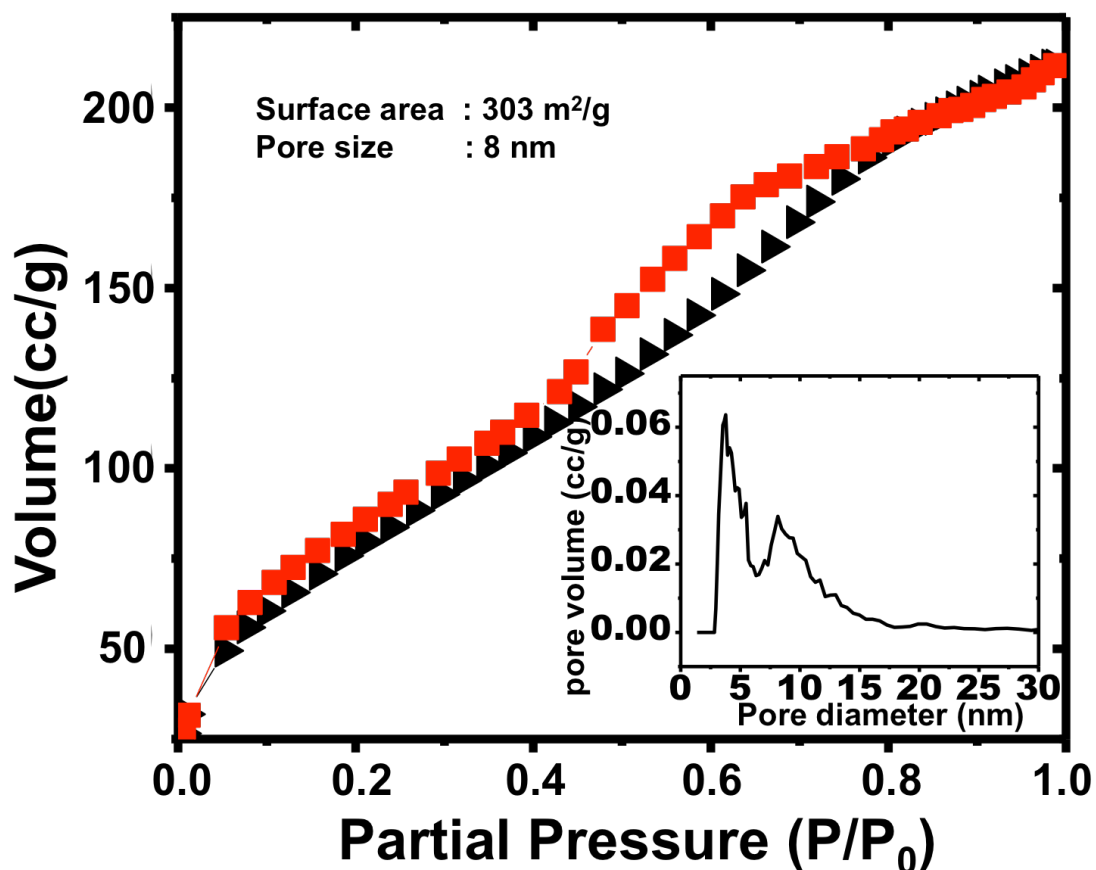


Figure 6.23. Hysteresis of Au@SiCN Sample with inset of corresponding pore size distribution plot.

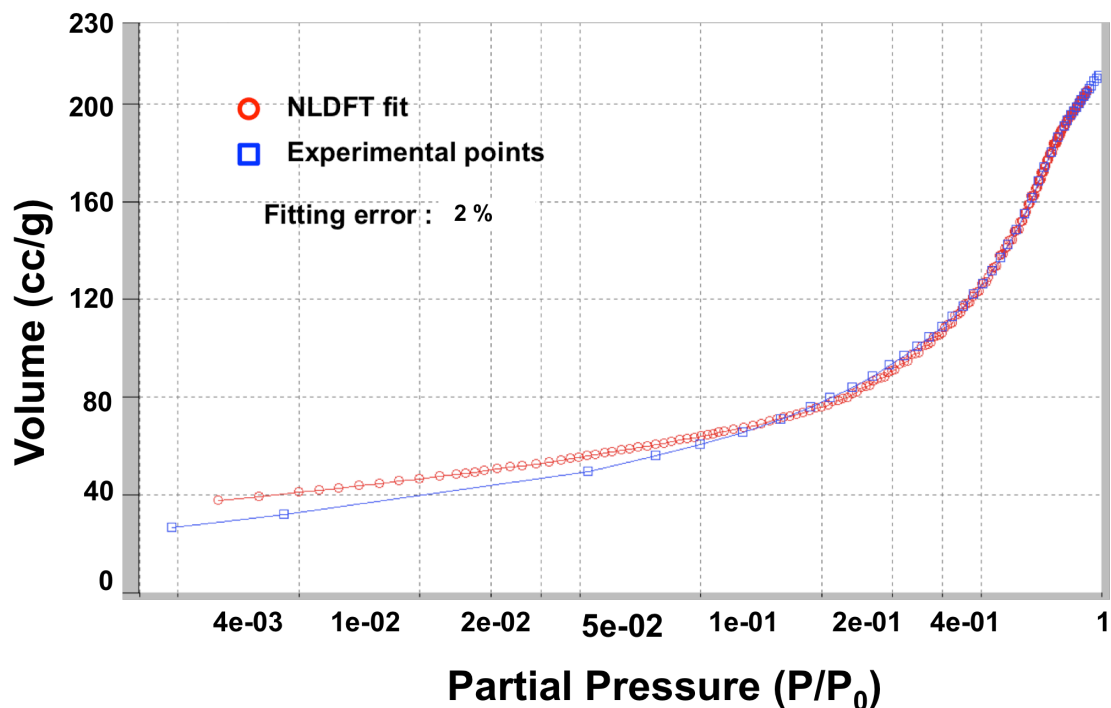


Figure 6.24. Experimental isotherm of Au@SiCN and fit from NLDFT cylinder/sphere adsorption model.

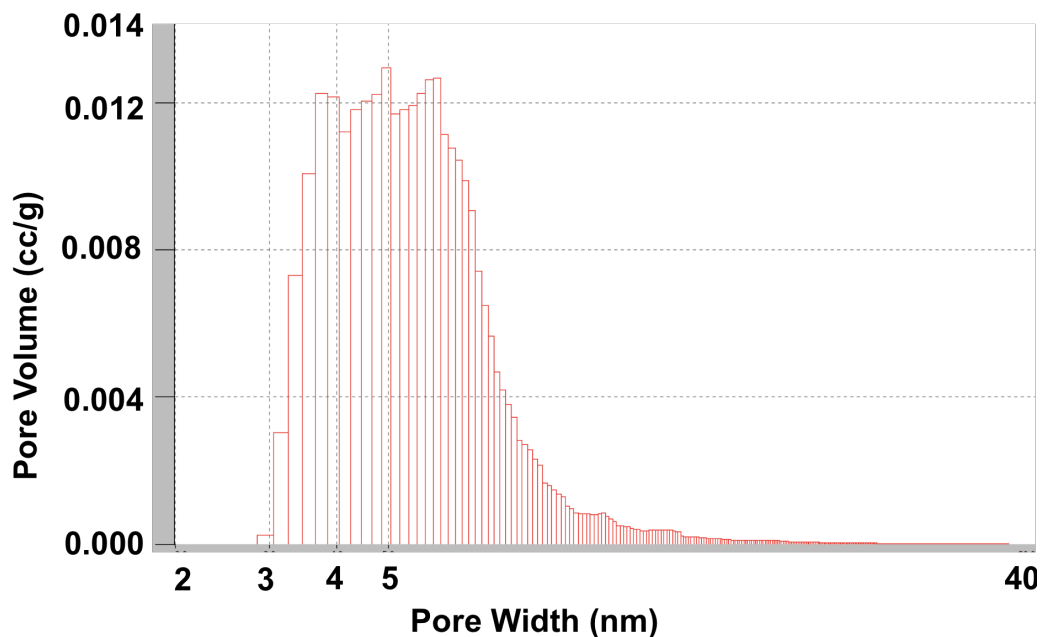


Figure 6.25. Volume histogram of Au@SiCN sample matching the pore size distribution of 8 nm.

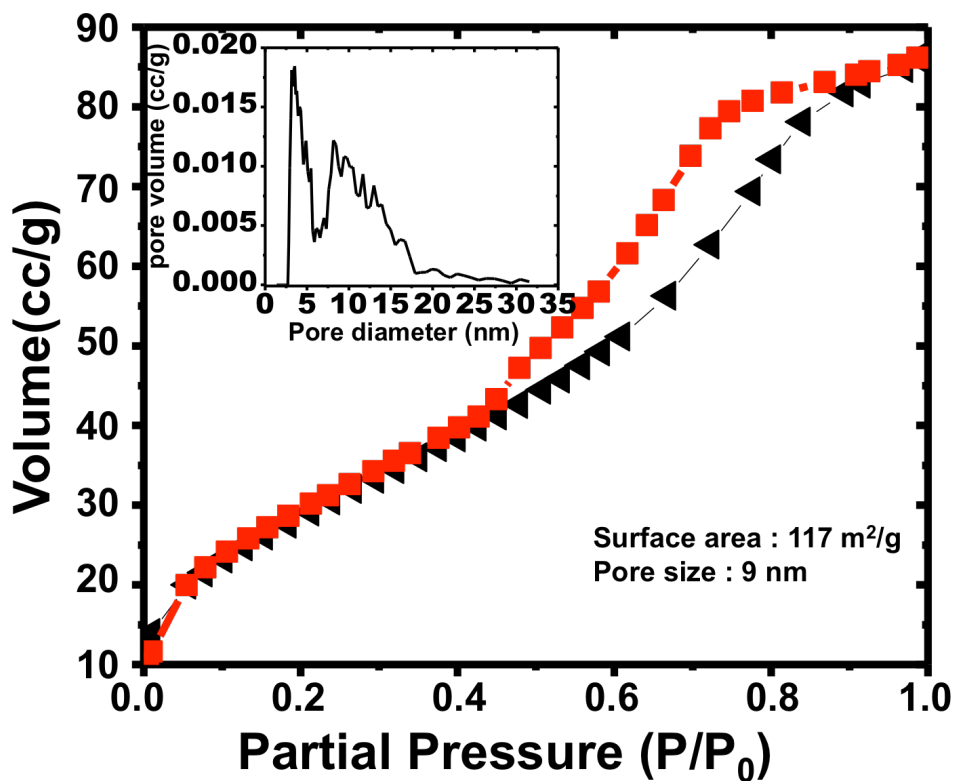


Figure 6.26. Hysteresis of SiCN (70% HTT1800 / 30% PE-OH) sample with inset of corresponding pore size distribution plot.

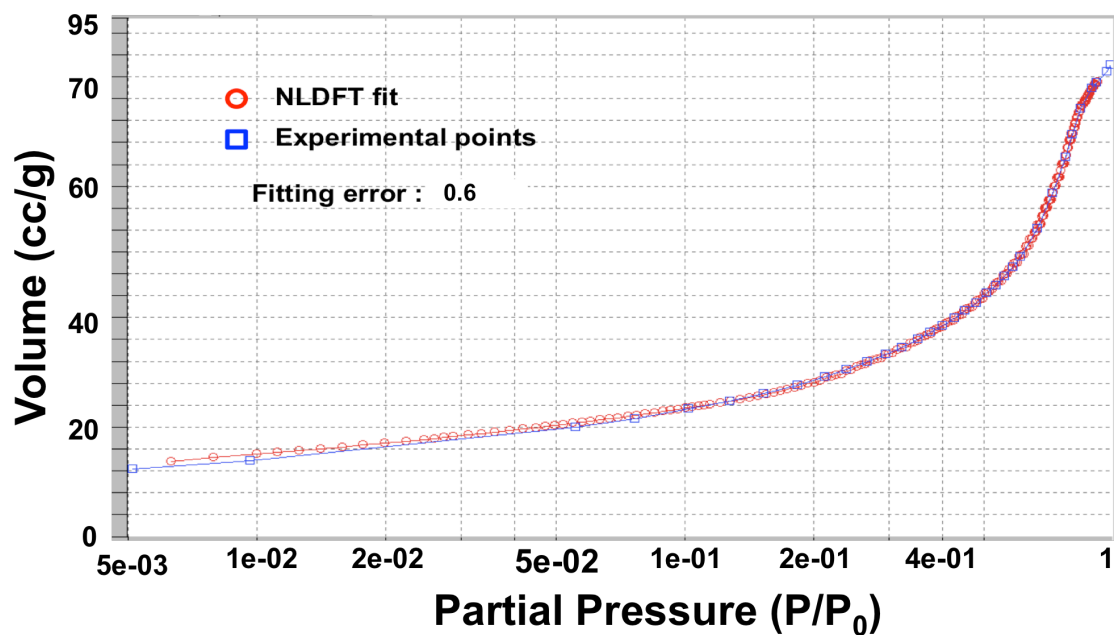


Figure 6.27. Experimental isotherm of SiCN (70% HTT1800 / 30% PE-OH) and fit from NLDFT cylinder/sphere adsorption model.

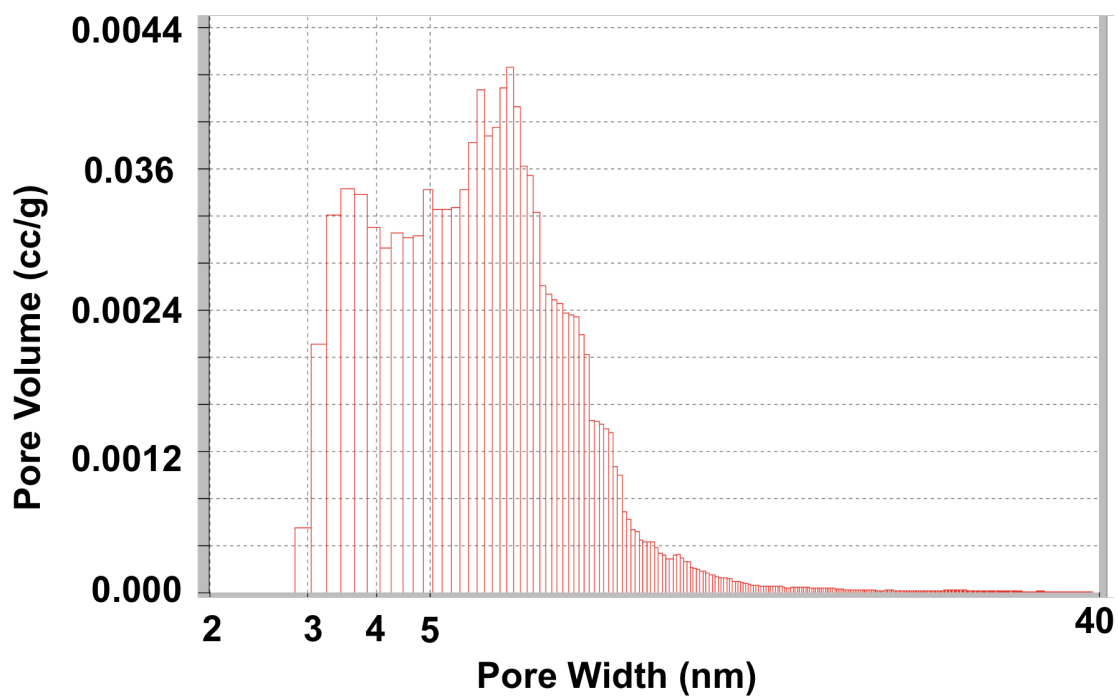


Figure 6.28. Volume histogram of SiCN (70% HTT1800 / 30% PE-OH) sample matching the pore size distribution of 9.316 nm.

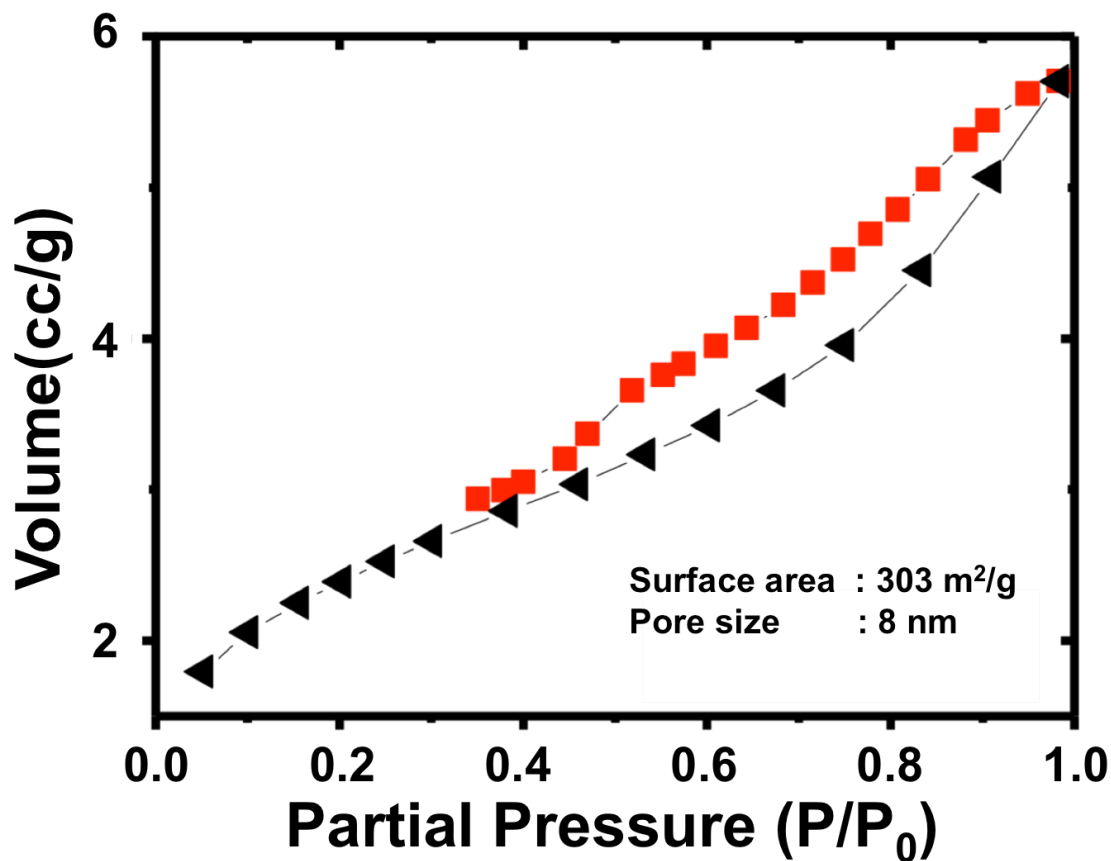


Figure 6.29. Hysteresis of Au@SiCN mesofibers sample.

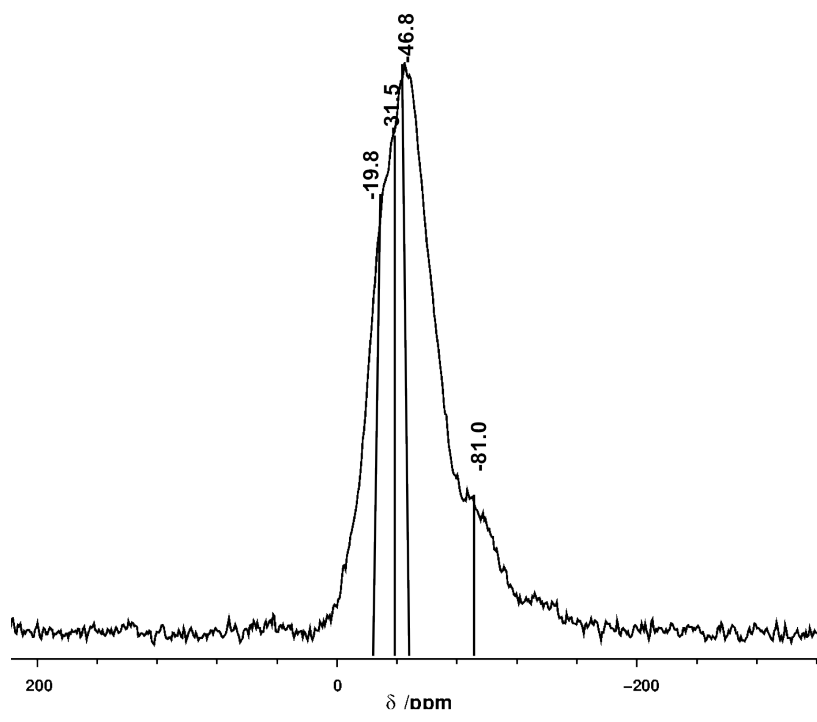


Figure 6.30. MAS ²⁹Si NMR spectrum of the Au@SiCN catalyst pyrolyzed at 1000 °C in an Ar-atmosphere. The main signal at -31.5 ppm is assigned to the formed SiCN₃ environments. Whereas the shoulder at -19.8 ppm and

the smaller signal at -46.8 ppm corresponding to SiC₄ and SiN₄ environments, respectively^{S7}. A distinct peak at 81.0 ppm is assigned to the SiCO₃ environment^{S8}. The signals and the respective chemical shifts are characteristic for a ceramic material formed from a polymeric SiCN-precursor at temperatures above 900 °C.

6.7.4. Acknowledgements

Financial support from the Deutsche Forschungsgemeinschaft, SFB 840, is gratefully acknowledged. We thank Dr. Yamini Avadhut for recording the MAS NMR spectra and Dr. Wolfgang Milius for XRD studies. We also thank Dr. Christene Denner for SEM and Sandra Ganzleben for TGA measurements. Markus Hund is acknowledged for assisting AFM measurements. Authors acknowledge Julia Ewert for the suggestions on the figures. Supporting Information is available online from Wiley Inter Science or from the author.

6.8. References

- [S1] R. Kempe, P. Arndt, *Inorg. Chem.* **1996**, *35*, 2644-2649.
- [S2] G. Glatz, G. Motz, R. Kempe, *Z. Anorg. Allg. Chem.* **2008**, *634*, 2897–2902.
- [S3] S. Brunauer, L. S. Deming, W. E. Deming, E. J. Teller, *J. Am. Chem. Soc.* **1940**, *62*, 1723–1732.
- [S4] D. E. Sullivan, *Phys. Rev. B*, **1979**, *20*, 3991-4000.
- [S5] P. Tarazona, *Phys. Rev. A*. **1985**, *13*, 2672-2679.
- [S6] R. Kempe *Chem. Eur. J.* **2007**, *13*, 2764.
- [S6] a) G. Ziegler, H.-J. Kleebe, G. Motz, H. Müller, W. Weibelzahl, S. Traßl, *Mater. Chem. Phys.* **1999**, *61*, 55-63; b) S. Traßl, D. Suttor, G. Motz, E. Rößler, G. Ziegler, *J. Eur. Ceram. Soc.* **2000**, *20*, 215-225.
- [S6] S. J. Widgeon, S. Sen, G. Mera, E. Ionescu, R. Riedel, A. Navrotsky, *Chem. Mater.* **2010**, *22*, 6221-6228

7. List of Publications

The following publications have been published or “to be submitted” during the work on this thesis

- 1) Saravana K.T. Pillai, Winfried P. Kretschmer, Martin Trebbin, Stephan Förster, Rhett Kempe, Tailored Nano-Structuring of End-Group Functionalized HD-Polyethylene Synthesized via an Efficient Catalytic Version of *Ziegler’s* “Aufbaureaktion”, *Chem. Eur. J.* **2012**, *18*, 13974–13978.
- 2) Saravana K.T. Pillai, Winfried P. Kretschmer, Christine Denner, Günter Motz, Markus Hund, Andreas Fery, Martin Trebbin, Stephan Förster, Rhett Kempe, SiCN nanofibers with a diameter below 100 nm synthesized via concerted block copolymer formation, microphase separation, and crosslinking, *Small* **2013**, *9*, 984–989.
- 3) Saravana K.T. Pillai, Winfried P. Kretschmer, Torsten Irrgang, Martin Friedrich, Justus Hermannsdörfer, Günter Motz, Rhett Kempe, Robustly supported Au@SiCN and their activity in oxidation of alkenes using Air/O₂ as an oxidant.

8. Danksagung/Acknowledgement

My first and foremost gratitude goes to the principle investigator and advisor Prof. Dr. Rhett Kempe for his constant encouragement, timeless suggestions, and priceless motivation. For his selfless devotion of time and energy for correcting me on both professional and personal development, I offer my most sincere thanks to Prof. Dr. Rhett Kempe. He was always patient, generous, and encouraged my independent thinking, which improved my problem solving and chemical intuition. Perhaps most of all, I want to thank for maintaining a positive and encouraging work environment. My respect and admiration are immeasurable.

I acknowledge Prof. Dr. Josef Breu for accepting to be the second reviewer of the examination board. I thank, Prof. Dr. Stephan Förster, the chair of examination board. My thanks also goes to Prof. Dr. Mukundan Tilakkat for being part of examination board.

My sincere thanks to Dr. Winfried Kretschmer for his suggestions on polyethylene part and his encouragement for the completion of the thesis. I also thank Dr. Torsten Irrgang for his suggestions on catalysis part and his time spent on training for GC analysis.

I would like to thank Danial Forberg for his friendly support in the lab. I would also like to extend my thanks to Julia Ewert for making suggestions on most of the figures included in my thesis and many thanks also to her for keeping the music on in the lab to bring jovial environment.

I am heavily indebted to Marlice for helping very often with contracts, moving files, and visa related questions. My special thanks goes to Anna for introducing me to homeopathy medicine and also being as a mother same as

at home. My thanks also go to Simonne and Heidi as well. I also thank the glass blowers and store keepers in downstairs for making their best on my requests.

I would like to thank Dr. Awal Noor for his friendly chitchats, cricket match discussions, and more for being as a good friend in the group. My deliberate thanks to Johannes Obenauf and Martin Friedrich. I also thank Toni Hille, Sina Rösler, Dr. Sadaf Qayyum, Susanne Ruch, Adam Sobaczynski, Gabi, Sonja Lippert, and Johannes Steinbauer.

I thank Dr. Christine Denner for providing friendly atmosphere in the bigining and also for SEM measurements. I would like to thank Zaheer Muhammed for demonstrating aminopyridinato complexes. I also extend my thanks to Justus Hermannsdörfer for his time prviding for the TEM measurements.

My thanks goes to Martin Trebbin for measuring SAXS for all the samples with spending extra time on solving patterns for the structures. I would also like to thank Corinna Stegelmeier for initial introduction with SAXS and her time spening on measuring the SAXS for some of the samples.

I would like to thank Florian Wieberger for DSC measurements and for explaining the concept with processing the raw data. My deliberate thank goes to Sandra Ganzleben for measuining almost all of the samples with unexpected short time. I would also like tio thank Chistian Probst for DSC measurement. I also extend my thanks to Dr. Wolfgang Milius for powder XRD measurements.

I would like to thank Markus Hund for his time to train many and many times on AFM measurements and especially to the sample fixation part. I also thank Tebbe Moritz for help solving in weekends with laser position and

sample mounting. I extend thanks to Christoph Henske for laser etching of samples.

I would like to thank Renee Siegel for measuring solid state NMR and Dr. Yamini Avadhut for giving time to measure the samples during her busy schedule.

I would like to thank Dr. Syriac J. Palackal for his encouragement on doing catalysis and explaining the industrial importance of heterogeneous catalysts. His endless motivation and suggestion on personal life development is appreciable.

I would also like to thank my mother for her patience during the time of my Ph.D and also I would like to thank Prabhu and Ramya for their patience, support, and encouragement. I thank Roopa, Mr. And Mrs Jambulingam for their infinite patience. I thank Roopa for her infinite love, trust, and patience. I thank Bala for his friendly support and suggestions. I also thank Ashok, Prashant, Manohara, Hari, Daniel Schubert, Karthik, Murali, TK, Dr. Unde, Dr. Mondal, Imran, Somnath, Akbaba, Dr. Srimurugan Sangareswaran, Suresh, David, Krishna and Gundu Prabhu for all their infinite support; they have more than anyone helped me keep everything together over the years. I would like to thank the new neighbor and friend Meizen Zieden for chitchat in the fitness center and at the apartment.

It is certainly a worthwhile thanking to Prof. Dr. B. Viswanathan, Dr. James Hoefelmeyer, Dr. Ranjit Koodali, Prof. Dr. Alan Goldman and Prof. Dr. S. Vancheesan (late) for all their constant support for continuing my education without whom I have not be in the current position.

Above all, I am thankful and grateful to the DFG SFB 840 for financial support for the completion of my Ph.D.

9. Declaration/Erklärung

(§ 5 Nr. 4 PromO)

Hiermit erkläre ich, dass keine tatsachen vorliegen, die mich nach den gesetzlichen bestimmungen über die führung akademischer grade zur führung eines doktorgrades unwürdig erscheinen lassen.

(§ 8 S.2 Nr. 5 PromO)

Hiermit erkläre ich mich damit einverstanden, dass die elektronische fassung meiner dissertation unter wahrung meiner urheberrechte und des datenschutzes euner gesonderten Überprüfung hinsichtlich der eigenständigen anfertigung der dissertation unterzogen werden kann

(§ 8 S.2 Nr. 5 PromO)

Hiermit erkläre ich eidesstattlich, dass ich die dissertation selbständig verfasst und keine anderen als die von mir angegebenen quellen und hilfsmittel benutzt habve.

Ich habe die dissetation nicht bereits zur erlangung eines akademischen grades anderweitig eingereicht und habe auch nicht bereits diese oder eine gleichartige doktorprüfung endgültig nicht bestanden

(§ 8 S.2 Nr. 5 PromO)

Hiermit erkläre ich, dass ich keine hilfe von gewerbliche promotionsberatern bzw.- vermittlern in anspruch genommen habe und auch künftig nicht nehmen werde.

Bayreuth, 12-09-2013, Saravana Kumar Thaurman Pillai